MAKING ONE LIP AND NOSE FROM TWO: MORPHOGENETIC MECHANISMS OF ANTERIOR MIDFACE CONVERGENCE MODELED IN *UNICORN* AND *BEETLEJUICE* MICE

by

Brandi Renee Lantz

B.S. Biology, Marietta College, 2013

Submitted to the Graduate Faculty of

the School of Dental Medicine in partial fulfillment

of the requirements for the degree of

Doctor of Philosophy

University of Pittsburgh

2018

UNIVERSITY OF PITTSBURGH

SCHOOL OF DENTAL MEDICINE

This dissertation was presented

by

Brandi Renee Lantz

It was defended on

July 17, 2018

and approved by

Juan Taboas, Ph.D., Assistant Professor, Department of Oral Biology

Seth Weinberg, Ph.D., Associate Professor, Department of Oral Biology

Lance Davidson, Ph.D., Professor, Department of Bioengineering

Dissertation Advisor: Heather Szabo-Rogers, Ph.D., Assistant Professor, Department of Oral Biology

MAKING ONE LIP AND NOSE FROM TWO: MORPHOGENETIC MECHANISMS OF ANTERIOR MIDFACE CONVERGENCE MODELED IN *UNICORN* AND *BEETLEJUICE* MICE

Brandi Renee Lantz, PhD

Orofacial clefting is the most common craniofacial anomaly and consists of several distinct phenotypic categories that range from lateral to medial facial clefts (MFCs). MFCs range in severity from a small medial notch in the vermillion of the upper lip, to a large medial cleft lip that extends posteriorly through the alveolar ridge and secondary palate and anteriorly through the nose. In humans MFCs are rare, thus there is a paucity of animal models and hypotheses surrounding the molecular and morphogenetic etiology of MFCs. During normal development, the anterior midface develops from the medial convergence of paired medial nasal prominences (MNPs) forming the midline of the upper lip and nose. Failure of MNP convergence results in MFCs.

To understand MFCs at both ends of the phenotypic spectrum, I compared the development of the mild medial soft tissue cleft lip in *Prickle1*$^{Bj/Bj}$ embryos and the severe MFC in *Unicorn* embryos. *Unicorn* embryos develop a MFC that splits the nose into two independent nostrils and extends from the medial lip to the secondary palate. I observed the frontonasal ectodermal zone, a signaling center that is required for normal outgrowth of the upper face, is displaced posteriorly in *Unicorn* mutants resulting in the development of two independent nostrils supported by a bifurcated nasal septum. In normal embryos, I observed an epithelial to mesenchymal transformation (EMT) occurs in the medial MNP epithelium during medial convergence. I observed that both the *Prickle1*$^{Bj/Bj}$ and *Unicorn* medial MNP epithelia has decreased apical-basal polarity and failed to undergo EMT by E11.5, the stage of completion in control embryos.

Furthermore, I used histological analysis in wildtype animals, as well as, lineage tracing with an inducible cartilage-specific Cre recombinase (*Collagen2-creER^{T})* driver to describe normal nasal septum development. These experiments revealed that the nasal septum begins developing as two independent rods of *Collagen2-Cre* positive cells approximating the midline of the MNPs as early as E10.5. By E11.5, the *Collagen2-cre* positive rods are fusing together in the anterior to posterior direction resulting in a single nasal septum.

In conclusion, my work has uncovered novel morphological and genetic mechanisms that control midfacial convergence.

TABLE OF CONTENTS

LIST OF TABLES

LIST OF FIGURES

ABBREVIATIONS

BrdU: Bromodeoxyuridine
Cbfa1: Core-binding factor alpha 1
E: Embryonic day
EGFP: Enhanced green fluorescent protein
ENU: N-ethyl-N-nitrosurea
EMT: Epithelial to mesenchymal transformation
Erm1: *Ezrin-radixin-moesin*
FEZ: Frontonasal ectodermal zone
FGF: Fibroblast growth factor
FNP: Frontonasal process
Gli1: Glioma-associated oncogene homolog 1
HH: Hedgehog
LNP: Lateral nasal process
MEE: Medial edge epithelium
MET: Mesenchymal to epithelial transformation
MD: Mandibular process
MNP: Medial nasal process
MXP: Maxillary process
Na: Nasal
NS: Nasal septum
PHH3: Phosphohistone H3
aPKCι: Atypical protein kinase C iota type
PMX: Premaxilla
PPMX: Palatal process of maxilla
PPPL: Palatal process of palatine
PPPX: Palatal process of premaxilla
PS: Presphenoid
Ptc1: *Patched1*
Sox9: SRY-Box9
TUNEL: Terminal deoxynucleotidyl transferase dUTP nick end labeling
V: Vomer
WT: Wildtype

1.0 INTRODUCTION

1.1 OROFACIAL CLEFTING

Early craniofacial morphogenesis occurs during an incredibly critical time during development filled with complex molecular and morphogenetic mechanisms that help to shape the morphological complexity of the face. Given the intricacy of the developmental events that must occur seamlessly at precise time points, it is no wonder that one-third of all birth defects are accompanied by some form of craniofacial developmental anomaly (Gorlin et al. 1990). Though phenotypical variation of craniofacial anomalies that can occur is quite large, the most common site for a craniofacial developmental anomaly to occur is within the oral cavity. Cleft lip with or without cleft palate affects approximately 1/700 live births, and is the most common craniofacial birth defect (Cox 2004; Dixon et al. 2011; Jiang et al. 2006; Leslie and Marazita 2013). While clefting cases can present with a large range of severity, it can also vary amongst ethnic groups, geographical origins, socioeconomic status, and environmental exposures. Albeit orofacial clefting does not typically cause infant mortality in developed countries, it does inflict a large financial burden upon the family, as well as, difficulties speaking, hearing, feeding, as well as, psychosocial interactions for the child. Given the prevalence of clefting, and that much about the morphogenetic mechanisms of orofacial clefting has yet to be discovered, it is of utmost importance to understand the morphogenic and molecular processes that occur during the development of orofacial clefting.

Facial morphogenesis begins during the 4^{th} week of human pregnancy (Jiang et al. 2006). During this time, lip development begins to occur during the 4^{th} week of pregnancy and fusion of the lip occurs by the end of the 6^{th} week of pregnancy (Jiang et al. 2006). After lip fusion, the

secondary palate subsequently begins to develop during the 6th week of pregnancy (Jiang et al. 2006). Finally, secondary palatal fusion occurs by the 8th week of human embryogenesis (Jiang et al. 2006). Thus, any morphogenetic disruptions that interfere with growth and fusion in the orofacial region during the 4th to 8th week of human embryogenesis has the potential to cause an orofacial cleft to occur.

Traditionally, orofacial clefting has been subdivided into two broad phenotypic categories: 1) isolated cleft palate and 2) cleft lip with or without cleft palate (Figure 1). Cleft lip is visible from the face and is present asymmetrically in the upper lip (Figure 1 B). Clefts of the lip can range in severity from a small notch in the upper lip to a complete separation of the upper lip extending into the nasal cavity. Clefting of the lip also has the potential to extend through the alveolar ridge to the incisive foramen (Figure 1 C, G). Cleft lip may present with a cleft palate; however, the cleft palate is likely a consequence of the large cleft in the alveolar ridge that prevents normal palate development (Figure 1 D, H). Cleft lip may be unilateral and only affect one side of the upper lip and palate, or bilateral and thus affect both sides of the upper lip and palate (Figure 1 B-D, F-H). Intriguingly, unilateral cleft lip cases are twice as likely to develop on the left side of the upper lip than the right side of the upper lip (Dixon et al. 2011). Isolated cleft palate occurs in the secondary palate, and can affect only the soft or hard palate, or in the most severe cases when the cleft extends into both the hard and soft palate (Figure 1 D, E, H). Additionally, several other types of orofacial clefting have the potential to occur, such as midfacial clefting, but reports of those cases are much more uncommon.

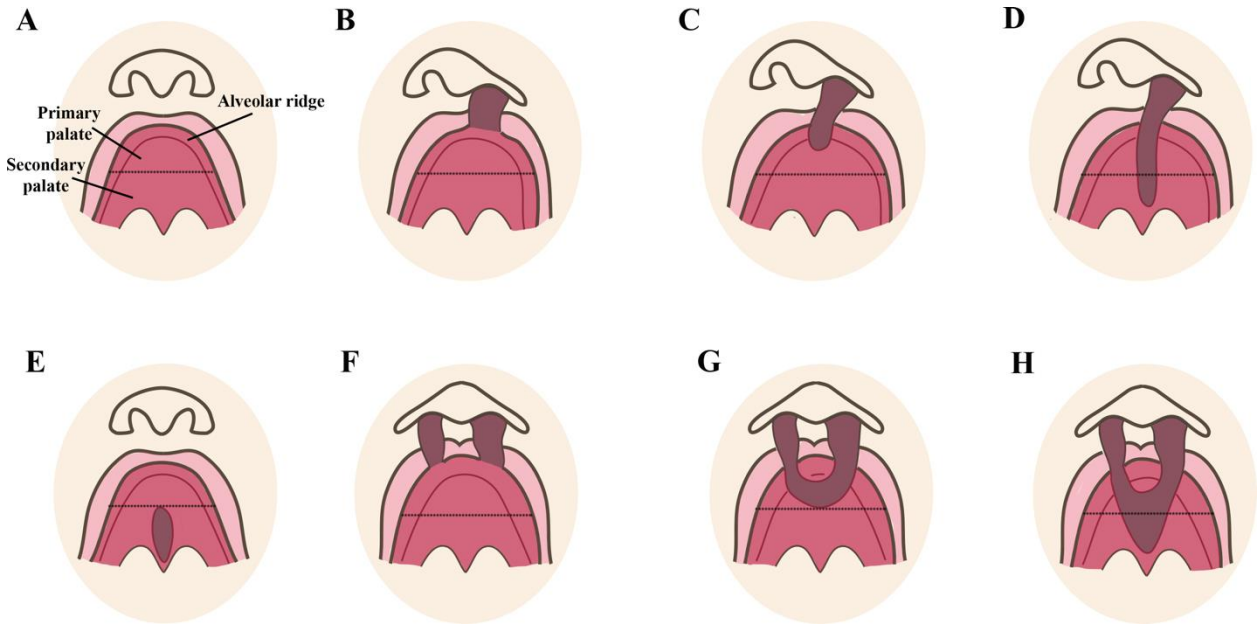

Figure 1. Normal and abnormal per lip and palate anatomy.

Schematic illustrations of normal and abnormal lip and palatal morphology looking up at the roof of an open mouth. (B-D) Phenotypic variations of unilateral cleft lip with or without cleft palate. (E) Isolated cleft palate and (F-H) phenotypic variations of bilateral cleft lip with or without cleft palate. The midline is normal in these subcategories of orofacial clefting. Illustrations were modified from (Dixon et al. 2011). (A) Normal perinatal lip and palatal morphology showing a complete upper lip, alveolar ridge, and secondary palate. (B) Unilateral cleft lip. (C) Unilateral cleft lip that extends through the alveolar ridge. (D) Unilateral cleft lip that extends through the alveolar ridge and the primary and secondary palate. (E) Isolated secondary cleft palate affecting the hard palate. (F) Bilateral cleft lip. (G) Bilateral cleft lip that extends into the primary palate to the incisive foramen. (H) Bilateral cleft lip that extends into the primary and secondary palate.

In 1967 DeMeyer originally described midfacial clefting in humans as “median cleft face syndrome” (DeMyer 1967). Since then, many terms have been used to describe the condition, such as frontonasal dysplasia, frontonasal dysostosis, craniofrontonasal dysplasia, frontonasal syndrome, Tessier number 0, and simply, midfacial clefting. Until 1996, roughly only 100 midfacial clefting cases had been reported worldwide (DeMyer 1967; Guion-Almeida et al. 1996; Pascual-Castroviejo et al. 1985). This unique subset of orofacial clefting is estimated to account for 0.43% to 0.73% of all craniofacial clefts, and to occur in approximately 1: 1,000,000 live births (Koh and Do Yeon Kim 2016; Urata and Kawamoto 2003). Midfacial clefting compromises the midline structures such as the upper lip, palate, and nose (Figure 2 B, C). The severity of these cases can range from a simple vermillion notch in the soft tissue to a very wide true cleft of the lip, palate, and nose that affects the soft tissue, as well as, the underlying skeletal structures, such as the nasal septum (Figure 2 B, C). Given the considerable variation of severity observed in midfacial clefting cases, it is uncertain whether midfacial clefting occurs considerably less than normal orofacial clefts or if less severe cases are underreported. Remarkably, the literature regarding cleft lip, and more specifically midfacial clefting of the midline structures is greatly lacking. Moreover, the developmental morphogenetics surrounding the anterior midfacial structures, such as, the lip and the nose are substantially unexplored.

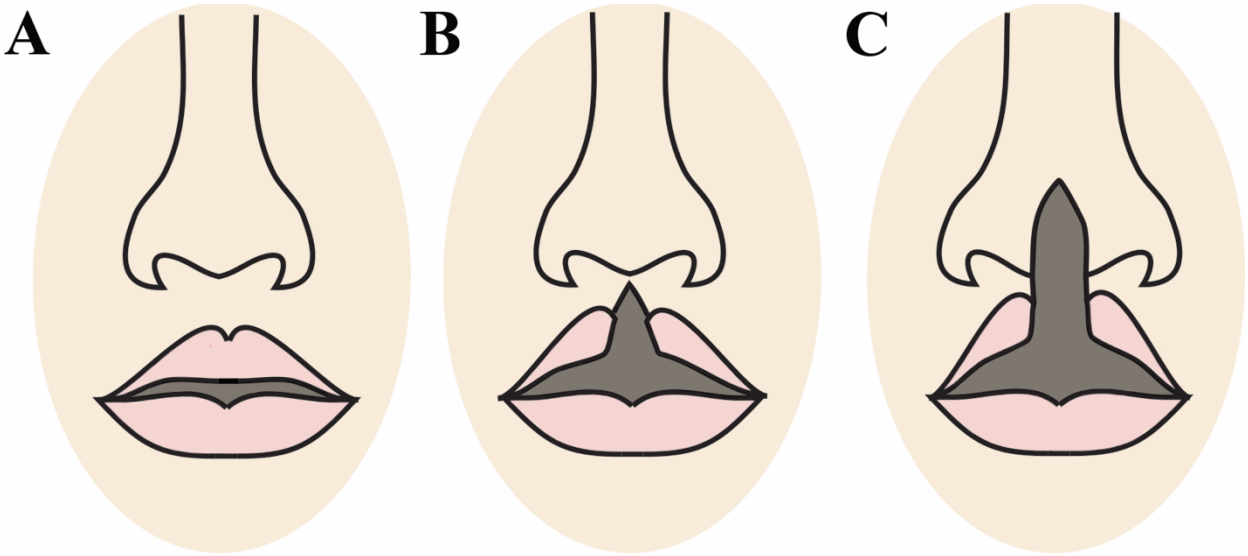

Figure 2. Phenotypic variation among cases of midfacial clefting.

Representative drawings of the phenotypic variation in patients that have midline orofacial clefting. (A) Normal midfacial anatomy. (B) In mild cases, patients can present with intact nasal and palatal morphology, but a medial notch in the upper lip. (C) In severe cases, the medial cleft lip is accompanied by a cleft in the midline of the nose. The most severe medial cleft face will impact the development and morphology of the lip, palate and nose. Images were modified from (Kolker et al. 2015).

Normal and abnormal development can typically be reiterated relatively closely to human pathogenesis in animal models, such as the mouse. Though, currently within the field of orofacial clefting there is substantially more understanding of palatal development relative to lip development. In humans, orofacial clefting is more likely to occur within the lip rather than the palate, and currently there are significantly more mouse models which develop an isolated cleft palate rather than a cleft lip (Gritli-Linde 2012; Gritli-Linde 2008; Watkins et al. 2014). Thus, it is difficult to understand normal, as well as, abnormal development of the anterior midfacial structures, such as the lip and the nose if there are a lack of animal models which can appropriately recapitulate the phenotype. Intriguingly, ciliopathic mouse embryos very frequently develop a midfacial cleft phenotype with a bifurcated nasal septum, but the complete etiology of the medial cleft morphogenesis is poorly understood. Another factor that may account for an inability to easily generate mouse models whom can recapitulate more common phenotypes such as clefting of the lip, but also more rare phenotypes, such as midfacial clefting could very well be due to the multifactorial etiology of orofacial clefting.

Orofacial clefting originates from a multifactorial etiology. The occurrence rate of orofacial clefting varies amongst populations, sex, socioeconomic status, and environmental exposures. American Indians and Asian populations have the highest rates of orofacial clefting reported at approximately 1 in 500 live births (Dixon et al. 2011). Populations originating from European ancestors have a much lower rate of orofacial clefting occurring at about 1 in 1,000 live births (Dixon et al. 2011). Populations originating from African lineages have the lowest reported birth rates of orofacial clefting occurring at approximately 1 in 2,500 live births (Dixon et al. 2011). Due to the facial shape diversity represented amongst different populations, it has been long suggested that facial shape variations can contribute to orofacial clefting, and there has been

evidence that facial shape can be a predisposing factor for orofacial clefting (Weinberg et al. 2008). Additionally, amongst the sexes, males are two times more likely to develop a cleft of the lip than females (Dixon et al. 2011). Contrarily, females are two times as likely to develop an isolated cleft of the palate than males (Dixon et al. 2011). Increased associations have also been found amongst the prevalence of children born with a cleft lip and/or palate and lower socioeconomic status (Clark et al. 2003). Furthermore, increased risks of orofacial clefting have been associated with environmental factors such as embryonic exposure to hypoxic conditions and certain teratogenic drugs during the development of the lip and the palate.

Though orofacial clefting occurs very early on during embryonic development, treatment of the cleft generally occurs in stages after the child is born. Treating a child affected by an orofacial cleft requires a team of healthcare providers such as, surgeons, speech therapists, ear nose and throat specialists, orthodontists, and psychologists. Thus, children with orofacial clefts can impose a large economic burden upon their families and society (Berk and Marazita 2002). More importantly though, children affected by clefts must receive numerous operations that will render their clefting site to become functionally and esthetically pleasing, thus allowing them to have an increased quality of life.

Given that orofacial clefting is the most common craniofacial anomaly to occur during embryonic development and that the etiology of the disorder is poorly understood, it is important to gain an in-depth understanding of the embryological origins of this developmental disorder. Owing to the multi-factorial causative etiology and variation of clefting types seen in human orofacial clefting, many aspects of the developmental disorder have yet to be resolved. In this dissertation, we were interested in determining the morphogenetic molecular mechanisms of the

medial nasal prominences during midfacial convergence. We also determined the role that surrounding developing facial organs play, such as the nasal septum, in midfacial convergence.

1.2 THE EMBRYONIC ORIGINS OF THE FACE

The human face is an intriguing complex as it is truly unique to each individual person, but fascinatingly the morphological processes that shape the craniofacial structures of each face are relatively the same. Morphogenesis of the human face requires many highly-orchestrated events and tissue interactions to occur in sync at precise points in time. The primitive face is reliant upon large scale interactions, such as facial prominence merging, but also upon more minute scale interactions, such as, cell to cell signaling interactions. Resultant of these early craniofacial morphogenetic events and subsequent growth and development, the silhouette of a more recognizable human face will soon begin to take shape.

Craniofacial morphogenesis begins to occur at a considerably early time during embryonic development, commencing with the cranial neural crest cells. Cranial neural crest cells that first emerge from the neural tube will subsequently migrate from the forebrain, midbrain, and hindbrain. Eventually, forebrain and rostral midbrain derived cranial neural crest cells will populate the frontonasal process, and caudal mid-brain derived cranial neural crest cells will populate the maxillary component of the first pharyngeal arch (Osumi-Yamashita et al. 1994; Trainor and Tam 1995). After differentiation and patterning processes, these forebrain and rostral midbrain cranial neural crest cells will populate the facial processes and ultimately give rise to the anterior midfacial bones, such as, the maxilla, ethmoid and palatine (Chai et al. 2000; Jiang et al. 2002; Yoshida et al. 2008).

The migrating neural crest cells migrate in and around the stomodeum. The stomodeum is the primitive mouth and is initially surrounded by facial processes which will give rise to the unique structures of the face. At approximately E (embryonic day) 9.5 in the mouse and 26 days gestation in humans, the frontonasal process is unpaired and laterally bordered by the maxillary

processes (Jiang et al. 2006). Within approximately half a day in mice (E10.0) and by 32 days gestation in humans, the surface ectoderm of the frontonasal process thickens bilaterally producing the nasal placodes (Jiang et al. 2006). As the frontonasal process continues to proliferate, it will begin to project laterally and medially around the nasal placodes, resulting in unambiguous partitioning of the face and the formation of bilateral nasal pits (Figure 3, Figure 4 A) (Hinrichsen 1985).

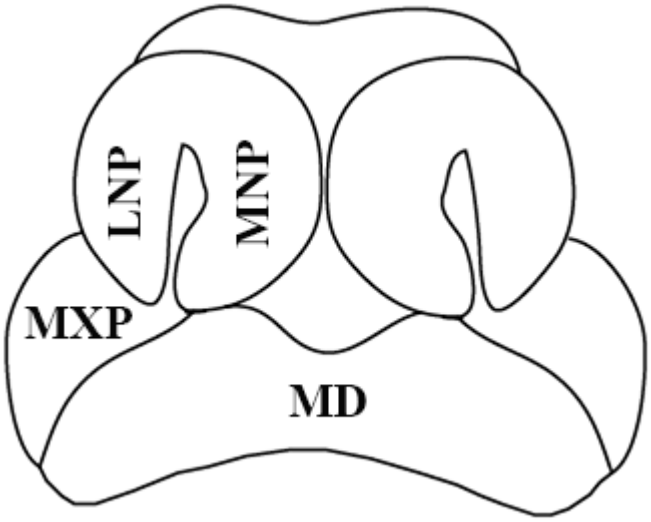

Figure 3. Phylotypic stage of facial prominence development.

The Phylotypic stage of facial development is characterized by individual facial prominences surrounding the stomodeum that eventually merge together and form continuous facial structures. The upper face is made from the lateral nasal process (LNP), medial nasal process (MNP), maxillary process (MXP). The lower portion of the face is formed from the mandibular process (MD). Midfacial clefting results from defects in MNP convergence, while defects in the fusion of the MNP, LNP, and MXP result in cleft lip phenotypes. Defects in the growth and development of the MXPs results in the development of cleft palate.

During this time in embryonic development, surrounding the stomodeum are a pair of maxillary prominences positioned laterally, lateral nasal prominences, medial nasal prominences positioned rostrally, and the mandibular prominence is caudal (Figure 3, Figure 4 A). The medial and lateral nasal prominences form a horseshoe of tissue surrounding the nasal pits (Figure 3).

The facial prominences are composed of an inner core of mesenchyme surrounded by an outer epithelial layer. The mesenchyme consists of neural crest and mesodermally derived cells. By E11.0 in mice and 38 days gestation in humans, continued growth of the medial nasal prominences and maxillary prominences helps to assemble the distal ends of the medial nasal prominence and lateral nasal prominence, and medial end of the maxillary prominence into direct contact in the zone of fusion (Figure 4 B) (Jiang et al. 2006). During this time, it is also crucial for the medial nasal processes to contact one another for the formation of the oblique seam in the primary palate. Shortly after, the epithelial seam surrounding the facial processes will begin to disappear, and the corresponding mesenchyme will begin to converge forming the lateral sides of the upper lip (Jiang et al. 2006). Mesenchymal convergence of the facial processes is essential for normal cranial development. As the medial nasal prominence, lateral nasal prominence, and maxillary prominence come together at the zone of fusion, the lateral nasal prominence is moved anteriorly as the maxillary prominence protrudes forward to make contact with the medial nasal prominence (Hinrichsen 1985). The medial nasal prominence and maxillary prominence will form the medial and lateral portions of the upper lip, respectively (Figure 4 C) (Ashique et al. 2002; Cox 2004; Sperber 2002; Sun et al. 2000).

While the fusion of the lateral sides of the upper lip is well studied, the development of the midline of the lip is understudied. Beginning at E11.5 in mice and approximately the 6th week of embryonic development in humans, rapid growth will continue to drive the paired nasal pits and

medial nasal prominences towards the midline. The convergence of the two medial nasal prominences creates a single "intermaxillary segment." The midline convergence of the two medial nasal prominences is essential for the development of the crest and tip of the nose, philtrum, and medial section of the upper lip (Figure 4 C).

The lateral nasal prominence will eventually form the alae of the nose, and the nasal pits will become the epithelium lining the nostrils following fusion of the medial nasal prominence and maxillary prominence with the lateral nasal prominence (Figure 4 C) (Hinrichsen 1985). The previously described convergence steps are completed by approximately E12.5 in mice and approximately 48 days of gestation in humans (Jiang et al. 2006).

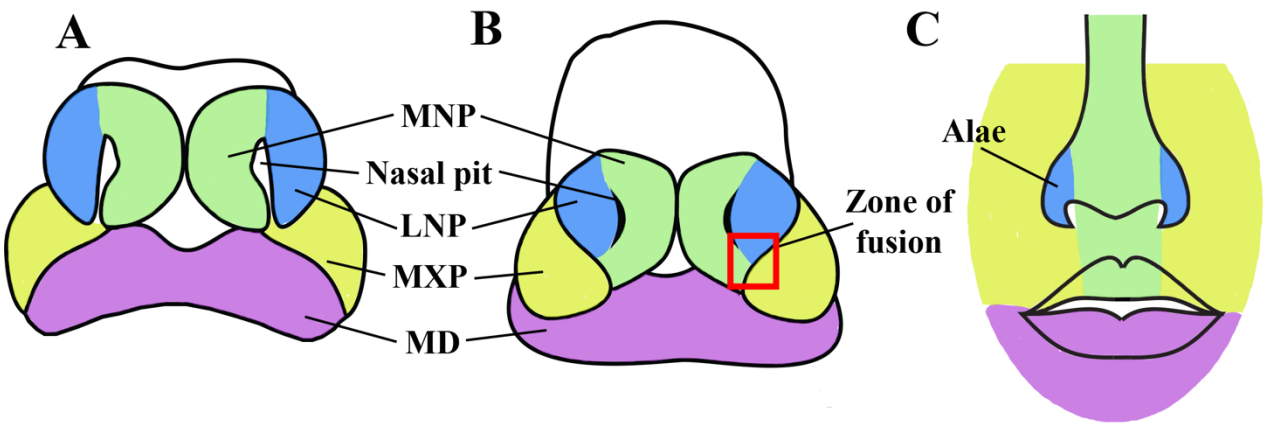

Figure 4. Developmental progression of midfacial morphogenesis.

Schematic of the phylotypic stages of facial development and adult facial regions derived from the embryonic facial prominences. (A) During the phylotypic stage of development (E10.5 in mouse; ~35 days of human gestation), the stomodeum is surrounded by a pair of maxillary prominences (MXP) positioned laterally, lateral nasal prominences (LNP), medial nasal prominences (MNP) positioned rostrally, and the mandibular prominence (MD) is caudal. (B) At E11.5 in the mouse and beginning at the 6th week of gestation in humans, the facial prominences begin to join together. The MNPs merge medially together. The MNPs, LNP, and MXP merge together at the zone of fusion (red box). The anterior facial prominences complete fusion by the end of the 6th week of human development. (C) In the human adult, the medial nasal prominences form the crest and tip of the nose, philtrum, and medial portion of the upper lip. The lateral nasal prominences form the alae of the nose. The maxillary prominences for the sides of the face, and the lateral portion of the upper lip. The mandibular prominence forms the mandible. Image modified from (Dixon et al. 2011).

In addition to facial prominence fusion leading to the development of the upper lip, fusion of the maxillary prominences are also required for palatal morphogenesis. As the bilateral medial nasal prominences fuse medially with one another, as well as, laterally with the maxillary prominences to form the upper lip, the intermaxillary segment, or primary palate is formed posterior to the lip (Cobourne 2004; Diewert and Wang 1992; Sperber 2002; Wang et al. 1995). Though the primary palate is formed much earlier in development than the secondary palate, the two must successfully fuse for functional palatal morphogenesis. In humans, it has been hypothesized that an early, severe cleft of the primary palate causes the formation of a cleft of the secondary palate (Burdi et al. 1972). The primary palate is finished developing by E11.5 in mice and by the beginning of 7 weeks gestation in humans, whereas the secondary palate finishes its development at E15.5 in mice and by the end of 8 weeks gestation in humans.

Secondary palatal development is initiated from lateral outgrowths of the maxillary prominences into the stomodeum as the facial prominences fuse together for facial morphogenesis at approximately E12 in mice and the end of the 6^{th} week of gestation in humans. At approximately E12.5 in mice and 7 weeks gestation in humans, the palatal shelves will grow vertically alongside of the developing tongue towards the floor of the mandible (Figure 5 A). At this developmental stage, the tongue inhibits contact of the palatal shelves. By E13.5 in mice and approximately 7.5 weeks gestation in humans, the palatal shelves elevate horizontally above the tongue (Figure 5 B) (Brinkley et al. 1978; Diewert 1980a; Diewert 1983; Fulton 1957; Iizuka 1973; Luke 1976; Walker and Fraser 1956; Wood and Kraus 1962). It has been shown that during the time of palatal shelf elevation, the mandible begins to grow rapidly, thus helping the tongue to drop within the oral cavity (Diewert 1974; 1980a; 1982; Diewert 1976; 1978; 1979; 1980b). During the process of

palatal shelf elevation, the anterior region will elevate first, closely followed by the posterior region of the palatal shelves (Ferguson 1988; Iizuka 1973; Waterman and Meller 1974). Once the shelves have elevated, the palatal shelves will grow medially towards each other and above the tongue until the medial edge epithelial cells make contact at the midline (Diewert 1983; Farbman 1969; Hayward 1969). The palatal shelves will first meet at the midline at E14.75 and subsequently fuse at E15.5 in mice and approximately the end of the 8th week of gestation in humans (Figure 5 C) (Bush and Jiang 2012). Also during this time, in the nasal cavity, the nasal septum extends inferiorly from the frontonasal process and fuses with the palate (Figure 5 C).

Embryonic craniofacial morphogenesis occurs relatively quickly at a very early stage of development when a large portion of expectant mothers are still unaware that they have conceived. To be able to truly understand orofacial clefting, it is essential to first understand normal craniofacial morphogenesis. During normal orofacial development, the craniofacial tissues are proliferating, migrating, signaling, and merging together. A deficit in any process at any point in development has the potential to cause a cleft of the lip and/or the palate to occur.

A

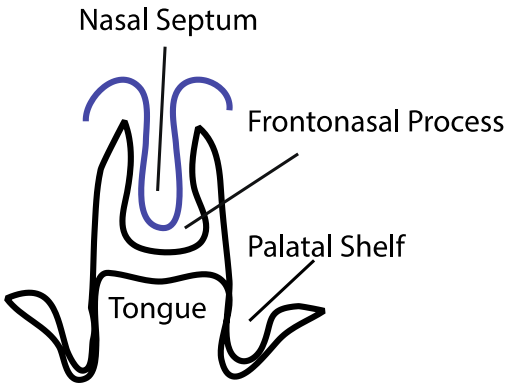
Nasal Septum
Frontonasal Process
Palatal Shelf
Tongue

B

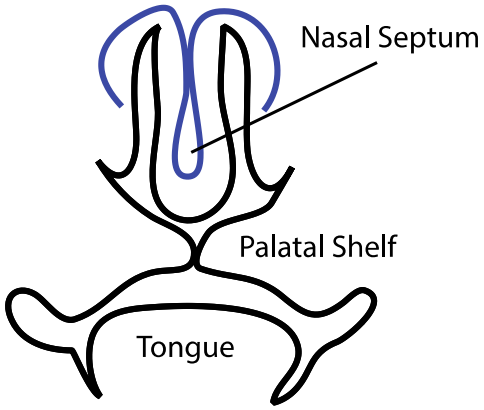
Nasal Septum
Palatal Shelf
Tongue

C

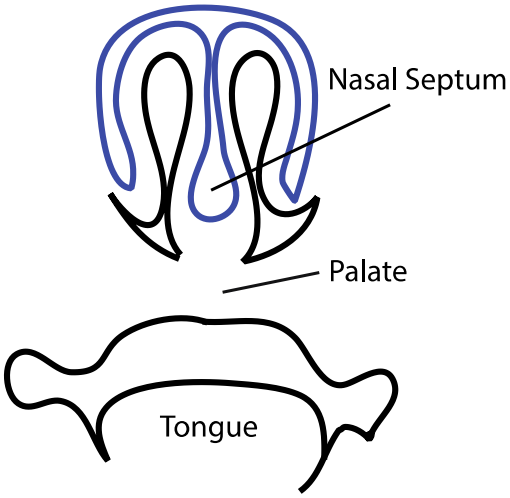
Nasal Septum
Palate
Tongue

Figure 5. Schematic of palatal and nasal septum development.

Schematic of secondary palate fusion including merging with the frontonasal process. (A) The secondary palatal shelves grow out of the intraoral edge of the maxilla and vertically alongside of the tongue, while the nasal septum matures in the midline of the upper face. (B) The palatal shelves elevate into a horizontal position, and grow towards each other until juxtaposed in the midline. At the same time, the nasal septum approximates the nasal edge of the palatal shelves. (C) The fusion of the palatal shelves separates the oral and nasal cavity. Merging of the nasal septum with the palate divides the nasal cavity into left and right nostrils. Image modified from Ten Cate's Oral Histology textbook and Virginia Diewert (Diewert 1983).

1.3 THE NASAL SEPTUM IS A CRITICAL MIDFACIAL ORGAN

Facial symmetry is unknowingly one of the first evaluations that take place during human interaction. Even an average individual who is not trained to look for facial asymmetries can be drawn to very minor facial differences. The most central organ of the face, the nose, is a fundamental structure that helps to determine facial symmetry. The upper respiratory organ is composed of a complex structure that is derived from differential embryonic origins that work to provide support and function. A large part of that support comes from the nasal septum.

The nasal septum is an osteocartilaginous organ that partitions the nasal cavity into left and right nasal passages. Anatomically, the nasal septum is continuous superiorly with the perpendicular plate of the ethmoid, as well as, posteriorly with the vertical plate of the vomer as seen in Figure 6. During embryological development, the vomer is formed by means of two intramembranous ossification sites located within the mucoperichondrium during the 9th week of human development (Fawcett 1911; Macklin 1914; Macklin 1921; Müller and O'Rahilly 1980). Interestingly, during embryonic development of the ethmoid, ossification of the ethmoid takes place endochondrally by means of three ossification sites (Sperber et al. 2001). In addition to the osteogenic derivatives, the anterior portion of the nasal septum is composed of hyaline cartilage (Figure 6). The cartilage of the nasal septum has been regarded by some authors as a principle component of midfacial growth. Growth of the nasal septum cartilage has been suggested to stretch the midfacial sutures, and therefore stimulate bone formation at the suture sites (Kvinnsland 1974; Sarnat and Wexler 1966; Scott 1953). Whereas other authors have theorized that the cartilaginous septum plays a passive role in craniofacial growth by merely supporting the nose and aiding in breathing (Moss et al. 1968; Stenstrom and Thilander 1970). Intriguingly though regarding both

views of the role of the nasal septum, there is very little is known about the development of this essential midfacial organ.

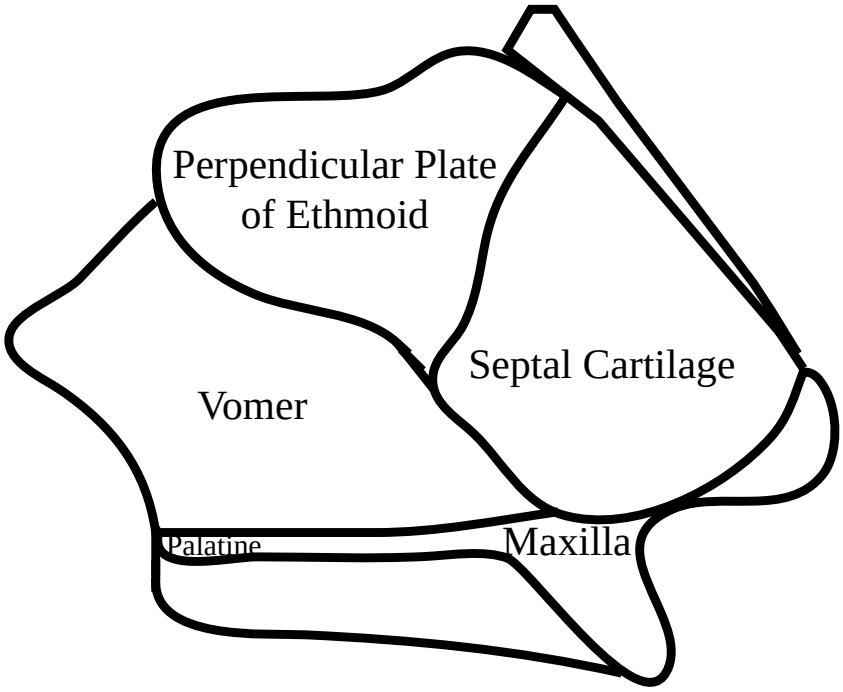

Figure 6. Hard tissue anatomy of the nasal septum wall in human adults.

The nasal septum divides the nasal cavity into left and right halves. The nasal septum is an osteocartilaginous organ. Superiorly, the nasal septum is formed from the perpendicular plate of the ethmoid. Posteriorly, the nasal septum is formed from the vertical plate of the vomer. Additionally, the anterior portion of the nasal septum is composed of hyaline cartilage. Image modified from the 1918 version of the Anatomy of the human body textbook (Gray 1918).

Whilst capturing the development of the palate in human embryos by means of serial sections, Virginia Diewert was fortunate to have also captured the development of the nasal septum (Diewert 1983). The literature since then has not been fruitful in identifying earlier stages of nasal septum development. Though from Virginia Diewert's work, it is known that at approximately 7 weeks in human embryonic development, the nasal septum is one midline organ that is located within the frontonasal process (Figure 5 A) (Diewert 1983). After the palatal shelves rise horizontally in order to fuse at the midline, the nasal septum will subsequently fuse with the palatal shelves (Figure 5 B, C) (Diewert 1983). The nasal septum should ideally be located within the midline of the nose and the face, but very commonly nasal septum dysmorphologies arise. By understanding the earlier morphogenic processes of the nasal septum, we can begin to identify its role in facial growth. Ideally, we could use the information to begin to attribute its role in normal morphogenesis, but to also identify its role in abnormal morphogenesis, such as orofacial clefting.

Nasal dysmorphologies are commonly associated with orofacial clefting. In unilateral clefting, it is common for the nose to become weakened and collapse on the side of the cleft site. In addition, the nasal septum can become deviated to the non-cleft side due to the pull of the orbicularis oris muscle and premaxillary segment. Interestingly, in cases of midline clefting, the nose itself can become split or bifid in addition to midline lip and palatal clefting. When this occurs, the nasal septum becomes bifurcated into two independent septal structures rather than one midline structure. This absence and/or lateral displacement of the midline bony structures then poses as a challenge to clinicians, as the main goals of orofacial surgery includes restoring symmetry and function to the face.

As the literature regarding nasal septum development is lacking, an in-depth knowledge of nasal septum morphogenesis will aid clinicians in understanding how the anomaly arose when

evaluating a patient with a nasal septal dysmorphology. This information would then aid the clinician to better categorize the dysmorphologies and to design the best treatment plan for the patient. Additionally, as we begin to understand how the nasal septum develops, we can also begin to make hypothesis as to how the nasal septum impacts the growth and development of the surrounding facial structures. In extreme nasal dysmorphology cases, we could then relay to the patient's family how surgery versus no surgery would impact their surrounding chondrocranial growth. In addition, understanding the timing of nasal septum development will also allow surgeons to plan their surgeries so that facial growth will not be affected. Ideally, clinicians could use their knowledge of very early nasal septum morphogenesis to restore symmetry to patients.

1.4 FRONTONASAL ECTODERMAL ZONE

Cranial morphogenesis is composed of incredibly complex processes which regulate both morphogenetic and molecular mechanisms to establish a blueprint early on during embryogenesis. A copious amount of signaling processes that are differential for individual tissue types at specified developmental stages are essential for precise patterning of the craniofacial prominences. The interactions amongst many shared signaling pathways within a defined region will ultimately contribute to the development of the head and neck.

Morphogenesis of the midface relies very specifically upon signaling interactions amongst the neural crest cells, surface ectoderm, and the forebrain. It has been previously shown that gene expression within the surface ectoderm can be regulated from signals from neural crest cells and the brain (Marcucio et al. 2005; Schneider and Helms 2003). In 2003, Diane Hu, Ralph Marcucio, and Jill Helms collectively identified the frontonasal ectodermal zone (FEZ), a region of epithelium in the chicken and mouse frontonasal process (Hu and Marcucio 2009; Hu et al. 2003). The FEZ is responsible for normal growth and patterning of the frontonasal prominence and subsequent upper jaw through ectodermal domains of Hedgehog (HH) and Fibroblast growth factor (FGF) expression (Hu and Marcucio 2009; Hu et al. 2003). Early signaling from the forebrain has been found to regulate expression domains in the FEZ (Chong et al. 2012). In addition to signaling, the FEZ is responsible for dorso-ventral polarity and promixo-distal extension of the upper jaw (Hu et al. 2003).

HH signaling is an essential signaling pathway that is involved in many aspects of development, including craniofacial morphogenesis. The twelve-pass transmembrane protein, Patched (Ptc) is a receptor for HH ligands (Marigo et al. 1996a; Stone et al. 1996). In the absence of HH ligands, Ptc inhibits smoothened (Smo), a seven pass-transmembrane protein, by preventing

its accumulation within cilia (Rohatgi et al. 2007). When a HH ligand binds to Ptc, Smo is released allowing the zinc finger transcription factors, Glioma-associated (Gli), to enter the nucleus and regulate gene expression (Kinzler et al. 1987; Lee et al. 1997; Marigo et al. 1996b). Interesting though, HH signaling has a regulatory feedback loop as Ptc is a downstream target of HH signaling (McMahon et al. 2003).

It has been previously found that early disruption of HH signaling can later affect HH expression within the FEZ subsequent facial prominence growth (Marcucio et al. 2005). Through the *Wnt1-Cre;Smo*$^{n/c}$ mice, it was demonstrated that by removing HH signaling responsiveness in the neural crest cells that patterning and growth of the facial primordia is greatly impacted (Jeong et al. 2004). The *Wnt1-Cre;Smo*$^{n/c}$ embryos were normal until e10.5, but thereafter began to exhibit cranial defects within NCC derived skeletal and non-skeletal components (Jeong et al. 2004). In 2010, it was found that the phenotypic severity that results from HH disruption is dependent upon a dose-response level of disruption of HH signaling (Young et al. 2010). Prior to these sets of experiments, Diane Hu and Jill Helms demonstrated that loss or gain of HH has consequential effects on the midfacial morphogenesis (Hu and Helms 1999). Removal of HH expressing ectoderm from the frontonasal prominence at specific stages of development resulted in a loss of Ptc expression, and the development of an orofacial cleft (Hu and Helms 1999). Additionally, even a transient inhibition of HH signaling in the frontonasal process was enough to cause the facial primordia to stop developing, and an orofacial cleft to develop (Hu and Helms 1999). When the investigators alternatively created a gain of HH, the embryos developed hypertelorism and ectopic midline skeletal structures (Hu and Helms 1999).

An additional pathway that surrounds the ectodermal HH domain is the fibroblast growth factor (FGF) pathway. FGF signaling molecules are involved in many aspects of craniofacial

development. FGF ligands bind to the tyrosine receptor kinase FGF receptor (FGFR) proteins to activate an intracellular cascade. Binding of a FGF ligand to the FGFR results in expression of FGF transcription factors, such as; Tbx27, Erm, Pea3, and Pax7 (Firnberg and Neubüser 2002). It has been previously shown that FGF8 regulates Erm expression in the nasal placodes (Firnberg and Neubüser 2002).

FGF signaling is involved in the development of the upper and lower jaws (Macatee et al. 2003; Trumpp et al. 1999), as well as, the olfactory placode (Bailey et al. 2006; Firnberg and Neubüser 2002), and olfactory epithelium (Kawauchi et al. 2005). In 2008 and 2009, Heather Szabo-Rogers showed that FGF signaling is a product of the nasal pits and is required for nasal capsule morphogenesis (Szabo-Rogers et al. 2008; Szabo-Rogers et al. 2009). It was additionally shown that FGF signaling from the upper portion of the nasal pits is responsible for cellular proliferation and survival (Song et al. 2004; Szabo-Rogers et al. 2008). Diane Hu, Ralph Marcucio, and Jill Helms have previously shown that in addition to HH expression, FGF expression within the FEZ is critical for beak growth (Hu et al. 2003). A year later, it was shown that the combination of extended FGF8 expression and increased proliferation in the frontonasal process in ducks contributed to ducks having a wider beak profile than chickens (Wu et al. 2004). Most intriguingly though, it has been shown through $FGF8^{Null/Neo}$ mice that Fgf8 is required for midfacial convergence and polarity in the nasal capsule (Griffin et al. 2013).

It is exceedingly apparent from all the pioneering work done that craniofacial morphogenesis is an extremely complex process that relies upon multiple signaling pathways. We know from the literature that midfacial morphogenesis is dependent upon FGF and HH signaling within the FEZ. We are interested in establishing how FEZ signaling pathways contribute to midfacial convergence of the MNPs.

1.5 DISAPPEARANCE OF THE EPITHELIAL SEAM

The facial prominences are initially composed of a mesenchymal core surrounded by an outer epithelial layer. As the facial prominences begin to proliferate rather rapidly and eventually make contact with one another, the outer epithelium of the facial prominences will form a bilayered epithelial seam. For normal facial development to occur, it is imperative for the epithelial seam to disappear and for the inner mesenchyme to merge and bridge together the facial prominences into one continuous structure. If the mesenchyme is unsuccessful in merging together the facial prominences for any reason, such as a failure of the surrounding epithelium to regress, then an orofacial cleft will very likely occur at that site. Intriguingly though, the exact mechanism for the disappearance of the surrounding epithelia is still unknown, although it probably goes through an epithelial mesenchymal transformation (EMT), apoptosis, and active cell extrusion.

Currently within the literature, the merging mechanisms of the anterior facial prominences that will eventually form the upper lip have been speculated to undergo the same epithelial seam disappearance mechanisms as the palatal shelves. Though remarkably and controversially, there is not one proven mechanism of action, but three proposed cellular mechanisms to explain the regression of the palatal epithelial seam. The proposed mechanisms for palatal epithelial regression include an epithelial to mesenchymal transformation (Fitchett and Hay 1989; Griffith and Hay 1992; Jin and Ding 2006; Martınez-Alvarez et al. 2000; Nawshad et al. 2004; Shuler et al. 1991; Shuler et al. 1992), apoptosis (Cuervo and Covarrubias 2004; Martınez-Alvarez et al. 2000; Mori et al. 1994; Taniguchi et al. 1995), and lateral migration of the epithelial cells (Carette and Ferguson 1992; Kim et al. 2015). Though there is more supporting evidence for the first two models, each theory is compelling and it is intriguing to wonder how this data from the palate will translate to the apicobasal polarized epithelium of the anterior prominences of the midface.

Beginning during embryonic development and lasting throughout the entire lifetime, epithelial plasticity is a vital cellular mechanism involved in embryonic morphogenesis, wound healing, cancer progression, and fibrosis. The plasticity phenotype of epithelial cells allows for the epithelial cells to transition to a mesenchymal cell phenotype (EMT) and back to epithelial phenotype (MET) as first described by Elizabeth Hay (Hay 1995). During EMT, structural epithelial cells that typically serve as protective boundaries via the integrity of their cell to cell interactions through tight junctions, gap junctions, cadherin-based adherhin junctions, desmosomes, and cell-ECM interactions will repress their epithelial characteristics. By doing so, the epithelial cells will acquire mesenchymal characteristics, such as, no defined cell polarity, migratory and invasive properties, and resistance to apoptosis.

Epithelial and mesenchymal cell markers listed below:

β-catenin:

β-catenin is a cytoplasmic plaque protein and transcription factor in the Wnt signaling pathway (Gavert and Ben-Ze'ev 2007). It is involved in the regulation of cell to cell adhesion within epithelial cells by linking the cadherin family receptors to the actin cytoskeleton, and thus forming a catenin-cadherin complex (Gavert and Ben-Ze'ev 2007). β-catenin enhances cell to cell adhesion via adherens junctions when bound to cadherin complexes.

E-cadherin:

E-cadherin is an intercellular adhesion molecule that is expressed by epithelial cells. These calcium dependent single-chain transmembrane glycoproteins are equipped with an extracellular domain, intracellular domain, and transmembrane domain and is responsible for forming key components of adherens junctions between epithelial cells (Mousa 2008; Scher et al. 1993; Takeichi 1990). E-cadherin is linked to the actin cytoskeleton via the cytoplasmic catenin proteins,

cytoplasmic elements, and forms the intracellular adherence junction (Hirano et al. 1987; Kato et al. 2005; Ozawa et al. 1989; Takeichi 1977; 1991).

Na, K ATPase:

Na, K ATPase is an oligomeric transmembrane protein that consists of α, β, and γ subunits that regulates intracellular sodium (Forbush III et al. 1978; Minor et al. 1998). The enzyme consists of a sodium potassium pump that is in the basolateral membrane of epithelial cells and creates a transmembrane sodium gradient across the plasma membrane. Na, K ATPase is involved in the formation of epithelial tight junctions, desmosomes, and epithelial polarity given that it localizes to the basolateral membrane of most epithelial cells (McNeill et al. 1990; Rajasekaran et al. 2001).

Atypical protein kinase C iota (aPKCι):

aPKC is an important component of generating apical cell polarity within epithelial cells (Henrique and Schweisguth 2003). aPKC forms a complex with Par3 and Par6 (Kemphues et al. 1988). The aPKC complex is also important for the formation of tight junctions in epithelial cells (Macara 2004; Ohno 2001). Two isoforms of aPKC exist, aPKCι and aPKC ς.

Vimentin:

Vimentin is a type III intermediate filament cytoskeletal protein that is found within mesenchymal cells. Vimentin is an α-helical rod domain that is flanked by head and tail domains (Eriksson et al. 2009). It is widely used as a mesenchymal marker in cells undergoing an epithelial to mesenchymal transformation (Kalluri and Neilson 2003). An upregulation of vimentin intermediate filaments have been found to play a role in epithelial cell migration, invasiveness, and cell shape (Gilles et al. 1999; Lee et al. 2006; Mendez et al. 2010).

Conversely, the epithelium that forms the bilayer could simply undergo apoptosis. Under this model, once the barrier epithelial cells have undergone cell death, the mesenchymal cells can migrate and link the facial prominences together into one continuous piece of tissue. Apoptotic stain listed below:

TUNEL:

Terminal deoxynucleotidyl transferase (TdT)-mediated dUTP nick end labeling (TUNEL) is an assay used to detect cells undergoing apoptosis (Gavrieli et al. 1992). TdT labels the blunt end breaks in double stranded DNA. Labeled dUTPs are added to 3' hydroxyl located at the ends of the DNA, and can then be identified via histological staining (Negoescu et al. 1996).

1.6 FORWARD GENETIC SCREENING USING ENU MICE

Humans are a complex species that undergo intricate multiplex morphological processes during embryonic development. A developmental malformation of the face can not only produce functional difficulties, but also psychological issues. Approximately one-third of all birth defects are accompanied by some form of craniofacial developmental anomaly (Gorlin et al. 1990). To better understand the developmental etiology of birth defects, such as craniofacial malformations, scientists regularly utilize the mouse as a model organism. Mouse models are indispensable tools for advancing scientific knowledge as they are very often able to recapitulate the etiology of human disease and developmental pathology.

Very often mouse lines are created with a known mutation in mind to further study the etiology of the disease or malformation. Currently, researchers can target specific genes within certain cells, tissues, or globally throughout the entire organism at very specific time points by utilizing tools, such as, the Cre-loxP system. Though, an approach such as the Cre-loxP system is only useful if the researcher has a known gene of interest. It is important to note though, that currently not all developmental disorders can be completely explained. While the field has been very remarkable in identifying a substantial number of genes that are associated with various craniofacial malformations, there are still many that are unknown. A Cre-loxP mice engineering approach would be helpful in further elucidating the known genetic mutation causing the phenotype, but would not be as helpful in identifying novel genes that are causing craniofacial phenotypes to occur.

One unique approach to creating a novel mouse model is to design a forward genetic screen that screens for a specific phenotype rather than the genotype. This type of approach is performed by utilizing a mutagen that can efficiently generate new mutations within the genome. In the 1970s,

scientists began using N-ethyl-N-nitrosurea (ENU) to induce point mutations within the spermatogonial stem cells (Russell et al. 1979). The ENU causes random single base pair mutations by alkylating the nucleic acids (Justice et al. 1999). The most common reported mutations are AT to GC transitions or AT to TA transversions. This new methodology was a breakthrough as the ENU is easy to administer to the mice, titratable to induce a certain number of mutations, and the mutagenized father could be used to create several lines.

There are several methods to screen for ENU induced phenotypes. To screen for recessive mutations, commonly a backcross and/or an intercross breeding schema is used (Li et al. 2015). In the backcross method, female progeny are mated back with the father whom is known to pass the phenotype of interest. In this method, the genotype of the father remains fixed while some embryos of the female carriers will have the phenotype, but embryos of non-carrier females will not exhibit the phenotype. Another method is to use an intercross method (Figure 7). In this method, the progeny are intercrossed together and the embryos are scanned for phenotypes (Figure 7). Though both forms of breeding are successful, it is thought that the number of multiple unlinked loci are reduced when carrying out an intercross methodology relative to the phenotypic contributions from multiple unlinked loci from a backcross methodology. Multiple unlinked loci can also be bred out of the ENU derived mouse line by out breeding to a WT mouse (Figure 8).

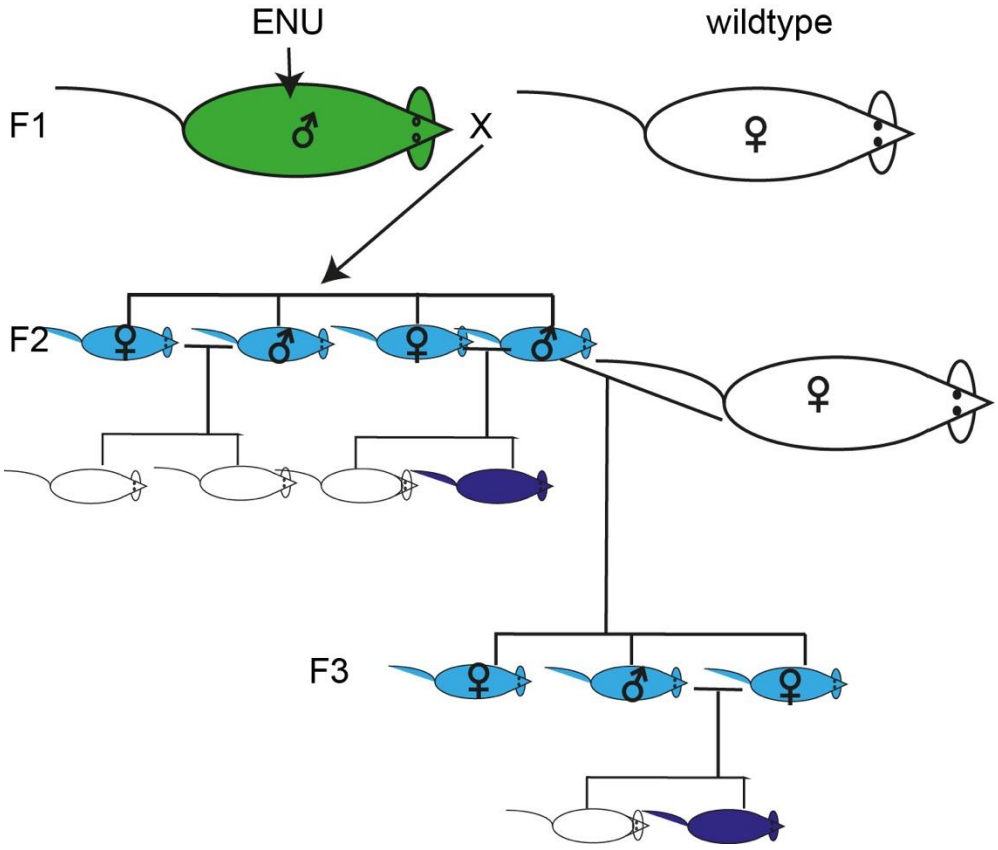

Figure 7. Breeding schema used to screen for a homozygous recessive allele resulting in craniofacial phenotypes.

A founder male mouse (green) (F1) is given an injection of ENU at a concentration to produce 80-90 mutations in the founder male (Li et al. 2015). After recovery, the founder male is bred out to a wildtype female (white), the pups from this breeding will be the F2 generation (light blue). The F2 generation are test-crossed together, and the embryos are phenotyped. The male who produced a phenotypic embryo is then crossed to another wildtype female to produce the F3 generation. The breeding schema of test-crosses and generation production is repeated is until the desired generation.

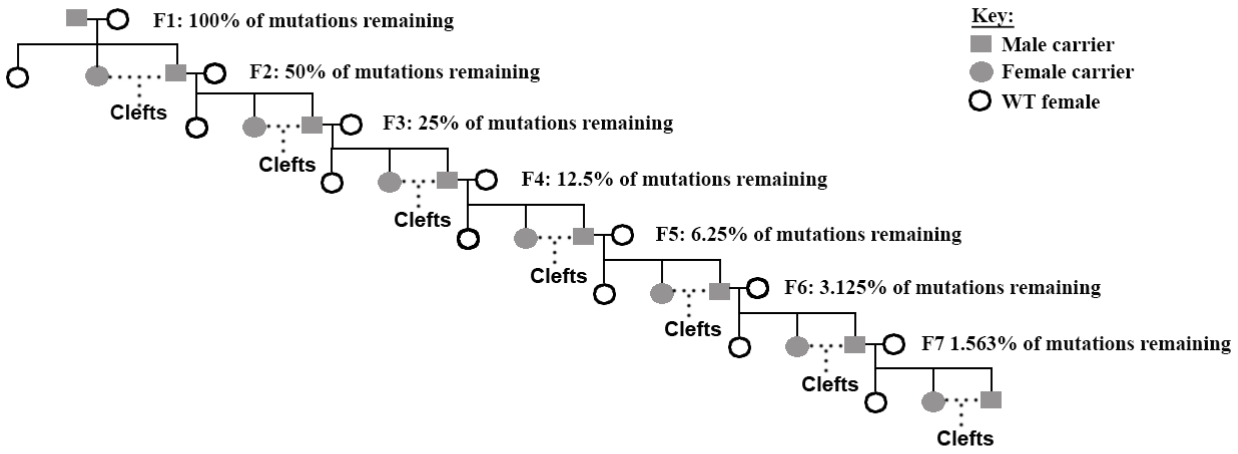

Figure 8. Genetic rationale for the homozygous recessive breeding schema to dilute the number of ENU- induced mutations.

Recessive test-cross schema for identifying the region of interest. At each generation, pups are crossed to each other, and the resulting litter is screened for craniofacial anomalies. The males that transmit the defect are crossed to a wildtype female. The resulting pups are test crossed and then a new generation is bred by crossing the productive male with a wildtype female. By crossing to a wildtype female at each generation, we reduce the number of ENU mutations by half with each cross. By breeding phenotypic productive males to 8 generations, if the founder male was dosed with ENU to create 100 mutations, theoretically there are only be 1 or 2 ENU-induced mutations maintained. Phenotypic pups from the F8 can be whole genome sequenced to identify the causative mutations responsible for the observed phenotype.

2.0 THE ROLE OF *PRICKLE1* IN ANTERIOR MIDFACIAL CONVERGENCE AND SUBSEQUENT OROFACIAL MORPHOGENESIS

2.1 INTRODUCTION

During morphogenesis of the anterior midface, bilaterally paired medial nasal prominences (MNPs) shift from a lateral to a more medial position prior to their subsequent convergence at the midline. Compromised fusion of the MNPs can result in midline clefting that can range dramatically in severity from a simple vermillion notch in the soft tissue to a very wide true cleft of the upper lip, palate, and nose. Midline clefting of the upper lip is a unique subset of orofacial clefting that has not been well characterized clinically nor mechanistically within animal models. The open questions on the development of midfacial clefts likely results from mild cases that are classified within normal levels of variation and do not require medical intervention. Because mild midfacial clefts are described as within normal variation, there prevalence is underreported. Inadequate characterization of this broad-spectrum phenotype could be in part due to a lack of understanding of normal midfacial morphogenesis, and very few animal models whom can adequately recapitulate a midline cleft of the lip phenotype.

The early face is reliant upon large scale interactions, such as facial prominence merging, but also upon more minute scale interactions, such as, cell to cell signaling interactions. The facial prominences are composed of an inner core of mesenchyme made up of neural crest and mesoderm surrounded by an outer epithelial layer. At embryonic day (E)10.5 in mice, the mesenchyme within the maxillary prominences begins to rapidly proliferate, thus pushing the MNPs towards the midline of the face (Jiang et al. 2006). By E11.5, rapid growth will continue to drive the nasal pits

and MNPs towards the midline. Temporospatial expression of FGF and HH signaling molecules within the frontonasal ectodermal zone (FEZ) which is located within the MNPs have been implicated in regulating proximal-distal and dorsal-ventral growth of the upper jaw (Hu and Marcucio 2009; Hu et al. 2003). A final critical step to midfacial convergence is regression of the outer epithelial seam surrounding the facial processes allowing the corresponding mesenchyme to join (Jiang et al. 2006).

Currently within the literature, the merging mechanisms of the anterior facial prominences has been speculated to undergo the same epithelial seam regression mechanisms as the palatal shelves (Cox 2004; Gaare and Langman 1977; Jiang et al. 2006; Sun et al. 2000). Though remarkably and controversially, there is not one proven mechanism of action, but three proposed cellular mechanisms to explain the regression of the palatal epithelial seam. The proposed mechanisms for palatal epithelial regression include an epithelial to mesenchymal transformation (Fitchett and Hay 1989; Griffith and Hay 1992; Jin and Ding 2006; Martınez-Alvarez et al. 2000; Nawshad et al. 2004; Shuler et al. 1991; Shuler et al. 1992), apoptosis (Cuervo and Covarrubias 2004; Martınez-Alvarez et al. 2000; Mori et al. 1994; Taniguchi et al. 1995), and lateral migration of the epithelial cells, and active cell extrusion (Carette and Ferguson 1992; Kim et al. 2015). Though the evidence supporting each hypothesis is compelling, an open question in the field is whether these principles from palatal fusion will translate to the fusion of the apical basal polarized epithelium of the anterior prominences of the midface.

The *Prickle1*$^{Bj/Bj}$ embryos develop a midline notch resulting in a soft tissue cleft of the lip. The *Prickle1*^{Beetlejuice} allele is a missense mutation in *Prickle1* resulting from ENU mutagenesis. The *Prickle1*^{Bj} allele encodes a C161F mutation. The mutation occurs in a cysteine knot within the first LIM domain rendering the protein nonfunctional (Gibbs et al. 2016). *Prickle1* is a core

component of the non-canonical Wnt/Planar cell polarity pathway (Wnt/PCP) (Gibbs et al. 2016; Gubb et al. 1999; Katoh and Katoh 2003; Liu et al. 2014; Tree et al. 2002; Zallen 2007). It has been previously shown that *Prickle1*$^{Bj/Bj}$ embryos exhibit ciliary defects, compromised polarized cell morphology, as well as, difficulty with directional cell migration (Gibbs et al. 2016). Intriguingly, *Prickle1* has previously been identified as a causative variant in secondary palatal clefting in mice, as well as, single nucleotide polymorphisms in *Prickle1* are associated with orofacial clefting in human populations (Yang et al. 2014).

We hypothesize that given *Prickle1*'s prominent role within the Wnt/PCP pathway that epithelial cells of the MNPs will not undergo successful EMT due to faulty cell polarity and cell signaling.

2.2 METHODS

Mouse lines and animal husbandry:

Founder *Prickle1*$^{Bj/+}$ animals were obtained from Dr. Cecelia W. Y. Lo at the University of Pittsburgh Department of Developmental Biology and maintained on a C57/BL6J background (Gibbs et al. 2016). The *Prickle1*^{Bj} mouse line was genotyped using an Invitrogen custom SNP assay with Taqman Genotyping MasterMix and read on a StepOnePlus machine. Timed matings were performed for embryo collections at e10.5, e11.5, e15.5, and e17.5. Presence of a plug was designated as day (e) 0.5. For BrdU labeling, 10 mg/kg of BrdU in sterile PBS was injected intraperitoneally one hour prior to collection. Pregnant dams were euthanized via CO2 inhalation followed by cervical dislocation, and embryos were harvested via C-section. Animal care and use was conducted in accordance animal protocols approved by the Institutional Animal Care and Use Committee of the University of Pittsburgh.

Skeletal preparations:

Heads of e15.5, e17.5 and P0 *Beetlejuice* animals were fixed in 95% ethanol and stained with Alizarin Red and Alcian Blue. Samples were clearing in KOH:Glycerol solution followed by storage and imaging in a 1:1 glycerol: ethanol solution.

In situ hybridization:

Gene expression patterns in *Prickle1*$^{Bj/Bj}$ littermates and WT embryos were evaluated either via 10 µm paraffin sections or wholemount using standard protocols (Szabo-Rogers et al. 2016). RNA probes were Digoxigenin labeled and detected with BM Purple. RNA probes used: Prickle1, Ptch1, Gli1, Erm1. At least 3 littermates were analyzed per each RNA probe.

Immunohistochemistry:

GD e10.5 and e11.5 *Prickle1*$^{Bj/Bj}$ littermates were fixed in 4% PFA, stored in 70% ethanol, and embedded in paraffin wax. Embryos were sectioned frontally 10 µm thick. Microwave antigen retrieval was conducted using Sodium Citrate Buffer. Sections were blocked in 5% goat serum in 1% Triton X-100 for 1 hour prior to being incubated overnight incubation of the primary antibodies at 4°C. Primary antibodies used: P-Histone H3 (S10) produced in rabbit, Cell Signaling #9701S; Purified mouse Anti-β-catenin 1:100, BD Biosciences #610153; Purified mouse Anti- E-cadherin, BD Biosciences #61018; Purified mouse Anti-Protein Kinase C (PKCι), BD Biosciences # 610175; Monoclonal Anti-Vimentin antibody produced in mouse, Sigma #V2258; Rabbit monoclonal Anti-Sodium Potassium ATPase, Abcam #ab76020. Secondary antibodies used: Biotinylated goat anti-rabbit IgG – Included in Vectastain ABC-HRP Kit; Alexaflour 488 rabbit anti-mouse, Invitrogen A11059; Alexaflour 488 donkey anti-rabbit, Invitrogen A21206. Samples were mounted with Prolong-Gold with Dapi (Invitrogen). PHH3 positive cells were detected using ImmPACT DAB. At least 3 littermates were analyzed per each antibody.

Proliferation and cell death studies:

BrdU samples were pretreated with Exonuclease III, Dpn1, and Proteinase K. RPN202 primary antibody (GE Healthcare Life Sciences) and Alexa Fluor 488 rabbit anti-mouse secondary antibody were used to detect BrdU activity. Samples were mounted with Prolong-Gold with Dapi (Invitrogen). ApopTag Plus Peroxidase *In Situ* Apoptosis Detection Kit was used to evaluated apoptosis (Sigma). TUNEL positive cells were detected using ImmPACT DAB.

Cell counting:

BrdU positive cells and DAPI stained nuclei were counted in similar anatomical regions in 2 areas in the MNP mesenchyme (150x150 pixels) and 1 epithelial (150 pixels) region in E10.5 embryos. BrdU positive cells and DAPI stained nuclei were counted in similar anatomical regions in 2 areas in the MNP mesenchyme (125x125 pixels) and 2 epithelial (125 pixels) regions in E11.5 embryos. A ratio was calculated from BrdU positive cells and DAPI stained cells via positive BrdU cells/all cells. TUNEL (200x200 pixels) and PHH3 (175x175 pixels) positive cells were counted in the same regions on near-adjacent sections and plotted in a scatterplot. A χ-squared test was used to evaluate PHH3 and TUNEL-positive cells between *Prickle1*$^{Bj/Bj}$ littermates and *Prickle1*$^{+/+}$ ($p<0.05$). A paired Students t-test was used to compare BrdU labelling between midfacial clefted and control embryos ($P<0.05$).

Imaging:

Whole mount images were captured on a Leica M165FC dissecting microscope using a DFC 450 camera and Leica LAS software. Histological images were captured on a Zeiss AXIO microscope with an AxioCam MRc 35 camera and Zen software. Fluorescence images were obtained at the Center for Biological Imaging at the University of Pittsburgh on an Olympus Fluoview 1000 confocal and analyzed using NIS software and presented as deconvolved maximal projection stacks.

2.3 RESULTS

2.3.1 *Prickle1*$^{Bj/Bj}$ develop a midline soft tissue cleft of the lip.

The craniofacial bones of *Prickle1*$^{Bj/Bj}$ embryos develop abnormally. Though all present, the bones are shortened and wider, and consequently lead to secondary craniofacial malformations such as; microcephaly, increased cranial base width, and orofacial clefting (Figure 9). As SNPs near PRICKLE1 have been implicated in human orofacial clefting, we focused our studies on the medial cleft lip phenotype recovered in *Prickle1*$^{Bj/Bj}$ embryos. *Prickle1*$^{Bj/Bj}$ embryos have a 100% (n=50/50) prevalence rate of developing a medial cleft lip (Figure 9 E). The bony premaxilla of *Prickle1*$^{Bj/Bj}$ embryos is not clefted at E15.5 through p0, thus indicating that the midline cleft of *Prickle1*$^{Bj/Bj}$ embryos is a median soft tissue cleft of the lip (Figure 9 E, F, G, H). Additionally, half of the *Prickle1*$^{Bj/Bj}$ embryos develop a cleft palate (Figure 9 M, N). Reflecting the absence of fusion in the secondary palate, the palatal process of the maxilla and the palatal process of the palatine do not approximate each other in the midline and expose the underlying vomer and presphenoid (Figure 9 J, K, M, N).

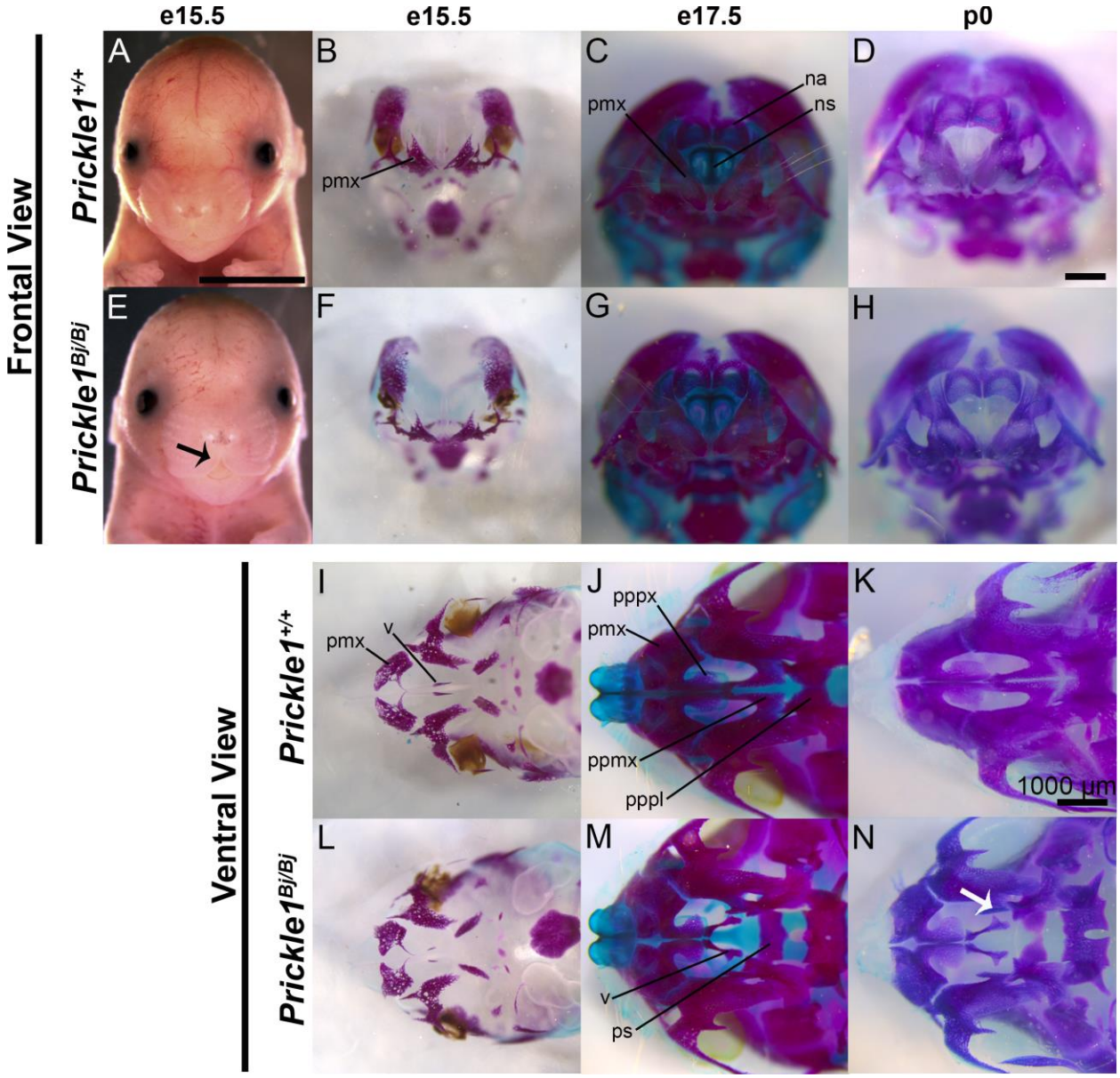
e15.5
e15.5
e17.5
p0
Frontal View
Prickle1+/+
Prickle1Bj/Bj
A
B
C
D
E
F
G
H
pmx
na
ns
Ventral View
I
J
K
L
M
N
v
pppx
ppmx
pppl
ps
1000 µm

Figure 9. *Prickle1*$^{Bj/Bj}$ embryos develop a soft tissue midline cleft lip and secondary palate.

Craniofacial morphology of *Prickle1*$^{Bj/Bj}$ (**E-H, L-N**) and their littermate controls (**A-D, I-K**) during fetal stages. (**A, E**) External morphology of the control and *Prickle1*$^{Bj/Bj}$. (**B-D, F-H, I-N**) Alcian blue and alizarin red stained embryos showing the cartilage and bone morphology respectively. (**A-H**) Frontal view, (**I-N**) ventral view of palate with the mandible removed. (**A, E**) *Prickle1*$^{Bj/Bj}$ develop a midline soft tissue cleft lip as evidenced by the notch below the nostrils (**E**, black arrow). (**B-D**, **F-H**) Frontal view of stained sections from E15.5, E17.5, and P0. In both the littermates and *Prickle1*$^{Bj/Bj}$, the paired premaxilla are the same distance apart, and have similar morphology. Suggesting the notch of the *Prickle1*$^{Bj/Bj}$ upper lip only develops from defects in the soft tissue and not the underlying bone. (**I-N**) The *Prickle1*$^{Bj/Bj}$ secondary palate cleft is apparent between the palatal processes of the maxilla and palatal processes of the palatine bone exposing the underlying vomer and presphenoid (white arrow). All scale bars are 1000 μm. Abbreviations: pmx, premaxilla; na, nasal; ns, nasal septum; v, vomer; pppx, palatal process of premaxilla; ppmx, palatal process of maxilla, pppl, palatal process of palatine; ps, presphenoid.

2.3.2 *Prickle1* is normally expressed in the MNPs prior to lip fusion

To better understand the role of *Prickle1* in the development of a medial cleft lip, we next inquired if and where *Prickle1* is normally expressed in the facial prominences of normal embryos. At E9.5 in WT embryos, *Prickle1* is expressed ubiquitously in the frontonasal prominence, as well as, the maxillary prominence and the mandibular prominence (Figure 10 A, B). By E10.5, one day prior to facial prominence fusion, *Prickle1* expression becomes more restricted within the facial prominences of WT embryos. *Prickle1* is expressed in the zone of fusion where the MNP, lateral nasal prominence, and maxillary prominences join for lip development (Figure 10 C). *Prickle1* is also located medially on the anterior tips of the mandibular prominence (Figure 10 C, D). Most intriguingly though, *Prickle1* is located at the inferior medial edge of the MNPs one day prior to midline merging of the MNPs (Figure 10 D).

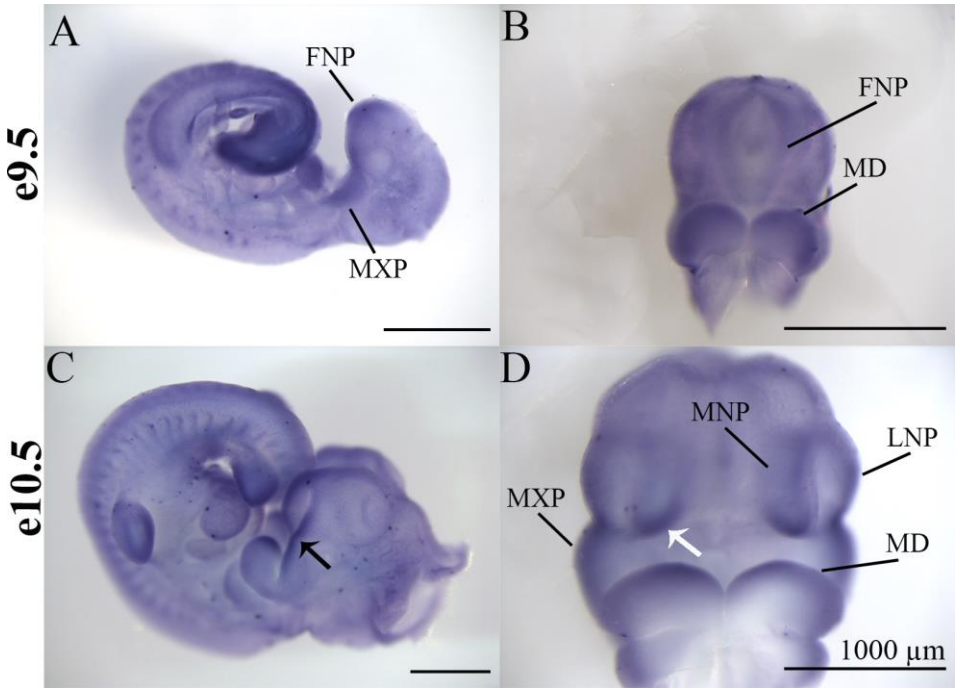

Figure 10. *Prickle1* localizes to the facial prominences in wildtype embryos.

In situ hybridization to *Prickle1* in wildtype embryos at E9.5 (**A, B**) and E10.5 (**B, C**). (A) *Prickle1* is expressed in the dorsal root ganglia, the forelimb bud, the tail, and the head at E9.5. (B) *Prickle1* is ubiquitously expressed in the frontonasal prominence, maxillary prominence, as well as, the mandibular prominence. (C) *Prickle1* is expressed in the dorsal root ganglion, the fore and hind limbs, the heart, and the head. (D) *Prickle1* is localized to the inferior medial edge of the medial nasal prominences (white arrow). *Prickle1* is also localized to the edges of the lateral nasal processes, maxillary processes, and the mandible at e10.5 in WT mice. *Prickle1* is expressed at the zone of fusion where the maxillary, medial nasal, and lateral nasal prominences meet (black arrow). Scale bars are 1000 µm. Abbreviations: FNP, frontonasal prominence; MXP, maxillary prominence; MD, mandibular prominence; LNP, lateral nasal prominence; MNP, medial nasal prominence.

2.3.3 *Prickle1*$^{Bj/Bj}$ FEZ patterning is disrupted during medial lip fusion.

The signaling pathways, Hedgehog (HH) and Fibroblast growth factor (FGF), are found within the frontonasal ectodermal zone (FEZ), and have been demonstrated to be essential for normal patterning and proximal distal outgrowth of the upper face. The level of HH signaling is evaluated by the expression of the HH receptor *Patched1* (*Ptc1*), and the transcription factor *Glioma-associated oncogene homolog 1* (*Gli1*). We evaluated FEZ patterning during (E10.5, E11.5) medial MNP fusion. We found that both HH and FGF signaling are down-regulated in the MNPs before and after MNP fusion (Figure 11 and 12). At E10.5, *Ptc1* expression is relatively unchanged amongst genotypes (Figure 11 A, B). *Ptc1* is expressed in the mesenchyme adjacent to the oral ectoderm at E10.5 (Figure 11 A, B). Though the *Ptc1* expression domain is similar at E10.5, its expression level fails to be maintained in *Prickle1*$^{Bj/Bj}$ MNP at E11.5 (Figure 11 C, D). *Gli1* expression is present adjacent to the brain in *Prickle1*$^{Bj/Bj}$ E10.5 embryos, but lacking in the mesenchyme adjacent to the nasal pit and within the medial edge epithelium (Figure 11 E, F). By E11.5, *Gli1* expression has initiated in the *Prickle1*$^{Bj/Bj}$ embryos, but has decreased expression in the mesenchyme of *Prickle1*$^{Bj/Bj}$ embryos in comparison to the littermate control (Figure 11 G, H).

The FGF pathway is also decreased in *Prickle1*$^{Bj/Bj}$ embryos. At E10.5, *Erm1* expression is decreased in the inferior nasal pit epithelium and within the medial edge mesenchyme (Figure 12 A, B). *Erm1* expression remains decreased in the nasal pit epithelium and mesenchyme surrounding the nasal pit in the *Prickle1*$^{Bj/Bj}$ mutants versus the littermate controls at E11.5 (Figure 12 C, D).

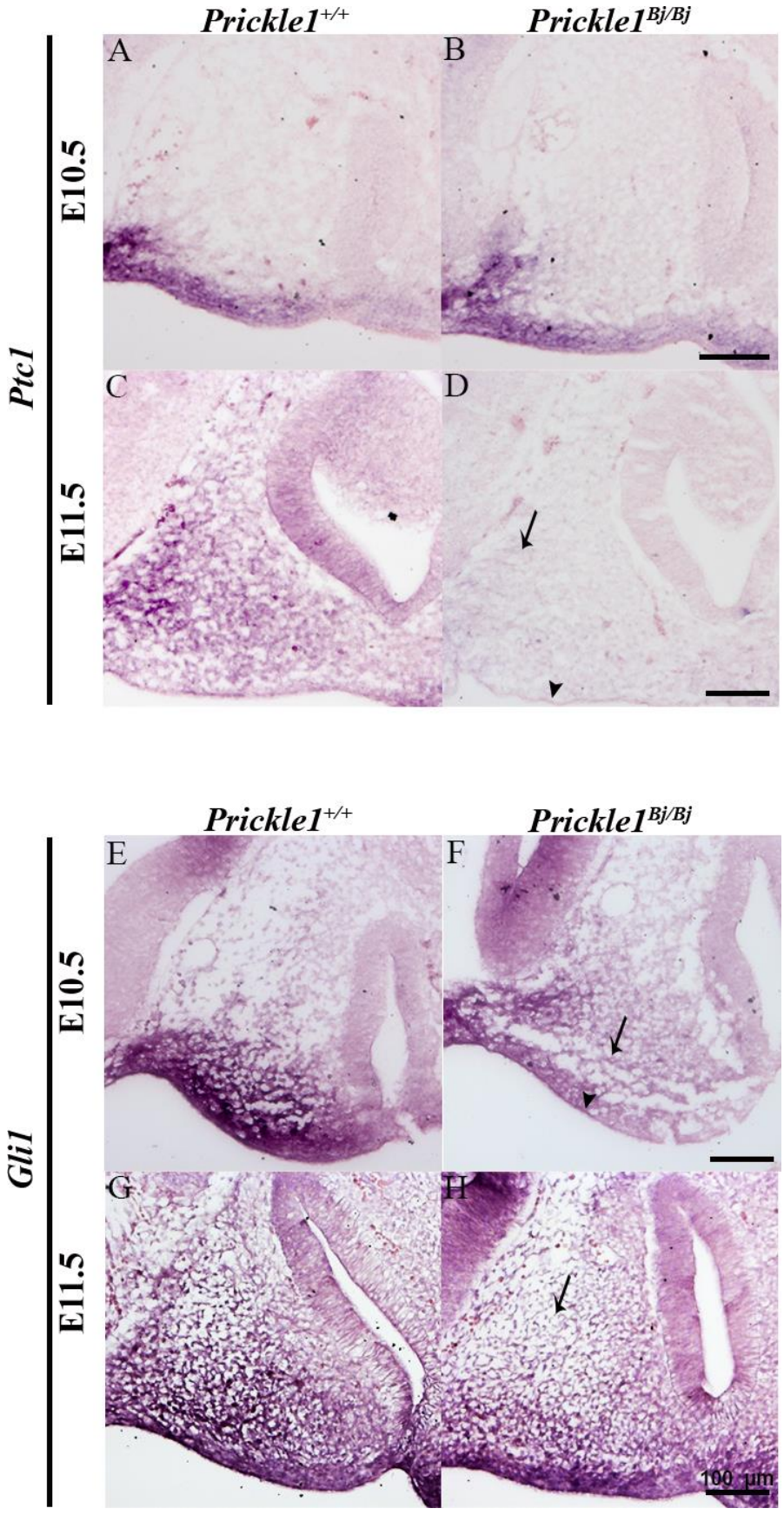
Prickle1+/+
Prickle1Bj/Bj
Ptc1
E10.5
E11.5
A
B
C
D
Prickle1+/+
Prickle1Bj/Bj
Gli1
E10.5
E11.5
E
F
G
H
100 µm

Figure 11. HH signaling is decreased in the *Prickle1*$^{Bj/Bj}$ FEZ.

Section *in situ* hybridization to HH signaling reporters, (**A-D**) *Ptc1* and (**E-H**) *Gli1*, at E10.5 and E11.5. (**A-B**) At E10.5, *Ptc1* expression is found in the mesenchyme adjacent to the oral ectoderm, its domain and expression level is similar between genotypes. (**C-D**) At E11.5, *Ptc1* expression fails to shift to the medial edge epithelium (arrow head) and mesenchyme (arrow) of *Prickle1*$^{Bj/Bj}$ embryos. (**E-F**) *Gli1* is decreased within the mesenchyme (arrow) and epithelium (arrow head) of *Prickle1*$^{Bj/Bj}$ embryos at e10.5. (**G-H**) At E11.5, *Gli1* expression is similar in the epithelium, but is decreased in the mesenchyme (arrow) of *Prickle1*$^{Bj/Bj}$ embryos**.** Scale bars are 100 μm.

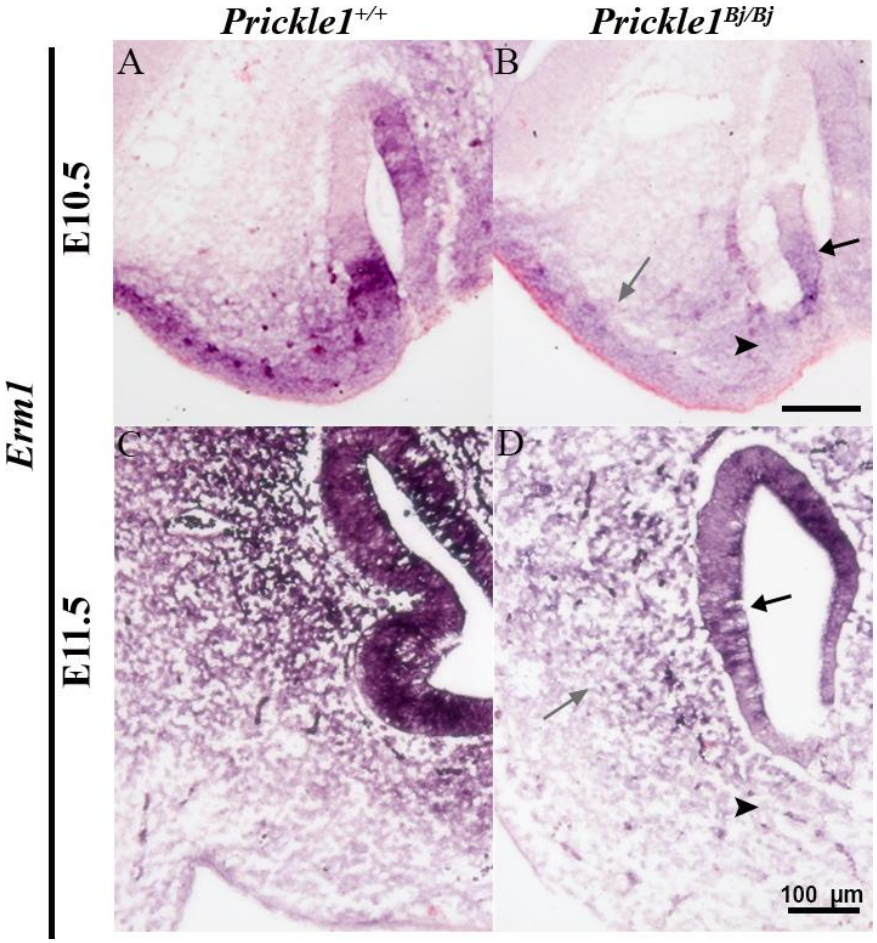
Prickle1+/+
Prickle1Bj/Bj
Erm1
E10.5
E11.5
A
B
C
D
100 µm

Figure 12. FGF signaling is decreased in the *Prickle1*$^{Bj/Bj}$ FEZ.

Section *in situ* hybridization to FGF signaling reporter, *Erm1* at (**A-B**) E10.5 and(**C-D**) E11.5. (**B, D**) *Erm1* expression is decreased in the most inferior tip of the MNP mesenchyme (arrow head) both at E10.5 and E11.5. (**B**) Erm1 expression is decreased in the inferior region of the medial edge mesenchyme (grey arrow) at E10.5 in *Prickle1*$^{Bj/Bj}$ embryos. (**D**) *Erm1* expression is decreased in the mesenchyme (grey arrow) medial to the nasal pit epithelium at E11.5. (**B, D**) In addition, *Erm1* is also decreased in the nasal pit epithelium (black arrow) at E10.5 and E11.5 in *Prickle1*$^{Bj/Bj}$ embryos. Scale bars are 100 µm.

2.3.4 *Prickle1*$^{Bj/Bj}$ MEE cells fail to undergo an epithelial to mesenchymal transformation.

Due to *Prickle1's* role in the Wnt/PCP pathway, and past reports describing polarity defects within the *Prickle1*^{BJ} mouse line (Gibbs et al. 2016), I hypothesized that the midfacial notch arises through defects in polarity in the merging MNPs. We observed that the premaxillary bones were unaffected (Figure 9), and the epithelial layers near the merging MNPs had defects in FGF and HH signaling (Figure 11, 12). I hypothesized that the midfacial notch results from defects in the MNP medial edge epithelial (MEE) layer. To test this hypothesis, we tested the polarity of the MNP MEE with PKCι, and the balance of EMT in the MEE cells by evaluating the epithelial markers β-catenin, E-cadherin, and Na, K-ATPase, as well as, the mesenchymal marker vimentin. We investigated whether *Prickle1*$^{Bj/Bj}$ embryos have epithelial defects amongst their MNP MEE cells before (E10.5) and after medial lip fusion (E11.5).

Prickle1$^{Bj/Bj}$ embryos have increased β-catenin between the epithelial cells at E10.5 and E11.5 (Figure 13 B, D). Additionally, Na, K-ATPase, an essential component of epithelial tight junctions is largely up-regulated in the MEE of the MNPs at E10.5 and E11.5 (Figure13 F, H). A further inquiry into *Prickle1*$^{Bj/Bj}$ MEE cells revealed that levels of epithelial junction marker, E-cadherin, is increased in *Prickle1*$^{Bj/Bj}$ embryos at E10.5 (Figure 14 B), as well as, E11.5 (Figure 14 D). Intriguingly though, the *Prickle1*$^{+/+}$ embryos lose their epithelial marker, E-cadherin, within their MEE cells during medial lip fusion (E11.5) (Figure 14 A, C). *Prickle1*$^{Bj/Bj}$ MNP MEE cells have decreased cell polarity as visualized by a decrease of PKC at the apical surface of the epithelial cells at both E10.5 (Figure 14 F) and E11.5 (Figure 14 H).

At E10.5 in *Prickle1*$^{+/+}$ embryos, the mesenchymal marker, vimentin, is present with the MNP MEE cells (Figure 15 A). Vimentin levels increase within the MNP MEE of *Prickle1*$^{+/+}$

embryos at E11.5 (Figure 15 C). Intriguingly, *Prickle1*$^{Bj/Bj}$ MNP MEE cells obtain levels of vimentin comparable to *Prickle1*$^{+/+}$ embryos at E10.5 (Figure 15 B). Though, *Prickle1*$^{Bj/Bj}$ MNP MEE cells are unable to produce mesenchymal markers at the same level as *Prickle1*$^{+/+}$ embryos at E11.5 (Figure 15 D).

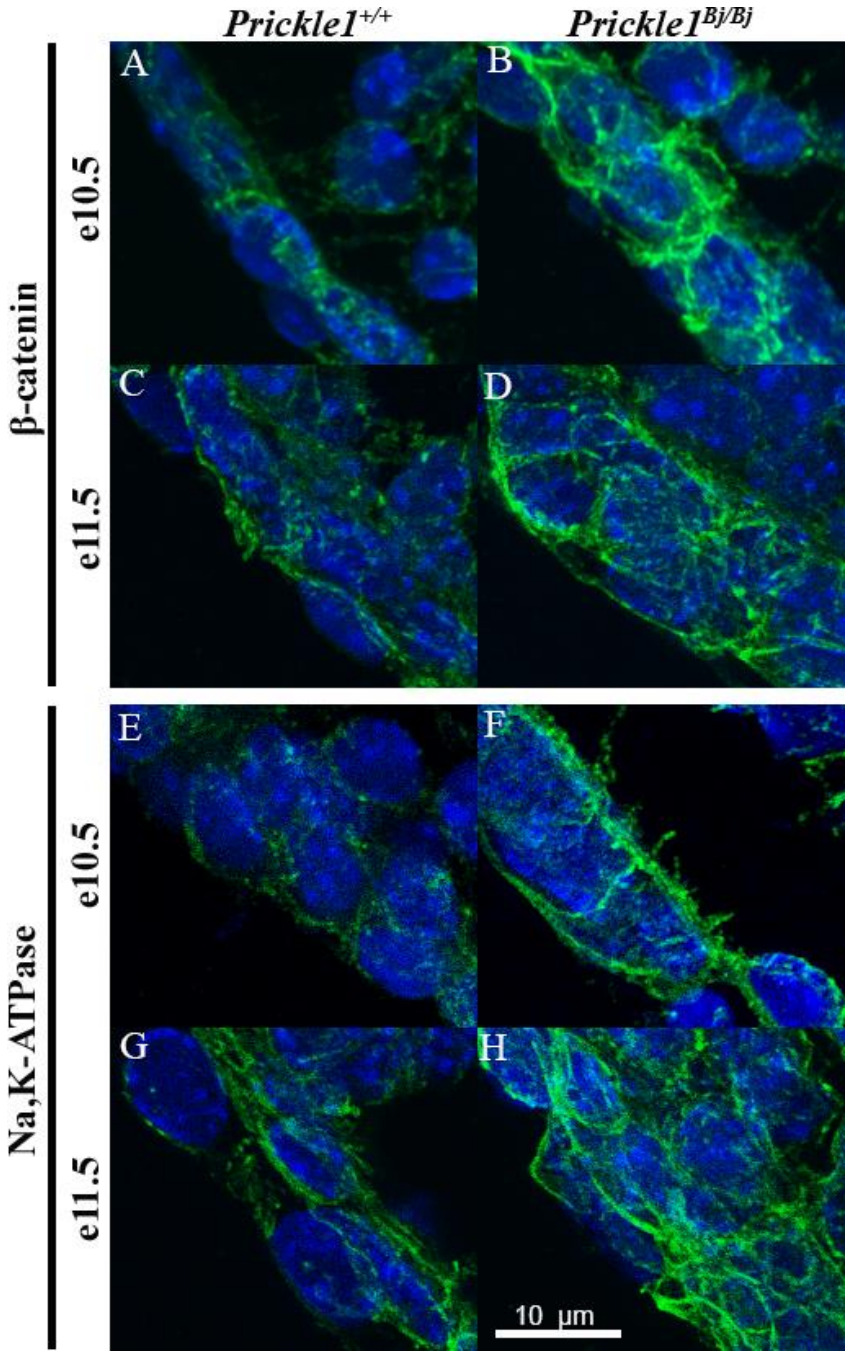
Prickle1+/+
Prickle1Bj/Bj
β-catenin
e10.5
e11.5
Na,K-ATPase
e10.5
e11.5
A
B
C
D
E
F
G
H
10 µm

Figure 13. *Prickle1*$^{Bj/Bj}$ have increased junctions within medial edge epithelium.

Maximal projection images showing immunofluorescent staining to β-catenin and Na, K-ATPase in the MNP MEE at E10.5 (**A-B, E-F**), and E11.5 (**C-D, G-H**). (**A-D**) *Prickle1*$^{Bj/Bj}$ MNP MEE have an increased amount β-catenin at E10.5 and E11.5 in comparison to their respective littermate controls. (**E-H**) Na, K-ATPase is increased in *Prickle1*$^{Bj/Bj}$ MNP MEE at E10.5 and E11.5. Scale bar is 10 μm.

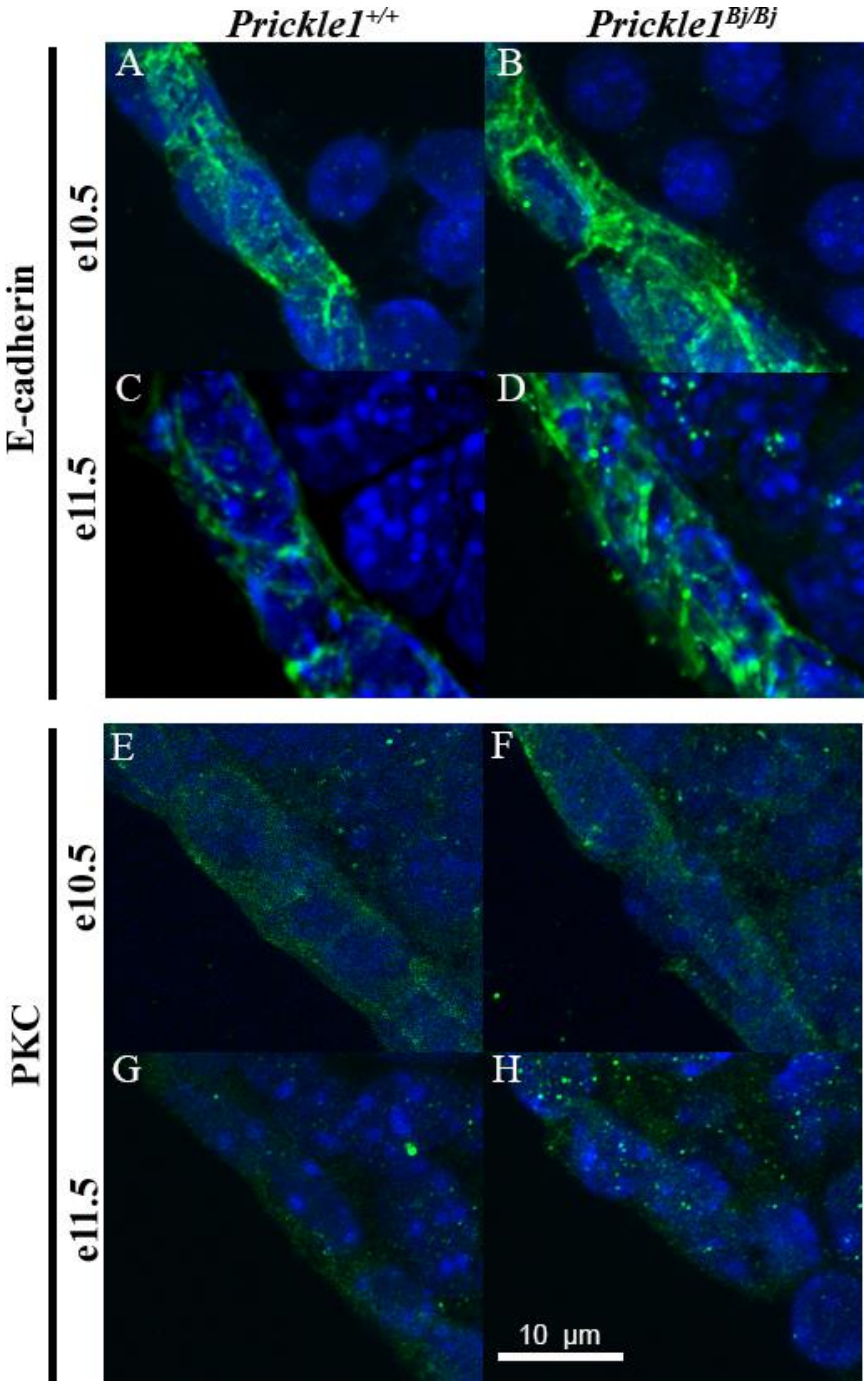
Prickle1+/+
Prickle1Bj/Bj
E-cadherin
e10.5
e11.5
A
B
C
D
PKC
e10.5
e11.5
E
F
G
H
10 µm

Figure 14. *Prickle1*$^{Bj/Bj}$ have increased junctions and decreased cell polarity in MNP medial edge epithelial cells.

Confocal stacks showing immunofluorescent staining to E-cadherin and PKC in the MNP medial edge epithelium at E10.5 (**A-B, E-F**), and E11.5 (**C-D, G-H**). (**A-D**) There is increased E-cadherin in *Prickle1*$^{Bj/Bj}$ MNP medial edge epithelial cells at E10.5 and E11.5 in comparison to their respective littermate controls. (**E-H**) *Prickle1*$^{Bj/Bj}$ embryos have decreased PKC around the apical surface of the MNP medial edge epithelium at E10.5 and E11.5. Scale bar is 10 μm.

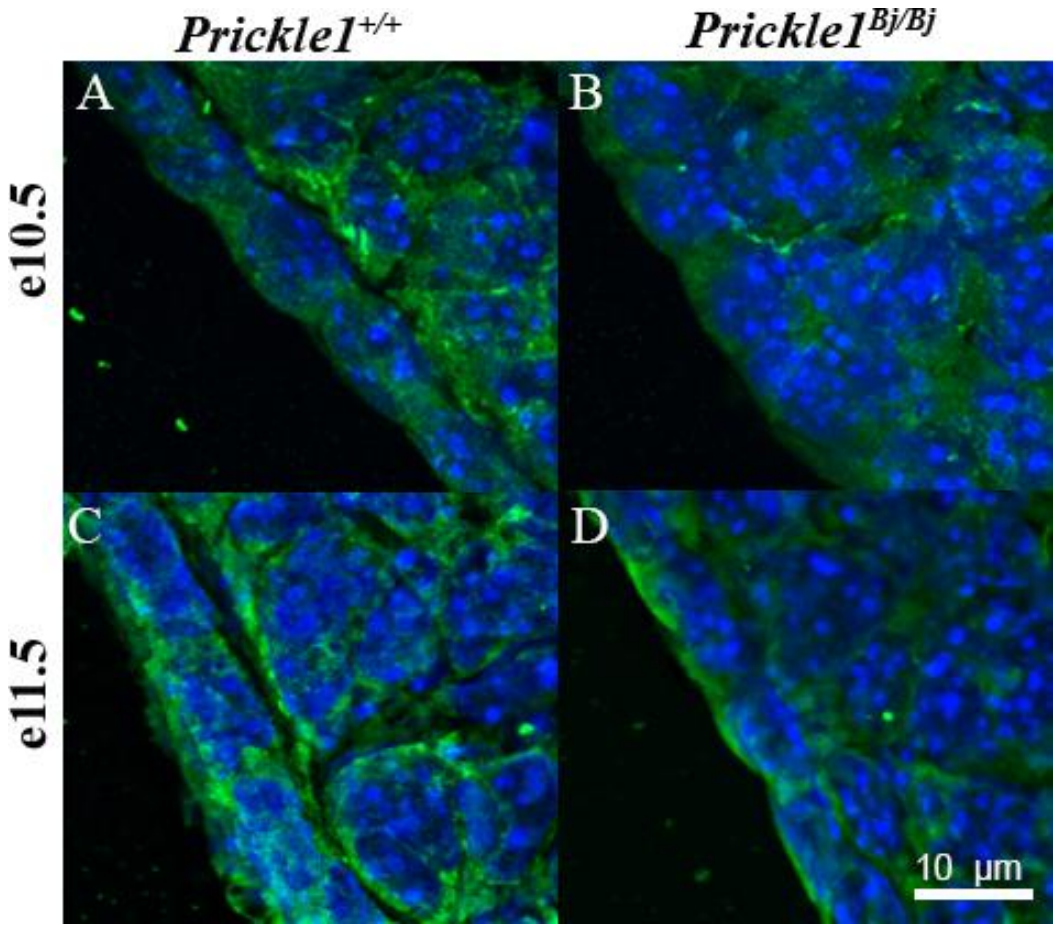
Prickle1+/+
Prickle1Bj/Bj
A
B
C
D
e10.5
e11.5
10 µm

Figure 15. *Prickle1*$^{Bj/Bj}$ medial edge epithelial cells fail to increase mesenchymal levels at E11.5.

Confocal stacks showing immunofluorescent staining to vimentin in the MNP medial edge epithelium at E10.5 (**A, B**) and E11.5 (**C, D**). (**A, B**) *Prickle1*$^{Bj/Bj}$ MNP medial edge epithelial cells can obtain the mesenchymal marker, vimentin at E10.5. (**C, D**) At E11.5, *Prickle1*$^{Bj/Bj}$ MNP medial edge epithelial cells have less vimentin levels. (**A-C**) Vimentin increases in *Prickle1*$^{+/+}$ MNP medial edge epithelial cells from E10.5 to E11.5. Scale bar is 10 μm.

2.3.5 *Prickle1*$^{Bj/Bj}$ embryos have decreased cell proliferation in their MNPs.

Due to the midline cleft present in the *Prickle1*$^{Bj/Bj}$ embryos, we investigated cellular proliferation in the MNPs at E10.5 and E11.5. We tested cellular proliferation in two ways, PHH3 and BrdU (Bromodeoxyuridine). It has been shown that histone H3 is phosphorylated when mitosis is occurring (Hendzel et al. 1997). During the M phase of mitosis, histone H3 is phosphorylated, thus indicating that the cell is undergoing division (Hendzel et al. 1997; Juan et al. 1998). BrdU, a thymidine analog, is incorporated into nuclear DNA during the S phase of replication, and demarcates the cells that are in the S-phase during the BrdU administration. Cells undergoing proliferation were counted in the cranial and caudal mesenchyme at both E10.5 and E11.5 (Figure 16-18 A). At E10.5, proliferating cells were counted in one area of the adjacent epithelium (Figure 16A, Figure 17 A). Two areas in the medial edge epithelium adjacent to the mesenchymal boxes were counted at E11.5 (Figure 16 A, Figure 18 A).

At E10.5, *Prickle1*$^{Bj/Bj}$ embryos have significantly less proliferation in the MNP medial edge epithelium when evaluated by BrdU (Figure 17 B, C). We found there to be less proliferating cells in the MNP medial edge epithelium when evaluated by PHH3, but no significance was found (Figure 16 B, C). No significant differences were found in *Prickle1*$^{Bj/Bj}$ embryos medial edge epithelium at E11.5 when evaluated via BrdU (Figure 18 B, C). Intriguingly though, when evaluating proliferation within the mesenchyme both BrdU and PHH3 revealed relatively similar numbers of cells undergoing the M and S phase of proliferation in the *Prickle1*$^{+/+}$ and *Prickle1*$^{Bj/Bj}$ embryos.

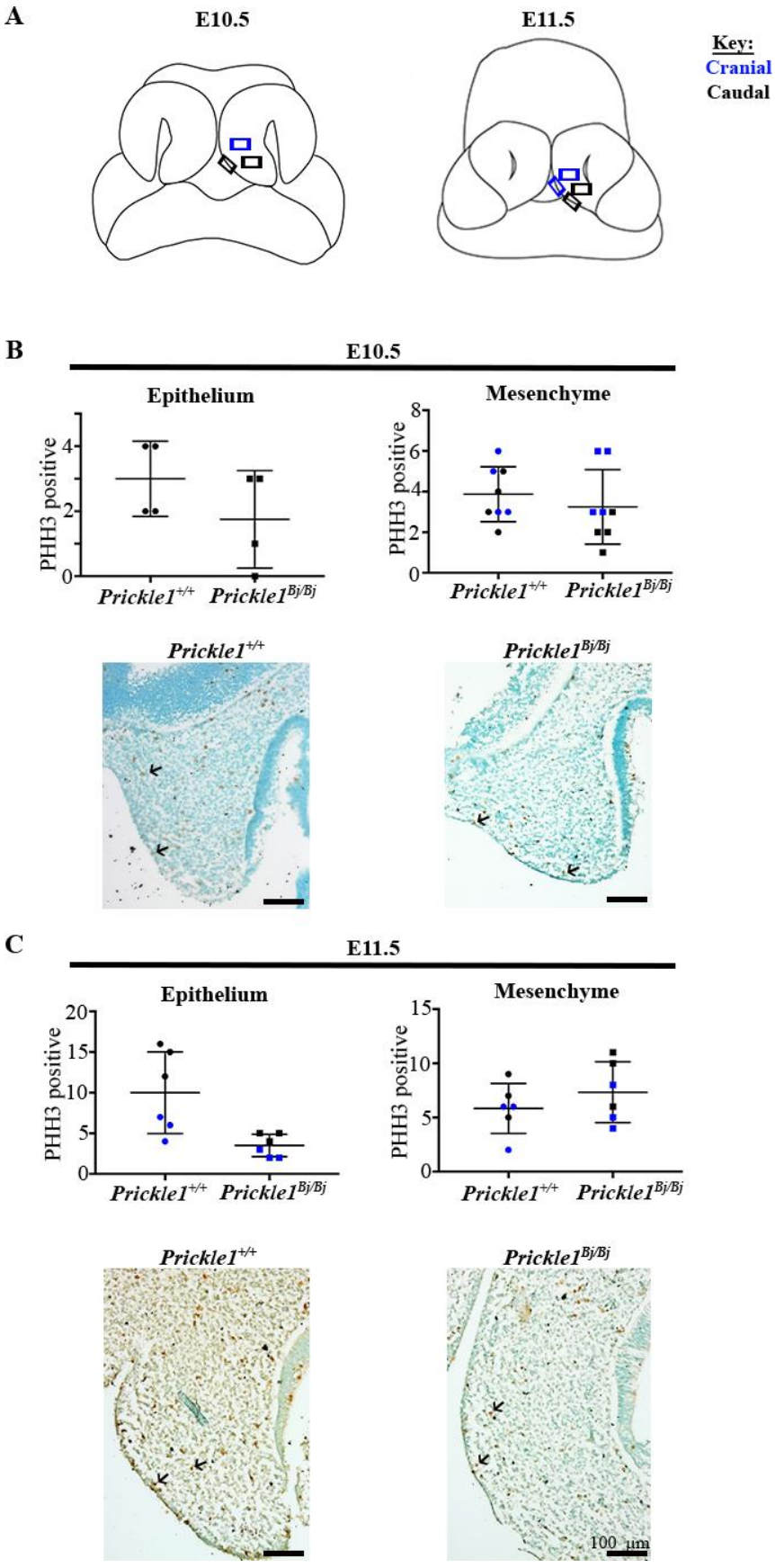
A
E10.5
E11.5
Key:
Cranial
Caudal
B
E10.5
Epithelium
Mesenchyme
PHH3 positive
Prickle1+/+
Prickle1Bj/Bj
C
E11.5
100 µm

Figure 16. *Prickle1*$^{Bj/Bj}$ have similar numbers of PHH3-positive cells in the MNP.

Proliferation measured in *Prickle1*$^{+/+}$ and *Prickle1*$^{Bj/Bj}$ epithelium and mesenchyme before (E10.5) and after (E11.5) MNP midline fusion. (**A**) Schematics of representing box placement for counting PHH3 positive cells. Two boxes were drawn and counted within cranial and caudal MNP mesenchyme of E10.5 and E11.5 embryos. One box was placed adjacent in the MNP medial edge epithelium of E10.5 embryos. Two boxes were placed in the MNP medial edge epithelium of E11.5 embryos. (**B**) Categorical scatterplots generated in Prism software for *Prickle1*$^{Bj/Bj}$ and *Prickle1*$^{+/+}$epithelial and mesenchymal PHH3 positive cells at E10.5. Representative images of *Prickle1*$^{+/+}$and *Prickle1*$^{Bj/Bj}$ MNP PHH3 stained sections at E10.5. (**C**) Categorical scatterplots for *Prickle1*$^{Bj/Bj}$ and *Prickle1*$^{+/+}$PHH3 positive cells, and representative images for E11.5 embryos. Significance evaluated by χ-square. Scale bars are 100 μm.

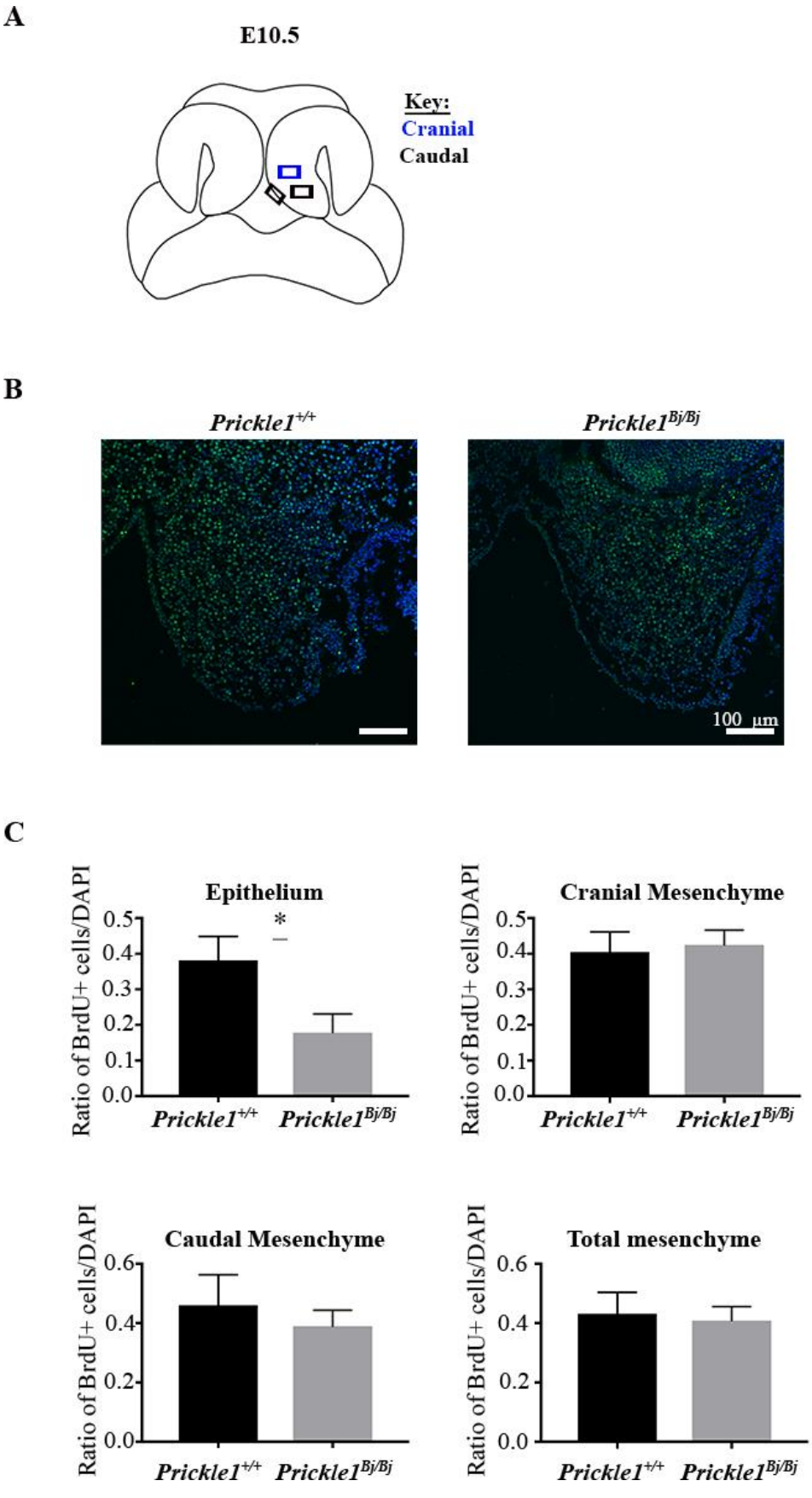
A
E10.5
Key:
Cranial
Caudal
B
Prickle1+/+
Prickle1Bj/Bj
100 µm
C
Epithelium
Ratio of BrdU+ cells/DAPI
0.5
0.4
0.3
0.2
0.1
0.0
*
Prickle1+/+
Prickle1Bj/Bj
Cranial Mesenchyme
Caudal Mesenchyme
0.6
Total mesenchyme

Figure 17. BrdU positive cells are decreased in *Prickle1*$^{Bj/Bj}$ MNP medial edge epithelial cells at E10.5.

(**A**) Schematic representing box placement for counting BrdU positive cells and DAPI nuclei. Two boxes were drawn and counted within the cranial and caudal mesenchyme of the MNP. One box was placed adjacent in the adjacent MNP epithelium. (**B**) Confocal stacks showing immunofluorescent staining to BrdU in the MNP at E10.5. (**C**) Ratios of BrdU positive cells/ total DAPI cells. Cells were counted in one area of the epithelium and two areas of the mesenchyme. Individual mesenchymal boxes were added together for the total mesenchyme. *Prickle1*$^{Bj/Bj}$ medial edge epithelial cells have significantly less BrdU positive cells at E10.5 (p-value= 0.01). Significance evaluated by students t-test.

A

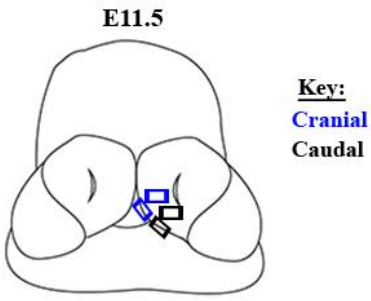
E11.5
Key:
Cranial
Caudal

B

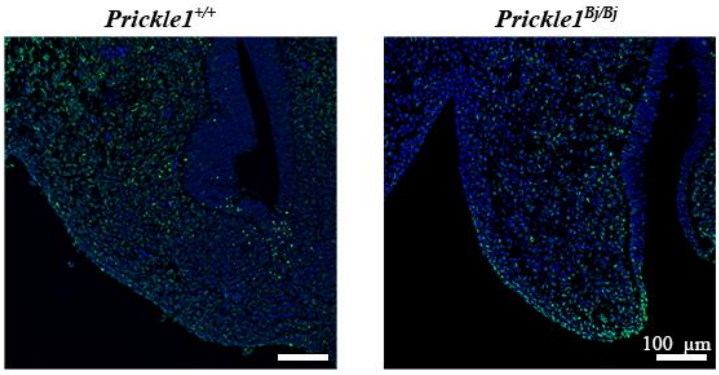
Prickle1+/+
Prickle1Bj/Bj
100 µm

C

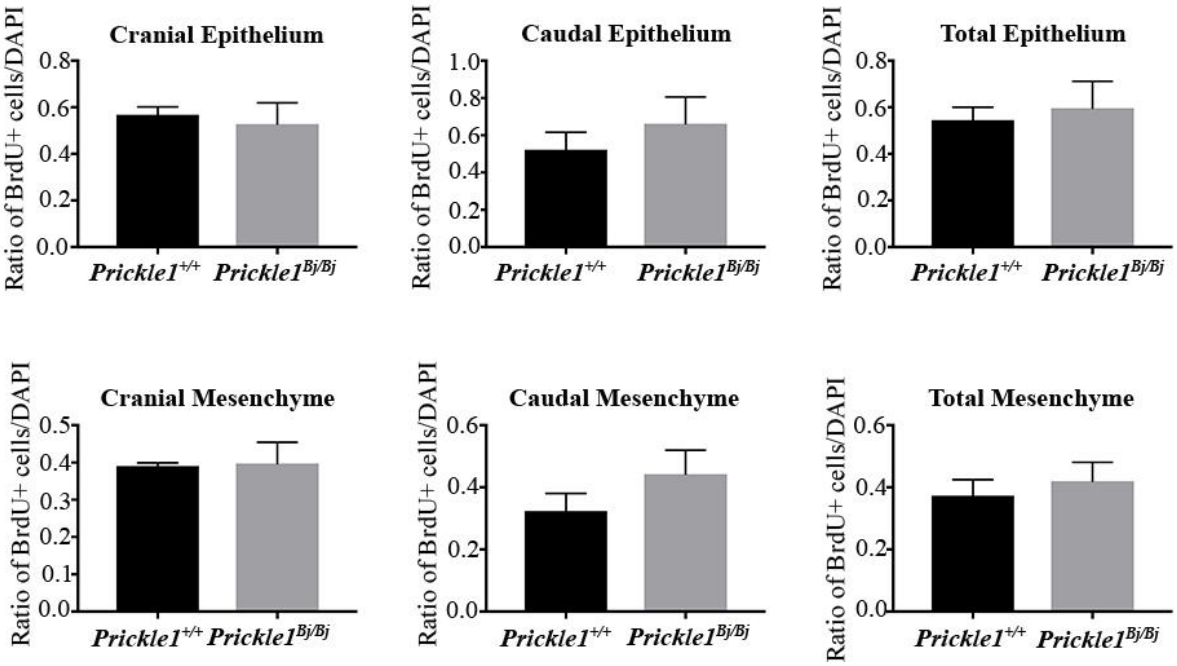
Cranial Epithelium
Caudal Epithelium
Total Epithelium
Cranial Mesenchyme
Caudal Mesenchyme
Total Mesenchyme
Ratio of BrdU+ cells/DAPI
Prickle1+/+
Prickle1Bj/Bj

Figure 18. *Prickle1*$^{Bj/Bj}$ MNPs have similar levels of proliferation at E11.5.

(**A)** Schematics of representing box placement for counting BrdU positive cells. Two boxes were drawn and counted within the cranial and caudal MNP mesenchyme. Two boxes were placed in the adjacent MNP epithelium. (**B**) Confocal stacks showing immunofluorescent staining to BrdU in the MNP at E11.5. (**C**) Ratios of BrdU positive cells/ total DAPI cells. Cells were counted in two areas in the epithelium and mesenchyme. Individual epithelial and mesenchymal boxes were added together for the total epithelium and mesenchyme. Significance evaluated by students t-test.

2.3.6 *Prickle1*$^{Bj/Bj}$ MNP cells do not have increased apoptosis during MNP fusion.

In the palate, there is evidence that the medial edge epithelial cells disappear via apoptosis (Cuervo and Covarrubias 2004; Martınez-Alvarez et al. 2000; Mori et al. 1994; Taniguchi et al. 1995). Apoptosis is a controlled process of cell death. Apoptotic cellular death is regulated by proteases, called caspases that mediate cleavage during early apoptosis. During later stages of apoptosis, endonucleases are activated and fragment the DNA. TUNEL (terminal deoxynucleotidyl transferase (TdT) nick end labeling) labels the cleaved DNA fragments. Due to the medial edge epithelium data in the palate, we tested whether *Prickle1*$^{Bj/Bj}$ have less apoptosis occurring in the MNP medial edge epithelium during MNP midline fusion.

Cells undergoing apoptosis were counted in the cranial and caudal mesenchyme at both E10.5 and E11.5 (Figure 19 A). At E10.5, apoptotic cells were counted in one area of the adjacent epithelium, and two areas in the epithelium at E11.5 (Figure 19 A). We did not find any significant apoptotic differences in the epithelium nor mesenchyme of the *Prickle1*$^{Bj/Bj}$ embryos at E10.5 or E11.5 (Figure 19 B, C). Though at E11.5, we did notice significantly more TUNEL positive cells located at the zone of fusion (Figure 19 C).

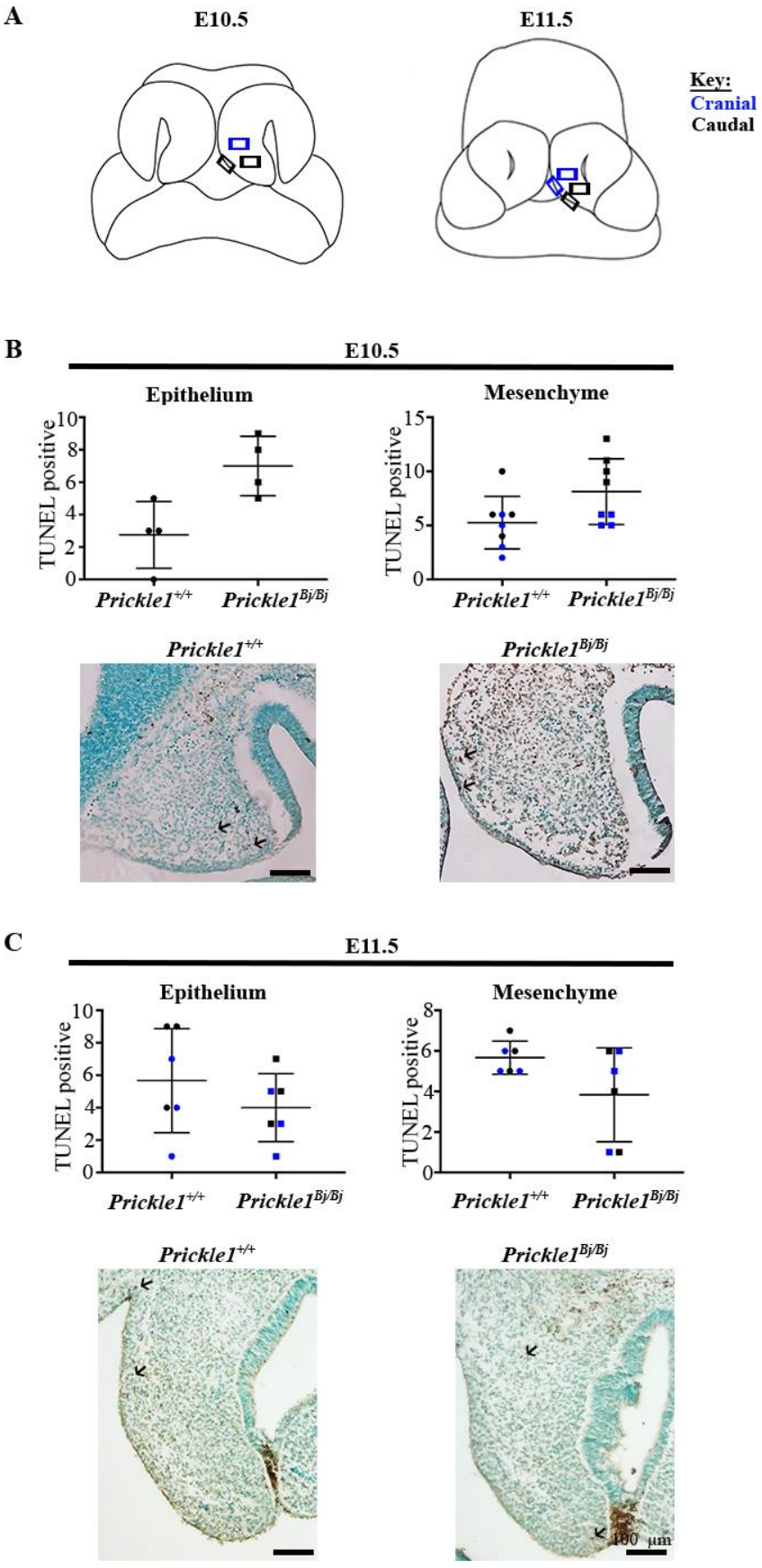
A
E10.5
E11.5
Key:
Cranial
Caudal
B
E10.5
Epithelium
Mesenchyme
TUNEL positive
Prickle1+/+
Prickle1Bj/Bj
C
E11.5
Epithelium
Mesenchyme
TUNEL positive
Prickle1+/+
Prickle1Bj/Bj
100 µm

Figure 19. *Prickle1*$^{Bj/Bj}$ MNP cells do not have increased apoptosis.

Apoptosis measured in *Prickle1*$^{+/+}$and *Prickle1*$^{Bj/Bj}$ epithelium and mesenchyme at E10.5 and E11.5 before and after MNP midline fusion. (**A**) Schematics of representing box placement for counting TUNEL positive cells. Two boxes were drawn and counted within cranial and caudal MNP mesenchyme of E10.5 and E11.5 embryos. One box was placed adjacent in the MNP epithelium of E10.5 embryos. Two boxes were placed in the MNP epithelium of E11.5 embryos. (**B**) Categorical scatterplots generated in Prism software for *Prickle1*$^{Bj/Bj}$ and *Prickle1*$^{+/+}$epithelial and mesenchymal TUNEL positive cells at E10.5. Representative images of *Prickle1*$^{+/+}$and *Prickle1*$^{Bj/Bj}$ MNP TUNEL stained sections at E10.5. (**C**) Categorical scatterplots for *Prickle1*$^{Bj/Bj}$ and *Prickle1*$^{+/+}$ TUNEL positive cells, and representative images for E11.5 embryos. (**B-C**) No significant differences were measured. Significance evaluated by chi-square test. Scale bars are 100 μm.

2.4 DISCUSSION

The *Beetlejuice* mutant mice are a novel orofacial clefting model that can accurately recapitulate mild midfacial clefting of the upper lip (Figure 9). The *Beetlejuice* mouse line is unique in that they have complete penetrance of a mild midfacial cleft lip, and an incomplete penetrant cleft palate phenotype responsible for 50% of the mutants developing a cleft palate (Figure 9). Similar to our *Beetlejuice* mutants, the *Prickle1*$^{C251X/C251X}$ mouse mutants also develop a cleft secondary palate. In addition, single nucleotide polymorphisms in PRICKLE1 are associated with human orofacial clefting (Yang et al. 2014). We have shown that in wild type embryos at E10.5 *Prickle1* is expressed in the inferior medial edge of the medial nasal prominences (Figure 10) suggesting that *Prickle1* plays a prominent role in midline fusion of the medial nasal prominences. In addition, past work in *Prickle1*$^{Bj/Bj}$ mice have described ciliary defects, compromised polarized cell morphology, and difficulty with directional cell migration (Gibbs et al. 2016). We hypothesized that loss of apical cell polarity of the medial nasal prominence medial edge epithelium would prevent the FEZ from coordinating cell signaling within the medial nasal prominences and ultimately impact epithelial molecular processes in the medial nasal prominences.

We verified that the *Prickle1*$^{Bj/Bj}$ embryos have a loss of apical cell polarity within the MNP medial edge epithelium at E10.5 and E11.5 (Figure 14 E-H). Additionally, we have shown that at both E10.5 and E11.5 HH and FGF signaling is decreased in the medial nasal prominences (Figures 11 and 12). In concordance with previous work in the palatal seam epithelium, we have demonstrated that an epithelial to mesenchymal transformation is essential in wildtype medial edge epithelium (Figures 13-15) (Fitchett and Hay 1989; Griffith and Hay 1992; Jin and Ding 2006; Martınez-Alvarez et al. 2000; Nawshad et al. 2004; Shuler et al. 1991; Shuler et al. 1992).

In the wildtype embryos, the medial edge epithelium loses its epithelial markers, such as E-cadherin, from E10.5 to E11.5 and at the same time gains mesenchymal markers, such as vimentin (Figures 14-15). However, in the *Prickle1*$^{Bj/Bj}$ embryos medial edge epithelium, levels of epithelial markers such as E-cadherin and β-catenin are increased at E10.5 and continue to stay higher than their control littermates at E11.5 (Figures 13-14). Additionally, levels of Na,K ATP-ase, an essential component in forming epithelial tight junctions is increased in the medial edge epithelium at E10.5 and levels continues to stay higher than their control littermates at E11.5 (Figure 13). It is intriguing to note that *Prickle1*$^{Bj/Bj}$ medial edge epithelium can obtain mesenchymal markers at E10.5, but the level of the mesenchymal marker does not increase at E11.5 as it does in the littermate control (Figure 15). We hypothesize that midline soft tissue cleft of the *Prickle1*$^{Bj/Bj}$ embryos presents as a mild cleft due to the medial edge epithelium being able to obtain some mesenchymal markers at E11.5.

Interestingly, we did not find significant differences in apoptosis in the MNPs, but did find a large amount of apoptosis occurring in the *Prickle1*$^{Bj/Bj}$ embryos lateral zone of fusion compared to the littermate control (Figure 19 C), suggesting that apoptosis is more important in the lateral zone of fusion of the primary palate rather than midline fusion of the MNPs. We did however find there was reduced cellular proliferation within the medial edge epithelium of the *Prickle1*$^{Bj/Bj}$ embryos at E10.5 and E11.5, but significant differences were only found at E10.5 when analyzed via BrdU (Figures 17-18). Additionally, proliferation within the mesenchyme when analyzed via BrdU and PHH3 were similar at E11.5 (Figures 17- 19). BrdU marks the S-phase, while PHH3 marks the mitosis phase of the cell cycle. This data suggests that the mild midfacial cleft could result from an elongation of the S-phase at E10.5 as a result of the *Prickle1*^{Bj} mutation.

In conclusion, the midline cleft lip present in the *Prickle1*$^{Bj/Bj}$ embryos has enabled us to understand normal midfacial morphogenesis. Through analysis of the *Beetlejuice* mice, we have been able to describe the molecular processes and signaling pathways that contribute to midfacial convergence. We conclude that decreased proliferation within the medial edge epithelial cells contributes to midfacial clefting, we can exclude defects in signaling pathways resulting from *Prickle1*^{Bj} as minorly contributing to the phenotype. Additionally, we believe that failure of the *Prickle1*$^{Bj/Bj}$ MNP medial edge epithelial cells to adequately gain mesenchymal markers inhibits the MNPs from fusing at the midline and ultimately causing a midline cleft to occur.

2.5 SUPPLEMENTAL FIGURES

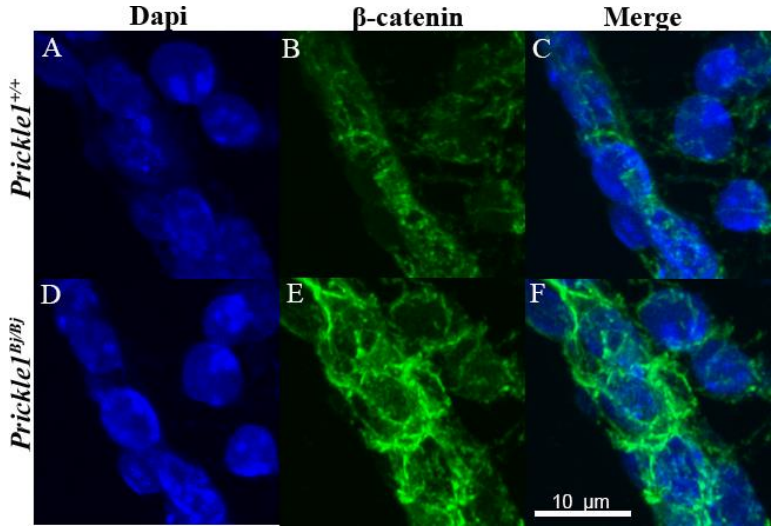

Figure 20. Supplemental 1. *Prickle1*$^{Bj/Bj}$ e10.5 β-catenin single channel

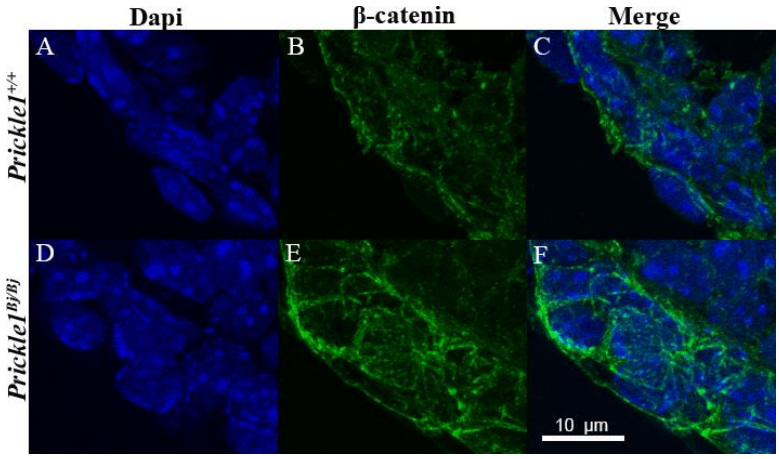

Figure 21. Supplemental 2. *Prickle1*$^{Bj/Bj}$ e11.5 β-catenin single channel

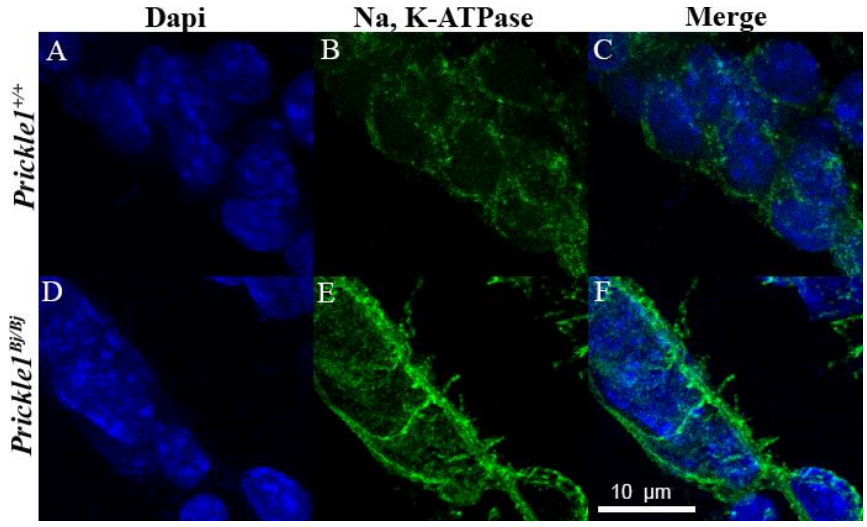

Figure 22. Supplemental 3. *Prickle1*$^{Bj/Bj}$ e10.5 Na, K-ATPase single channel

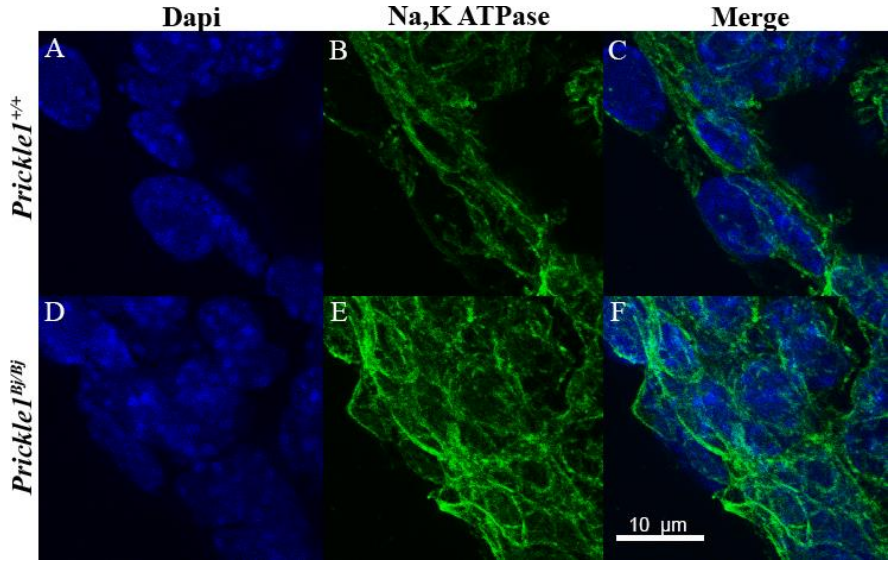

Figure 23. Supplemental 4. *Prickle1*$^{Bj/Bj}$ e11.5 Na, K-ATPase single channel

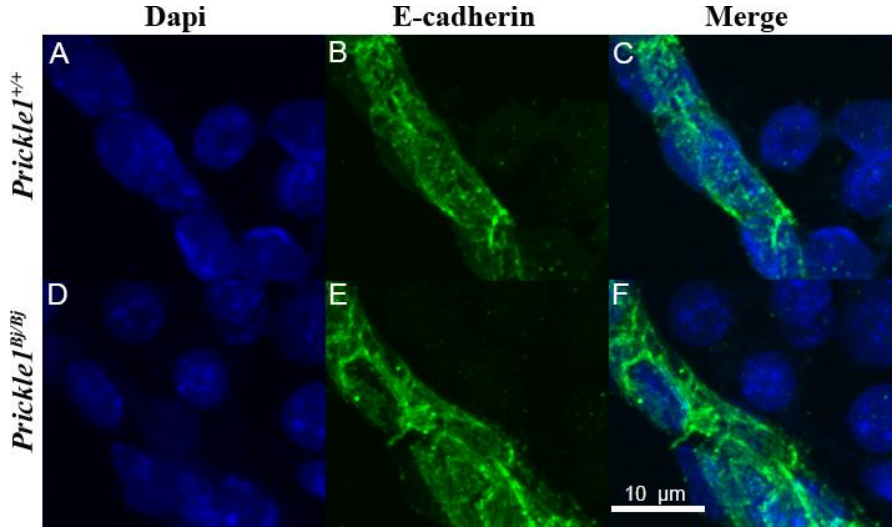

Figure 24. Supplemental 5. *Prickle1*$^{Bj/Bj}$ e10.5 E-cadherin single channel

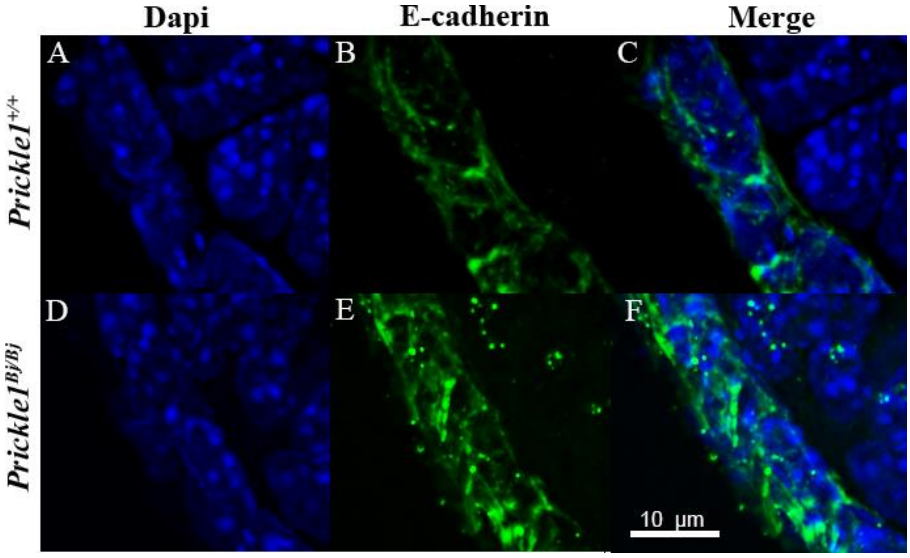

Figure 25. Supplemental *6. Prickle1*$^{Bj/Bj}$ e11.5 E-cadherin single channel

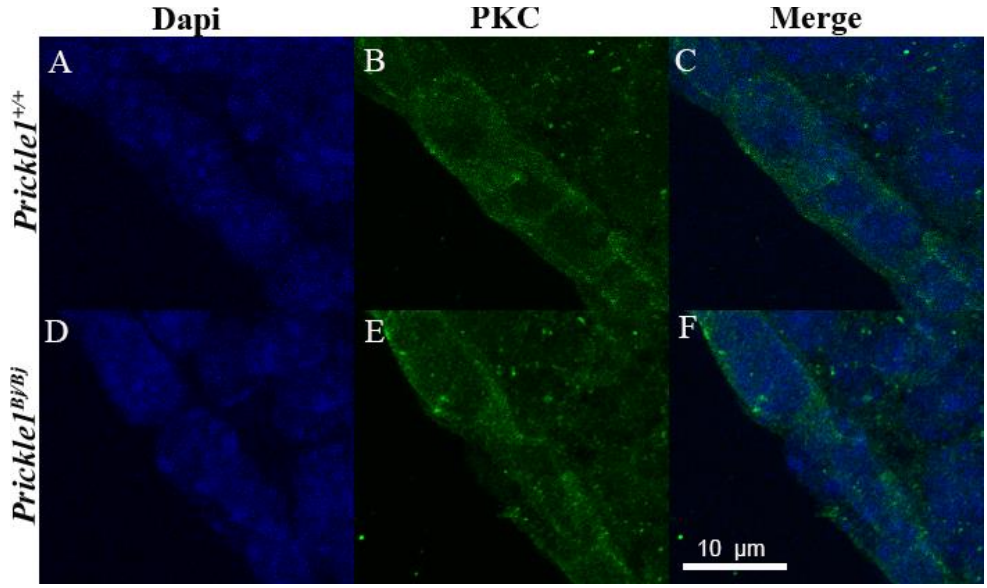

Figure 26. Supplemental 7. *Prickle1*$^{Bj/Bj}$ e10.5 PKC single channel

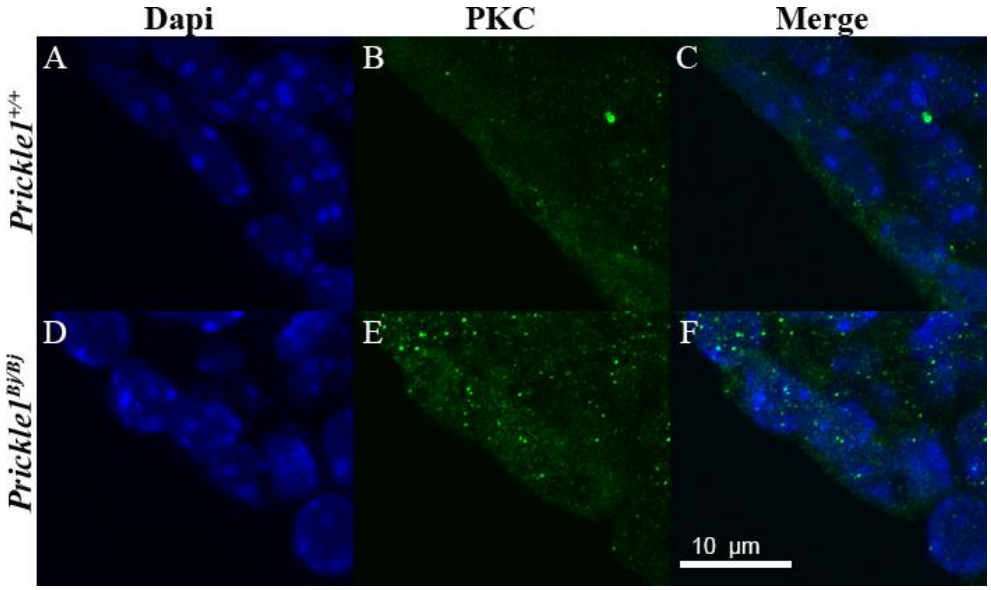

Figure 27. Supplemental 8. *Prickle1*$^{Bj/Bj}$ e10.5 PKC single channel

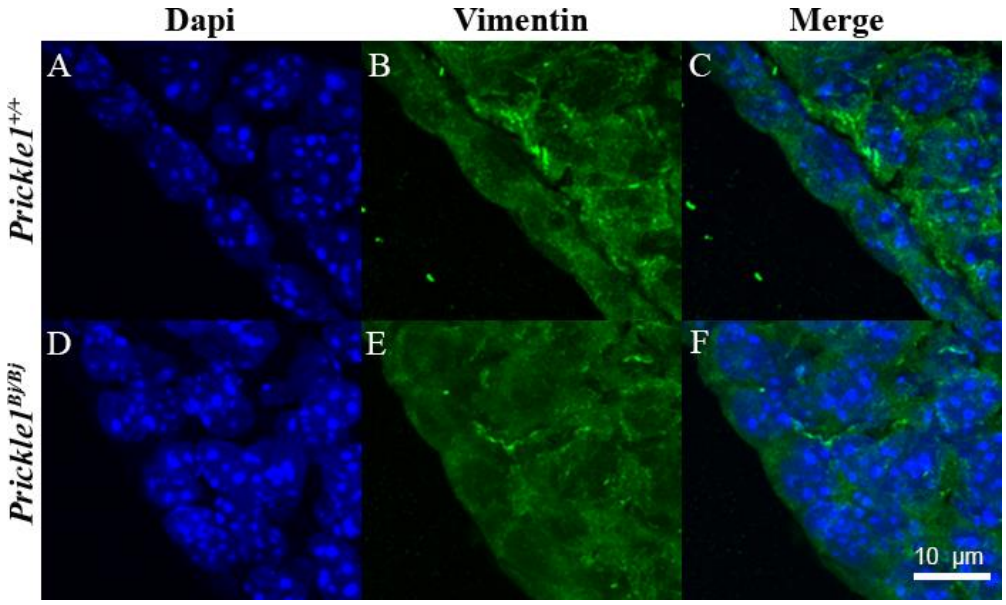

Figure 28. Supplemental 9. *Prickle1*$^{Bj/Bj}$ e10.5 Vimentin single channel

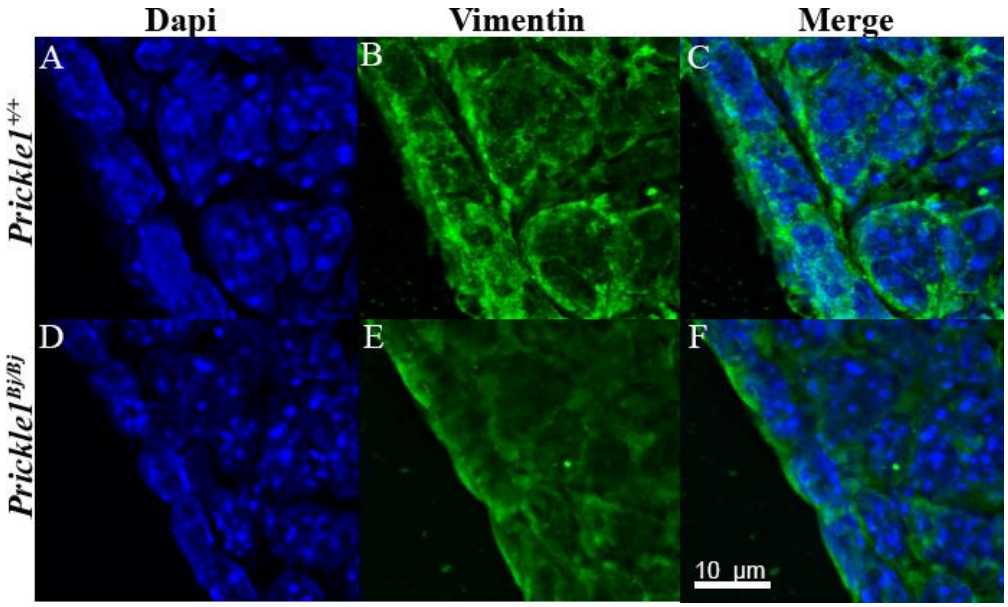

Figure 29. Supplemental 10. *Prickle1*$^{Bj/Bj}$ e11.5 Vimentin single channel

3.0 MAKING ONE NOSE FROM TWO: *UNICORN* MICE UNCOVER ANTERIOR MIDFACIAL MORPHOGENETIC MECHANISMS.

3.1 INTRODUCTION

The anterior midface is an intriguing complex as it is truly unique to each individual person, but fascinatingly, the morphogenetic processes that contribute to this uniqueness are relatively the same. During normal midfacial morphogenesis, the silhouette of the midface begins to take form after the bilaterally paired medial nasal prominences (MNPs) merge towards the midline until fusion is achieved at the center of the primitive face. Compromised midline convergence of the MNPs results in an intriguing subtype of orofacial clefting called, midfacial clefting. The severity of midfacial clefting can range from a simple vermillion notch in the soft tissue to a very wide true cleft of the upper lip, palate, and nose.

In addition to clefting of the orofacial and nasal structures, the nasal septum is commonly bifurcated in severe cases of midfacial clefting. The nose is typically symmetrical, but split through the midline with two adjacent nasal septa supporting the midface. This etiology poses an as interesting model to answer an open developmental question regarding early morphogenesis of the nasal septum: does the nasal septum begin as one midline structure, which is duplicated in severe cases of midfacial clefting; or does the nasal septum begin as two separate structures that must merge at the midline, and fails to in cases of midfacial clefting?

During early facial morphogenesis, convergence of the paired MNPs are responsible for forming the crest and tip of the nose, philtrum, medial portion of the upper lip, and the primary palate. The MNPs are composed of an inner core of mesenchyme, made up of mesoderm and

neural crest cells, and is surrounded by an outer epithelial layer. At embryonic day (E)10.5 in mice, the mesenchyme within the maxillary prominences begins to rapidly proliferate, thus pushing the MNPs towards the midline of the face (Jiang et al. 2006). By E11.5, rapid growth continued to drive the nasal pits and MNPs towards the midline. Proximal-distal and dorsal ventral growth of the upper jaw have been found to be regulated by the frontonasal ectodermal zone (FEZ) by regulating temporospatial expression of HH and FGF signaling molecules (Hu and Marcucio 2009; Hu et al. 2003). A final critical step to midfacial convergence is regression of the outer epithelial seam surrounding the facial processes allowing the corresponding mesenchyme to join (Jiang et al. 2006).

Midfacial clefting has not been well characterized clinically in humans postnatally, nor mechanistically within animal models prenatally. Inadequate characterization of this broad-spectrum phenotype could be in part due to a lack of understanding of normal fusion processes of the MNPs and early nasal septum morphogenesis. Throughout this paper, we introduce the *Unicorn* mice as a novel model for severe cases of midfacial clefting. We demonstrate the importance of FEZ patterning and molecular mechanisms of the epithelial layer in MNP midline convergence. We also delineate the earliest morphogenic stages of NS development using the Col2-cre mice, and demarcate the bifurcated NS etiology observed in the *Unicorn* mice.

3.2 METHODS

Mouse lines and animal husbandry:

Founder *Unicorn* (b2b1941Clo) animals were cryorecovered at Jackson Laboratory and maintained on a C57/BL6J background. The original phenotypes and exome sequencing, and cryopreservation were performed as described (Li et al. 2015). The mouse line was developed by chemically mutagenizing C57BL/6^J mice with ethylnitrosourea (ENU) and by completing a two-generation backcross breeding scheme (Li et al. 2015; Shen et al. 2006). The mice were maintained by outbreeding the line onto a C57/BL6J background. At each generation, I performed a test cross to ensure heritability of the phenotype between siblings, and then bred the productive male to wildtype C57/$BL6^J$ females. The original ENU treatment was designed to induce 100 mutations, each outcross to wildtype females reduces the ENU mutations by 50%. By the 8^{th} generation we expect to have selected 1 or 2 mutations that are maintained in the line and causative of our phenotype.

From the original exome sequenced, and phenotyped animals, we chose 5 homozygously mutated genes that we found to be expressed in the face at the time of lip fusion (Figure 46. Supplemental 1) to develop custom Invitrogen SNP assays to use with Taqman Genotyping MasterMix and read on a StepOnePlus machine. We genotyped the first 5 generations for all 5 genes, but by generation 4 we found that the phenotypes segregated with the mutations in Raldh2. Col2-$CreER^T$ (FVB-Tg(Col2a1-cre/ERT)KA3Smac/J) mice and Tdtomato (*Gt(ROSA)26Sor*$^{tm4(ACTB\text{-}tdTomato,\text{-}EGFP)Luo}$/J) mice were purchased from Jacksons Laboratories.

Presence of a plug was designated as day (E) 0.5, embryo collection was performed on embryonic day 10.5 (E10.5), E11.5, E12.5, and E15.5. The pregnant dams were euthanized on the appropriate day following timed matings via CO_2 asphyxiation and followed by cervical

dislocation. The embryos were harvested via C-section and embryo staging was confirmed by morphology.

Tamoxifen and BrdU administration*:*

For BrdU labeling, 10 mg/kg of BrdU in sterile PBS was injected intraperitoneally into the pregnant dams one hour prior to collection. Tamoxifen (50 ug/ml) dissolved in sterile sesame oil was injected intraperitoneally into pregnant dams on E9.5 and the embryos were collected at E10.5, and E11.5. Control embryos had no tamoxifen injection.

Animal care and use was conducted in accordance animal protocols approved by the Institutional Animal Care and Use Committee of the University of Pittsburgh.

Skeletal preparations:

Heads of e15.5 *Unicorn* and littermate control embryos were fixed in 95% ethanol and stained with Alizarin Red and Alcian Blue. Samples were stored and imaged in a 1:1 glycerol: ethanol solution.

Pseudo-SEM:

E10.5 and E11.5 embryos were fixed overnight in 4% PFA, and transferred to 0.01% ethidium bromide. Embryos were imaged using a Leica M165FC dissecting microscope and photographed using the DsRED filter under fluorescence illumination.

Morphometric analysis:

Three E10.5 and four E11.5 *Unicorn* and littermate control embryos were processed and imaged via pseudo-SEM protocol. Ten landmarks were placed on the images (Figure 32, Figure

33). The distance between the landmarks were measured in µm using the measure tool in Image J version 1.51w. ImageJ was calibrated so that 148 pixels = 10 µm. We observed that the mean width of the maxillary prominences (measurement 5, 6; Figure 32, 33) was the same in wildtype and *Unicorn* (E10.5 WT 4.67 µm +/- 0.20 µm, n=3; vs *Unicorn* 5.02 µm +/- 0.64 µm, n=3; E11.5 WT 7.78 µm +/- 1.09 µm, n=4; Unicorn 6.96 µm +/- 0.95 µm, n=4).

For each measurement, the landmark measurement width was normalized to the width of the maxillary prominences to give a normalized value. The normalized values for each animal, genotype and stage were averaged and represented as a bar graph. A paired Students t-test was used to compare normalized facial prominence widths between *Unicorn* and control embryos ($P<0.05$).

Histology analysis:

For histological analysis, E10.5 and E11.5 embryos were collected, fixed in 4% PFA overnight dehydrated and stored in 70% ethanol, followed by processing in a Leica ASP300s processor and embedded in paraffin wax with a Leica Histoembedder. Embryos were sectioned frontally at 10 µm and placed on triethoxysilylpropylamine (TESPA) coated Super-Frost coated slides. Adjacent slides were stained with H&E for histological analysis and Picrosirius red and alcian blue.

In situ hybridization:

Section *in situ* hybridization was performed using digoxigenin-labelled RNA probes, hybridized at 65°C, followed by high stringency washes and followed by incubation with anti-DIG antibody. Following washing to reduce non-specific antibody binding, the location of RNA probes were

detected with BM Purple (Szabo-Rogers et al. 2016). RNA probes used: *Ptc1*, *Gli1*, and *Erm1*. At least 3 littermates were analyzed per each RNA probe.

Immunohistochemistry:

Tissue sections were prepared for immunohistochemistry and immunofluorescence by sodium citrate buffer antigen retrieval in a microwave for 5 X 4 minutes. Sections were blocked in 5% goat serum in 1% Triton X-100 for 1 hour prior to being incubated overnight incubation of the primary antibodies at 4°C. Primary antibodies used: P-Histone H3 (S10) produced in rabbit, (Cell Signaling #9701S); Purified mouse Anti- β-catenin 1:100, (BD Biosciences #610153); Anti- E-cadherin, (BD Biosciences #61018); Anti-Protein Kinase C (PKCι) (BD Biosciences # 610175); Anti-Vimentin antibody (Sigma #V2258); Anti-Sodium Potassium ATPase, (Abcam #ab76020). Secondary antibodies used: Biotinylated goat anti-rabbit IgG- HRP (Vectastain); Alexaflour 488 rabbit anti-mouse, (Invitrogen A11059); Alexaflour 488 donkey anti-rabbit, (Invitrogen A21206). Following fluorescent antibody incubation, samples were mounted with Prolong-Gold with Dapi (Invitrogen). PHH3-positive cells were detected using the Vectastain amplification kit and ImmPACT DAB, and slides were mounted in Thermo Scientific mounting medium. At least 3 littermates were analyzed per each antibody.

Proliferation and apoptotic studies:

BrdU incorporation was detected using antigen retrieval with the endonucleases (Exonuclease III, and Dpn1), and Proteinase K. BrdU was detected with the RPN202 primary antibody (GE Healthcare Life Sciences) and Alexa Fluor 488 rabbit anti-mouse secondary antibody (Invitrogen A11059) were used to detect BrdU activity. Samples were mounted with Prolong-Gold with Dapi

(Invitrogen). TUNEL-positive cells were labelled following the manual for the ApopTag Plus Peroxidase *In Situ* Apoptosis Detection Kit (Sigma Millipore) was used to evaluate apoptosis.

Cell counting:

BrdU positive cells and DAPI stained nuclei were counted in similar anatomical regions in 2 areas in the MNP mesenchyme (150x150 pixels) and 1 epithelial (150 pixels) region in E10.5 embryos. BrdU positive cells and DAPI stained nuclei were counted in similar anatomical regions in 2 areas in the MNP mesenchyme (125x125 pixels) and 2 epithelial (125 pixels) regions in E11.5 embryos. A ratio was calculated from BrdU positive cells and DAPI stained cells via positive BrdU cells/all cells. TUNEL (200x200 pixels) and PHH3 (175x175 pixels) positive cells were counted in the same regions on near-adjacent sections and plotted in a scatterplot. A χ-squared test was used to evaluate PHH3 and TUNEL-positive cells between *Unicorn* and controls ($p<0.05$). A paired Students t-test was used to compare BrdU labelling between midfacial clefted and control embryos ($P<0.05$).

Imaging:

Whole mount images were captured on a Leica M165FC dissecting microscope using a DFC 450 camera and Leica LAS software. Histological images were captured on a Zeiss AXIO microscope with an AxioCam MRc 35 camera and Zen software. Fluorescence images were obtained at the Center for Biological Imaging at the University of Pittsburgh on an Olympus Fluoview 1000 confocal and deconvolved using NIS software. Images are presented as maximal projection stacks.

3.3 RESULTS

3.3.1 *Unicorn* mice develop a midfacial cleft with a bifurcated nasal septum.

The *Unicorn* mice develop a midfacial cleft that extends through the lip, palate, and nose (Figure 30 A b, d, Figure 31 F, H). With the exception of the midline cleft, the external anatomy of the *Unicorn* mice is grossly normal (Figure 30 A). The nose is fully formed with two nostrils and the lateral sides of the lip are normal (Figure 30 A b, d). The palatal shelves in the *Unicorn* embryos are also normal relative to the cleft. At E15.5, the palatal shelves elevated above the tongue, as in the control, but failed to make contact at the midline (Figure 31 A-D). Additionally, the patterning of the cranial bones and cartilages are present and normal at E15.5 considered the midfacial cleft phenotype (Figure 30 B c, d). Due to the clefting, the premaxilla and vomer are laterally displaced in comparison to the littermate control (Figure 30 B c, d, Figure 31 G, H).

In addition to the orofacial and nasal clefting phenotype, the nasal capsule cartilage of the *Unicorn* embryos is fully split (Figure 30 B c, d). Histological analysis of the cleft revealed the nasal septum to be fully bifurcated in *Unicorn* embryos at e15.5 (Figure 31 B, D, F). The nasal septum of the littermate control is present as one midline organ within the frontonasal process as it is making contact and fusing with the palatal shelves (Figure 31 A, C, E). The dual nasal septa of the *Unicorn* embryos at E15.5 is located within a widened frontonasal process that fails to make contact with the palatal shelves (Figure 31 B, D, F). Intriguingly, each of the two *Unicorn* nasal septa are approximately the same size individually as the one normal nasal septum present in the control embryos (Figure 31 A-F).

A

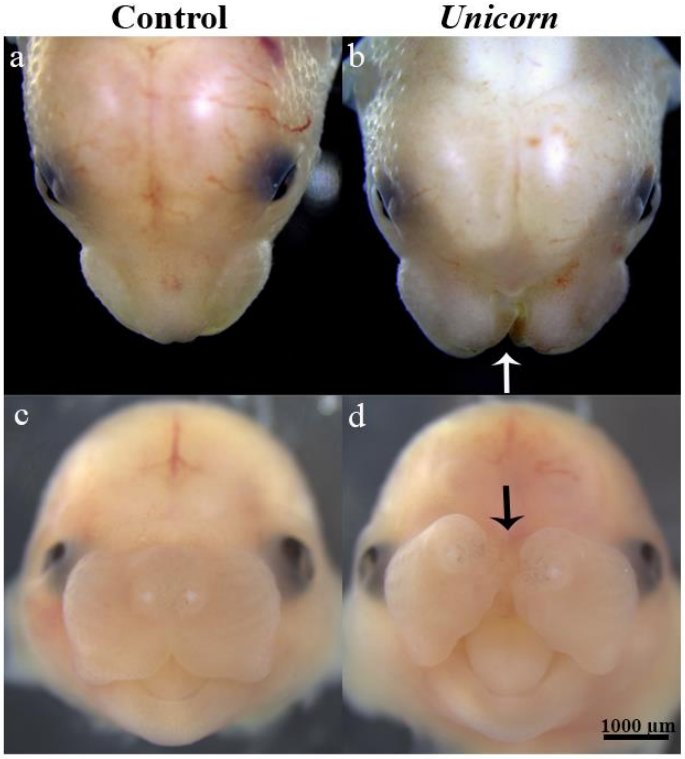
Control
Unicorn
a
b
c
d
1000 µm

B

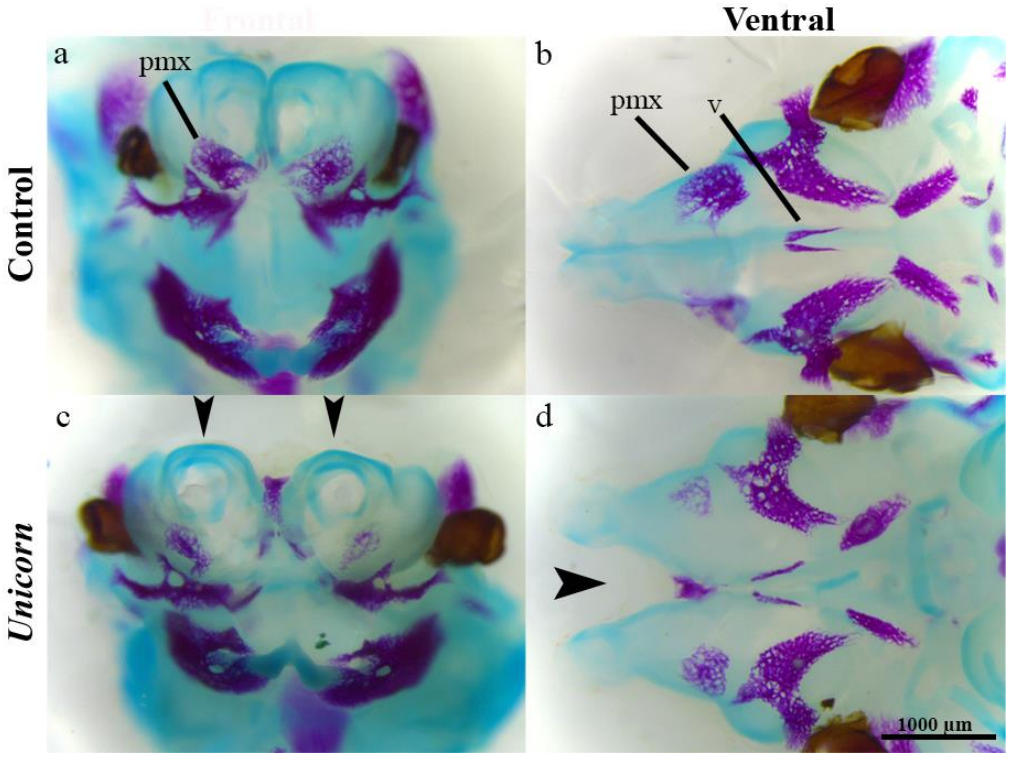
Ventral
Control
Unicorn
a
pmx
b
pmx
v
c
d
1000 µm

Figure 30. Gross morphological analysis of the midfacial cleft phenotype in *Unicorn* animals.

(**A**) External, birds eye view of the skull (**a, b**) and frontal view (**c, d**) at E15.5, showing the midfacial cleft phenotype of *Unicorn* mutants (arrows). (**b, d**) The midfacial cleft extends through the lip, palate, and the nose upon gross morphological phenotyping. (**B**) Alizarin red, and alcian blue staining of bone and cartilage staining respectively revealed that all cranial bones and cartilages are present in the *Unicorn* mice (**b, d**), and revealed that the nasal capsule is split in the *Unicorn* mice at E15.5 (arrow head**, c, d**). Scale bars are 1000 µm. Abbreviations: pmx, premaxilla; v, vomer.

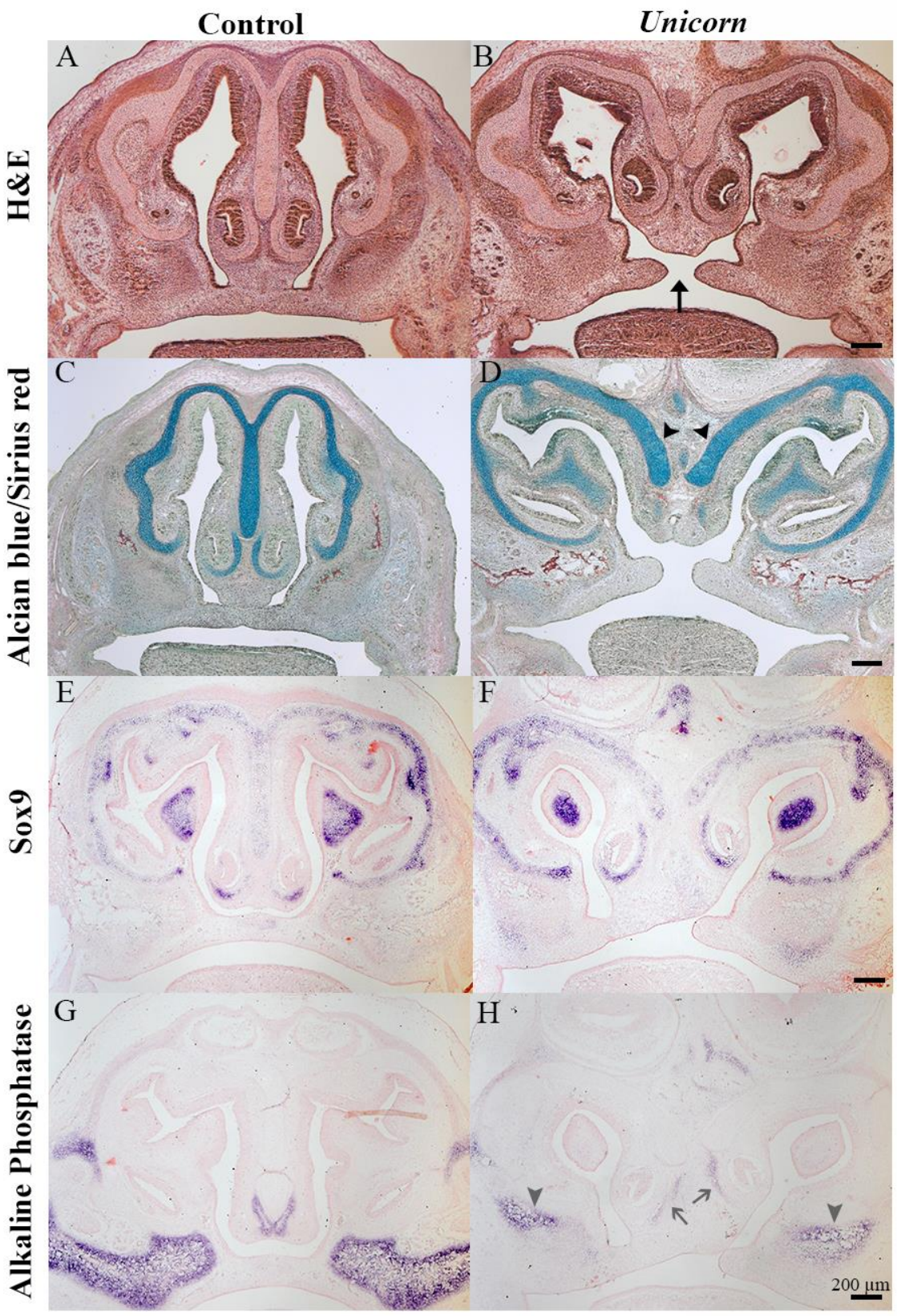
Control
Unicorn
H&E
Alcian blue/Sirius red
Sox9
Alkaline Phosphatase
A
B
C
D
E
F
G
H
200 µm

Figure 31. The nasal septum is duplicated in the *Unicorn* animals as revealed by histological analysis at e15.5.

Histological analysis of frontal sections capturing the nose and palate of *Unicorn* and control embryos, stained with **(A, B)** hematoxylin and eosin, **(C, D)** alcian blue and alizarin red, **(E, F)** *Sox9* **(G, H)** *Alkaline phosphatase* at E15.5. (**B, D, F, H**) The secondary palate of *Unicorn* individuals is clefted (**B**, black arrow). (**A, C**) Alcian blue and H&E staining display the nasal septum as one midline organ located in the frontonasal process in littermate control embryos. (**B, D**) In *Unicorn* embryos, there are two individual nasal septa organs located in the frontonasal process that are similar in size individually as the single littermate control nasal septum (black arrow heads). (**E, F**) *Sox9* expression is found in the duplicated septum at similar levels between wildtype and littermate controls. (**C-F**) All the *Sox9* expressing regions are positive for alcian blue staining in the *Unicorn* mutants as the littermate controls. (**G, H**) *Alkaline phosphatase* expression is present, but decreased in the palatal shelves (grey arrow heads) and vomer (grey arrows) of the *Unicorn* individuals. Scale bars are 200 μm.

3.3.2 The *Unicorn* face is abnormal by E10.5.

At E10.5 in mice, the MNPs begin to shift from a lateral to a more medial position prior to making contact and merging together at E11.5. We hypothesized that the midfacial cleft phenotype in the *Unicorn* embryos arose in part due to the MNPs failing to fuse at the midline fusion, and facial prominences morphological changes. To analyze the facial morphology changes occurring at E10.5 and E11.5, we placed facial morphometric landmarks upon the faces of *Unicorn* and control embryos (Figure 32 B, Figure 33, B).

At E10.5, I observed that the nasal pits of the *Unicorn* embryos face laterally, projecting towards the sides of the face (Figure 32 A), whereas in the littermate control, the MNPs have been shifted medially towards the midline of the face (Figure 32 A). Importantly, the width of most of the *Unicorn* facial prominences is not significantly different from the control embryos at E10.5 (Figure 32 C). The one exception is the distance from the lateral edge of the lateral nasal prominence to the inferior tip of the MNP (1, 6) which is significantly shorter in the *Unicorn* embryos (Figure 32 C).

Significant deviations from the littermate control embryos begin to occur at E11.5 in the *Unicorn* midfacial region (Figure 33). In the control embryos, the MNPs have made contact at the midline of the face and are beginning to merge together (Figure 33 A). The MNPs have shifted towards the front of the face, but a significant internasal distance separates the medial edges of the MNPs from making contact at the midline (3,3) (Figure 33 A, B, C). From the facial morphometric measurements, it was found that the *Unicorn* embryos were significantly wider through the lateral nasal prominence to the midline of the face (1, 7), nasal pit to the midline of the face (2, 7), nasal pit to nasal pit (2,2), zone of fusion to the opposing zone of fusion (6,6), lateral edge of the lateral nasal prominence to the opposing lateral edge of the lateral nasal prominence (1,1), and the

distance through the maxillary prominences (5,5; Figure 33 C). Surprisingly, the width of the *Unicorn* MNPs were not significantly different from the little mate control (2,3; Figure 33 C). Nor was the width of the later edge of the lateral nasal prominence to the medial edge of the MNP (1,3; Figure 33 C). In contrast to *Unicorn* embryos at E10.5, the distance from the lateral edge of the lateral nasal prominence to the inferior tip of the MNP is not were not significantly different from the littermate controls (1,6; Figure 33 C).

A

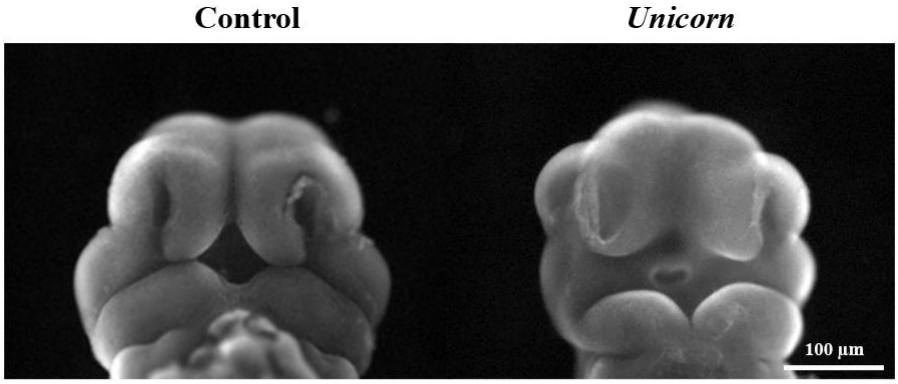
Control
Unicorn
100 µm

B

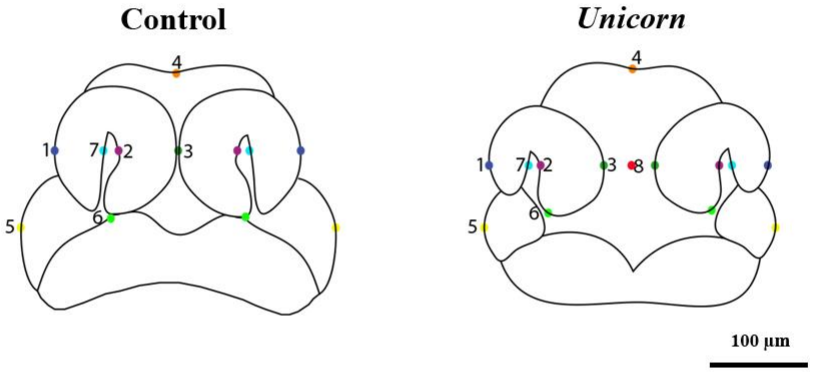
Control
Unicorn
1
2
3
4
5
6
7
8
100 µm

C

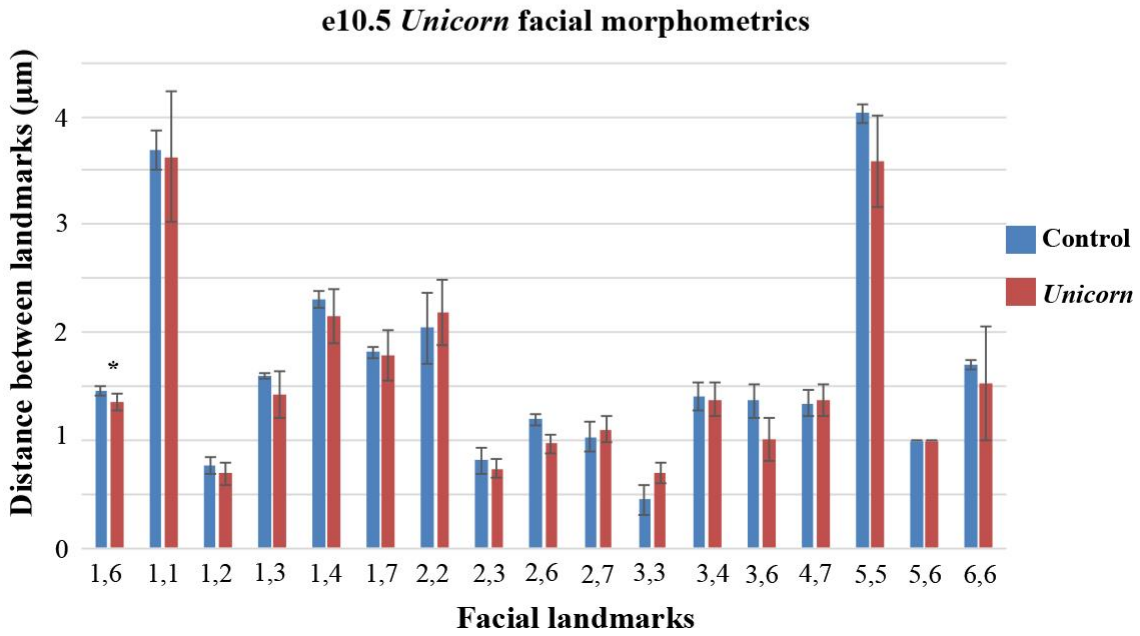
e10.5 *Unicorn* facial morphometrics
Distance between landmarks (µm)
0
1
2
3
4
*
1,6
1,1
1,2
1,3
1,4
1,7
2,2
2,3
2,6
2,7
3,3
3,4
3,6
4,7
5,5
5,6
6,6
Facial landmarks
Control
Unicorn

Figure 32. *Unicorn* facial prominences are of comparable width to littermate controls at E10.5.

(**A**) Frontal pseudo-SEM images of E10.5 *Unicorn* and littermate control embryos. (**A**) In the control mice, the MNPs have shifted to the center of the face. The MNPs of the *Unicorn* animals are turned laterally towards the side of the face. (**B**) Schematics of E10.5 control and *Unicorn* faces with numbered facial landmarks. (**C**) The width of the facial prominences are normal. The distance between the lateral nasal prominence and the distal tip of the MNP is shortened (1,6) (p-value 0.04). We measured 3 pairs of animals and the measurements were normalized to the maxillary prominence width (5,6) due to no differences observed in width. Significance levels: * < 0.05, ** < 0.005, *** < 0.005. Scale bars are 100 μm.

A

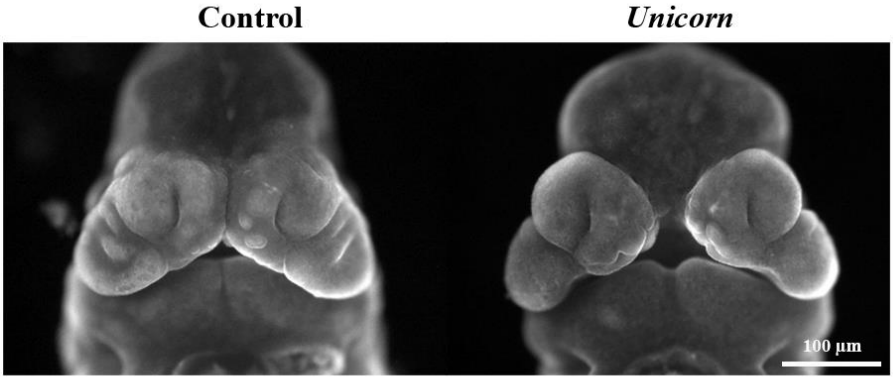
Control
Unicorn
100 µm

B

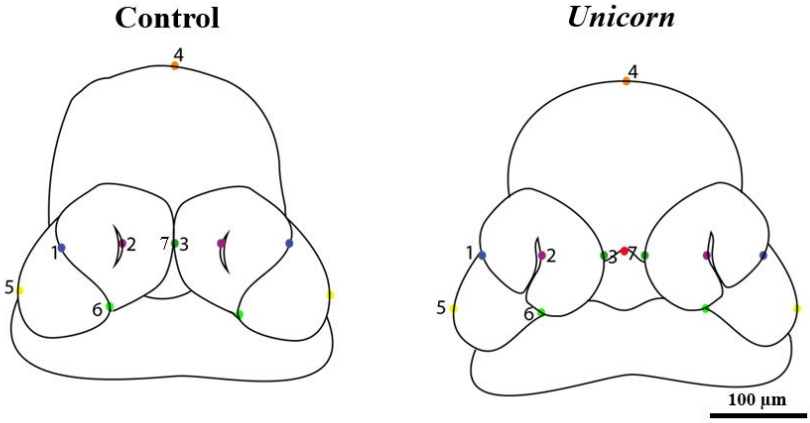
Control
Unicorn
1
2
3
4
5
6
7
100 µm

C

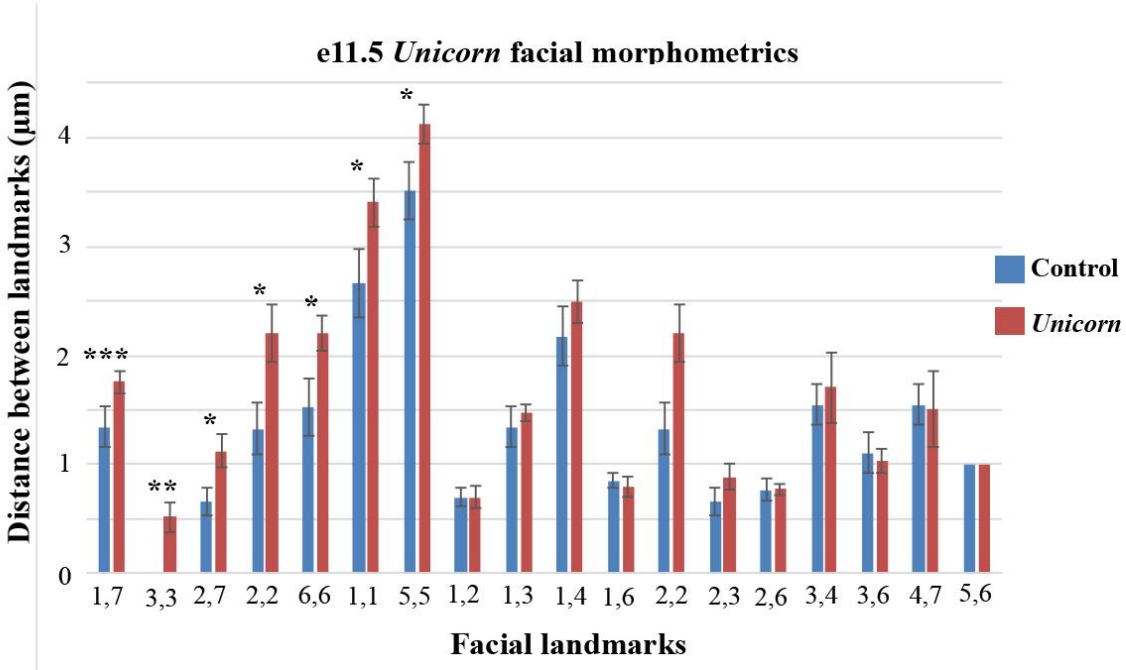
e11.5 *Unicorn* facial morphometrics
Distance between landmarks (µm)
0
1
2
3
4
***
**
*
*
*
*
*
1,7
3,3
2,7
2,2
6,6
1,1
5,5
1,2
1,3
1,4
1,6
2,2
2,3
2,6
3,4
3,6
4,7
5,6
Facial landmarks
Control
Unicorn

Figure 33. *Unicorn* facial morphology is significantly abnormal at e11.5.

(**A**) Frontal pseudo-SEM images of E11.5 *Unicorn* and littermate control embryos. At E11.5, the MNPs in the control mice have met at the midline. The *Unicorn* mice have a large internasal distance that separates the two MNPs. (**B**) Schematics of E11.5 control and *Unicorn* faces with numbered facial landmarks. (**C**) At E11.5, the midfacial region in the *Unicorn* mice have a significantly increased internasal distance between the MNPs (3,3) (p-value= 0.002). *Unicorn* embryos are significantly wider through the LNP to the midface (1,7) (p-value= 0.000026), the MNP (2,7) (p-value= 0.015), the lateral edge of the MNP to the corresponding lateral edge of the paired MNP (2,2) (p-value= 0.0099), medial edge of the maxillary prominence to the corresponding medial edge of the maxillary prominence (6,6) (p-value= 0.009), and the lateral edge of the lateral nasal prominence to the corresponding edge of the paired lateral nasal prominence (1, 1) (p-value= 0.017). We measured 4 pairs of animals and the measurements were normalized to the maxillary prominence width (5,6) due to no differences observed in width. Significance levels: * < 0.05, ** < 0.005, *** < 0.005. Scale bars are 100 µm.

3.3.3 *Unicorn* FEZ patterning is disrupted during medial lip fusion.

The signaling pathways Hedgehog (HH) and Fibroblast growth factor (FGF) are temporospatially located within the MNPs frontonasal ectodermal zone (FEZ), and are involved in regulating proximal distal growth of the upper face. We evaluated FEZ signaling before (E10.5) and after (E11.5) MNP convergence. HH signaling was evaluated by the expression of the HH receptor *Patched1* (*Ptc1*), and the transcription factor *Glioma-associated oncogene homolog 1* (*Gli1*) (Figure 34). At E10.5, both *Ptc1* and *Gli1* expression are greatly down-regulated (Figure 34 A). *Gli1* fails to be expressed in the inferior medial edge of the MNP mesenchyme (Figure 34 A a). In the control and *Unicorn* embryos, *Ptc1* is expressed in the mesenchyme adjacent to the brain and medial edge mesenchyme (Figure 34 A b, d). At E11.5, the amount of HH signaling has increased in the control MNPs (Figure 34 B). *Unicorn* embryos are able to upregulate *Gli1* expression at the zone of fusion and small amounts of expression in the mesenchyme of the medial edge mesenchyme (Figure 34 B c). The *Unicorn Gli1* domain fails to shift laterally though in the mesenchyme surrounding the nasal pit (Figure 34 B c). *Ptc1* expression is relatively ubiquitously expressed in the MNP mesenchyme at E11.5 in control embryos (Figure 30 b). The *Unicorn* embryos have slight *Ptc1* expression at the inferior tip of the MNP and around the medial edge mesenchyme (Figure 34 B d). Though, the *Ptc1* expression domain fails to be expressed within the anterior or central MNP mesenchyme where the MNP would fuse with the opposing MNP (Figure 34 B d).

The FGF pathway was evaluated by the expression of the transcription factor, *Ezrin-radixin-moesin* (*Erm1*). We found that *Erm1* expression was increased in the *Unicorn* embryos MNP before (E10.5) and after (E11.5) MNP fusion (Figure 35). In the control embryos, Erm1 is expressed in the MNP mesenchyme surrounding the medial edge epithelium and the mesenchyme

of the inferior tip of the MNP (Figure 35 a). In *Unicorn* embryos, *Erm1* expression is increased in the MNP mesenchyme and the domain shifts to cover the entire mesenchyme at E10.5 (Figure 35 c). Additionally at E10.5, *Erm1* expression is increased in the *Unicorn* nasal pit epithelium (Figure 35 c). At E11.5, the *Erm1* domain has shifted to the inferior tip of the MNP mesenchyme, and a very small amount of *Erm1* expression remains in the medial edge mesenchyme in the control embryos (Figure 35 b). In *Unicorn* embryos, the domain of *Erm1* expression is increased from the inferior tip of the MNP mesenchyme anteriorly alongside the nasal pit epithelium (Figure 35 d). *Erm1* expression is also increased in the nasal pit epithelium at E11.5 in *Unicorn* mutants (Figure 35 d).

A

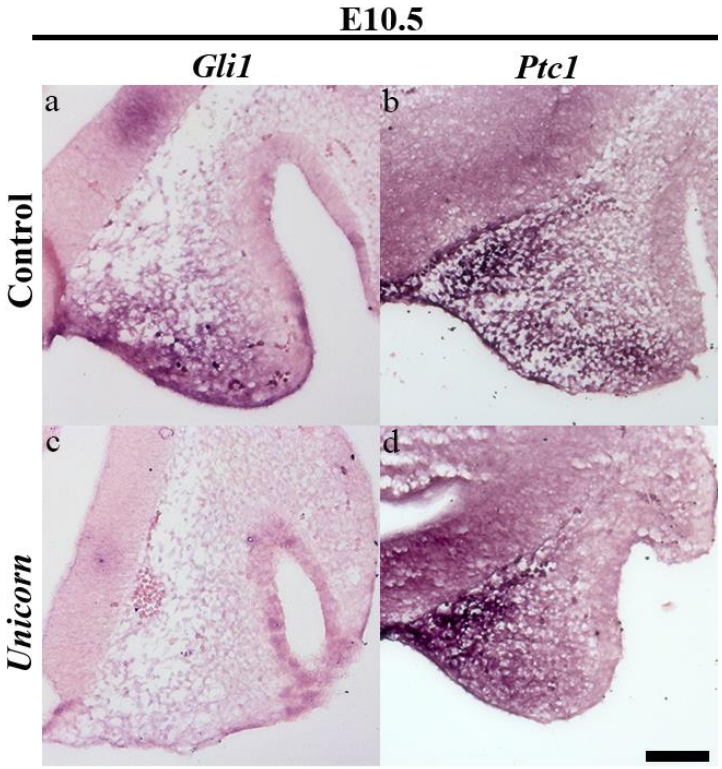
E10.5
Gli1
Ptc1
a
b
Control
c
d
Unicorn

B

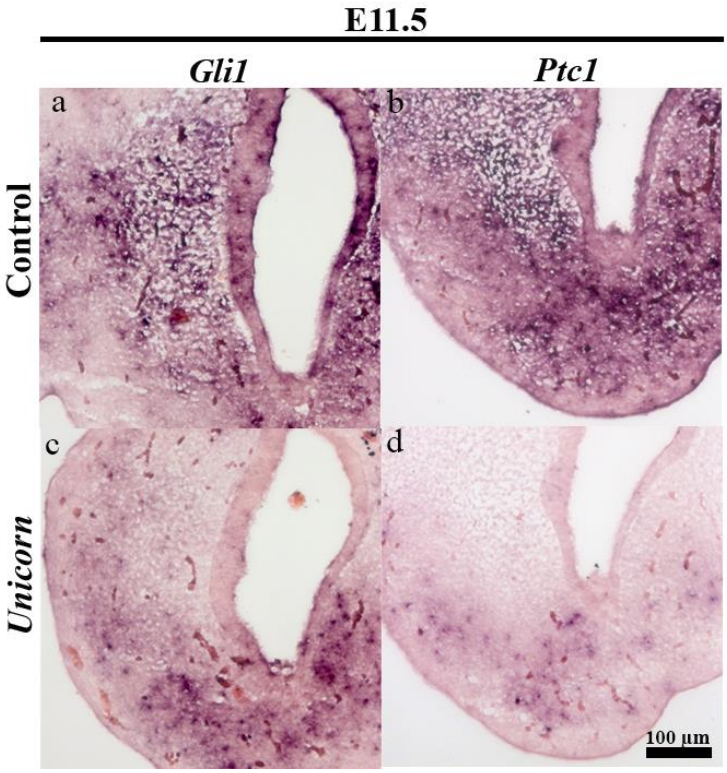
E11.5
Gli1
Ptc1
a
b
Control
c
d
Unicorn
100 µm

Figure 34. HH signaling is decreased in *Unicorn* FEZ.

Section *in situ* hybridization to HH signaling reporters, *Ptc1* and *Gli1* before (E10.5) and after medial lip fusion (E11.5). (**A a, c**) *Gli1* expression is decreased in the MNP mesenchyme and MEE at e10.5. (**B a, c**) At e11.5, *Gli1* expression is decreased in the nasal pit epithelium and mesenchyme lateral to the nasal pit. (**A b, d**) At e10.5, *Ptc1* expression is unchanged in the MNP mesenchyme adjacent to the brain and medial edge mesenchyme. (**B b, d**) *Ptc1* expression is decreased at e11.5 in the mesenchyme lateral and distal to the nasal pit epithelium. Scale bars are 100 μm.

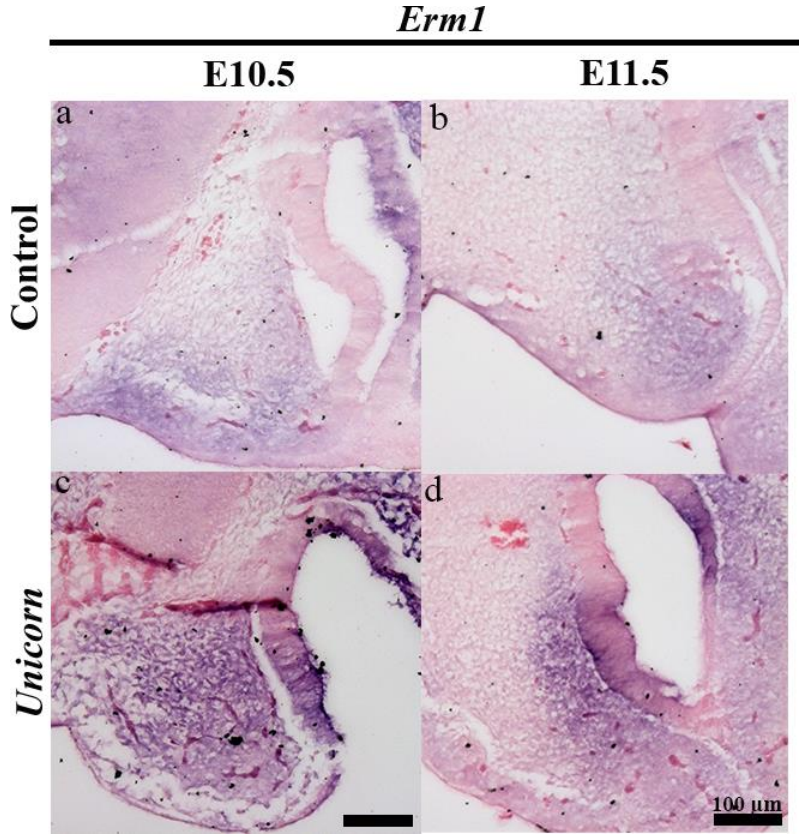
Erm1
E10.5
E11.5
Control
Unicorn
a
b
c
d
100 µm

Figure 35. FGF signaling is increased in *Unicorn* FEZ.

Section *in situ* hybridization to FGF signaling reporter, *Erm1* before (E10.5) (**a-b**) and after medial convergence (E11.5) (**c-d**). (**a, c**) *Erm1* domain is increased and expanded anteriorly in the MNP mesenchyme at E10.5. (**b, d**) *Erm1* expression is increased and the domain of expression shifted from the posterior tip of the MNP to lateral of the nasal pit in the *Unicorn* individuals at E11.5. (c, d) Erm1 is expressed in the nasal pit epithelium at e10.5 and e11.5 in *Unicorn* individuals. Scale bars are 100 µm.

3.3.4 *Unicorn* patterning is normal at E12.5.

At E12.5, one day after the MNPs have begun to converge at the midline, the MNPs are now one confluent piece of tissue called the frontonasal process. In E12.5 control embryos, *Cbfa1*, an osteoblast specific transcription factor, is expressed in the paired premaxillary bones (Figure 36 A). *Unicorn* embryos also have paired *Cbfa1* premaxillary expression zones inferior to the nostrils, however the domains are flaring laterally (Figure 36 B). *Sox9*, a chondrocyte specific marker, is expressed in the nasal capsule, singular midline nasal septum, and the lateral fins that project inferiorly from the midline of the nasal septum in control embryos (Figure 36 C). *Sox9* is expressed in the same anatomical regions of the nasal capsule, bifurcated nasal septum, and the inferior nasal septum fins in the *Unicorn* embryos (Figure 36 D). *Erm1* expression is unchanged in *Unicorn* and control embryos at E12.5 (Figure 36 E, F). In both control and *Unicorn* embryos, *Erm1* is expressed at similar levels in the mesenchyme surrounding the nasal pit and the nasal septum (Figure 36 E, F). Though in the *Unicorn* embryos, the *Erm1* domain is expanded superiorly between the oral ectoderm and cartilaginous condensations of the *Unicorn* embryos (Figure 36 F). *Gli1* is expressed in the same mesenchymal domains of *Unicorn* and control E12.5 embryos, though expression is higher in the control embryos (Figure 36 G, H).

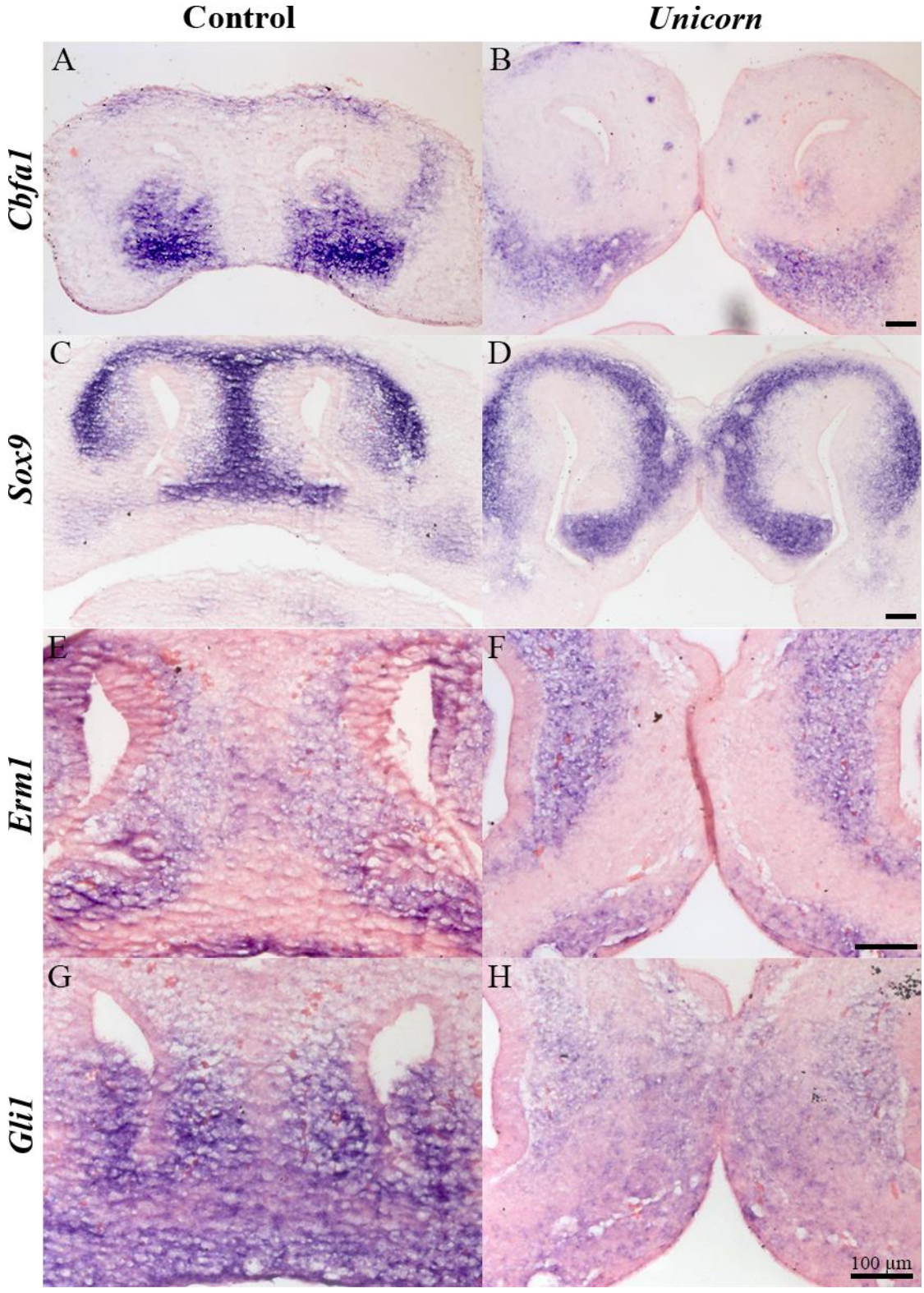
Control
Unicorn
A
B
C
D
E
F
G
H
Cbfa1
Sox9
Erm1
Gli1
100 µm

Figure 36. *Unicorn* mutants undergo normal mesenchymal patterning at E12.5.

E12.5 frontally sectioned *Unicorn* and littermate control embryos in situ hybridization of *Cbfa1* (**A-B**), *Sox9* (**C-D**), *Gli1* (**E-F**), and *Erm1* (**G-H**). (**A, B**) *Cbfa1* is expressed in the premaxilla of *Unicorn* and control embryos. (**C, D**) *Sox9* is expressed in the single nasal septum of the littermate control, as well as, in the duplicated nasal septum of the *Unicorn* embryos. (**E, F**) *Erm1* is expressed at similar levels and domains in the control and *Unicorn* embryos. The *Erm1* domain is expanded superiorly between the oral ectoderm and cartilaginous condensations of the *Unicorn* embryos. (**G, H**) *Gli1* expression surrounds the nasal septum in the control animals, as well as, in the (H) *Unicorn* embryos, though *Gli1* expression is decreased in the *Unicorn* embryos. Scale bars are 100 μm.

3.3.5 The presumptive nasal septum begins as a paired organ in the MNPs mesenchyme that converges into a midline organ during midfacial fusion.

Histological analysis of the *Unicorn* midfacial cleft phenotype revealed two nasal septa that were well formed, and individually the bifurcated nasal septa were approximately the same size as the singular midline nasal septum in the control embryos at E12.5 and E15.5 (Figure 31 A-F, Figure 36 C-D). The nasal septum is classically described as a singular midline organ, but earlier morphogenesis of the osteocartilaginous organ has not been well described within the literature. We hypothesized that the nasal septum develops within each MNP individually and merges at the midline during midline MNP convergence. Using the *Unicorn* mice, and Col2-Cre^{ERT} x Tdtomato mice, I will describe the earliest developmental steps during nasal septum morphogenesis.

At E15.5, the nasal septum is a singular midline organ located within the frontonasal process in control animals (Figure 31 A, C, E). At E12.5, the MNPs met at the midline one day prior (E11.5) and began to converge together. At this developmental stage in control animals, anteriorly the nasal septum is one midline organ. Intriguingly though, posteriorly at E12.5, the bottom of the nasal septum flares out laterally (Figure 36 C-D, Figure 37 D). One day prior, at E11.5, the anterior portion of the nasal septum is singular though much wider than found at E12.5 (Figure 37 A, B, Figure 38 F, I, I'). The posterior portion of the nasal septum again projects out laterally to the sides into the MNPs, and the posterior medial portion of the nasal septum assumes a more acute angle (Figure 37 A. B). However, in the *Unicorn* mice at stages E12.5 and E11.5, the nasal septum is bifurcated as it was at E15.5, but at these earlier developmental stages, the nasal septum was visualized as mesenchymal condensations within the MNPs (Figure 37 C, E). However, we could not identify the presumptive nasal septum in serial H&E sections at E10.5 in the *Unicorn* nor the control embryos.

We approached visualizing nasal septum morphology at stages earlier than E11.5 in normal embryos that express the reporter: Col2-Cre^{ERT};Tdtomato embryos (Figure 38). In these mice, prior to recombinase excision, cells express Tomato (mT), a membrane localized red fluorescent protein. Cre recombinase (mG) is expressed as green fluorescent protein in the membrane of cells that express Collagen 2, but only after the addition of tamoxifen. Tamoxifen binds to the Cre estrogen receptor and allows nuclear translocation and recombination in Collagen 2 cells. After injection of tamoxifen, the recombinase will excise a stop codon and prevent the expression of Tomato (mT) in the Cre recombinase expressing cells (Collagen 2). We controlled for recombinase activity by not injecting tamoxifen and collecting embryos at E10.5 (Figure 38 A, D, G). We induced Cre expression at E9.5 with 50 ug/ml Tamoxifen IP injections (Figure 38 E, F, H, I, J, K). We collected the Col2-Cre^{ERT} x Tdtomato embryos at E10.5 and E11.5, and photographed the labeled Collagen 2 expressing presumptive nasal septum cells in the MNPs (Figure 38).

Excitingly, we observed many labelled cells (green) near the medial edges of the MNPs at E10.5 (Figure 38 E, H, J). The cells seem to be assembled into bilateral rods-suggesting that the singular nasal septum starts as paired condensations between E9.5 and E10.5. These rods are similar to the bifurcated MNPs when the MNPs fail to fuse during early stages of *Unicorn* embryos at E11.5 (Figure 37 B, D). Between E10.5 and E11.5, *Collagen2-Cre* positive cells begin to migrate towards the midline and accumulate together in bilateral rods in the MNPs, as well as, caudally in the midline (Figure 38 F, I, K).

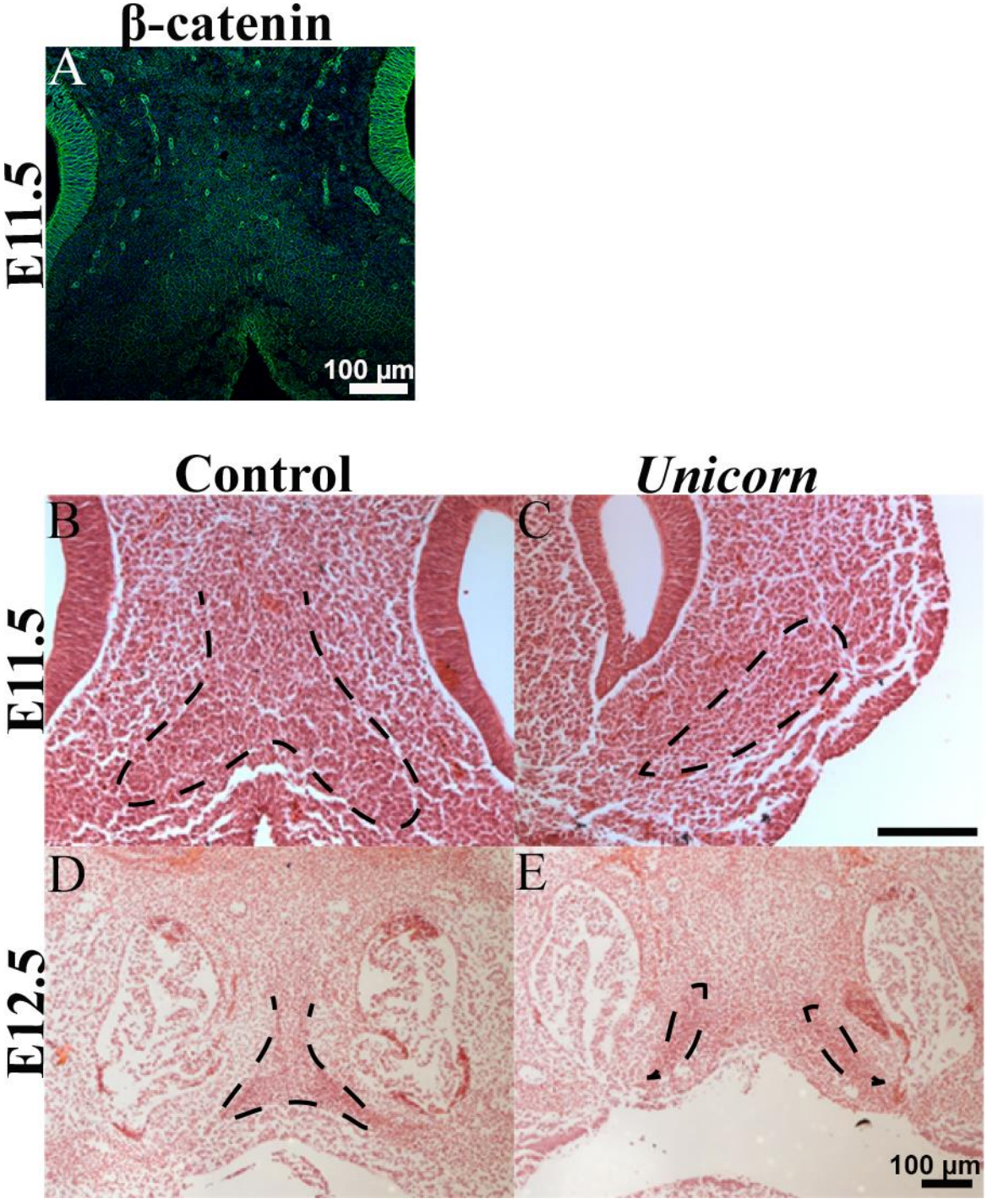
β-catenin
A
E11.5
100 µm
Control
Unicorn
B
C
E11.5
D
E
E12.5
100 µm

Figure 37. The *Unicorn* nasal septa are displaced laterally and develop autonomously within the MNPs.

(**A**) Confocal immunofluorescent stacks staining to β-catenin outlining the nasal septum at E11.5 in a control animal. (**B-E**) H&E stained sections of *Unicorn* and control embryos at E11.5 (**B-C**) and E12.5 (**D-E**). (**B**) In control embryos, at E11.5, the nasal septum is a single strut of cartilage cranially that then splits into two rods that extend laterally into the paired MNPs. (**C**) In the E11.5 *Unicorn* embryos, the nasal septum exists as a single condensation in each of the paired MNPs. (**D**) In control animals at E12.5, the anterior half of the nasal septum has become narrower, and the posterior fins of the nasal septum still project out laterally into the MNPs. (**E**) In contrast, the nasal septa of the *Unicorn* embryos at E12.5 remain as two individual cartilaginous condensations within the unfused MNPs. Scale bars are 100 μm.

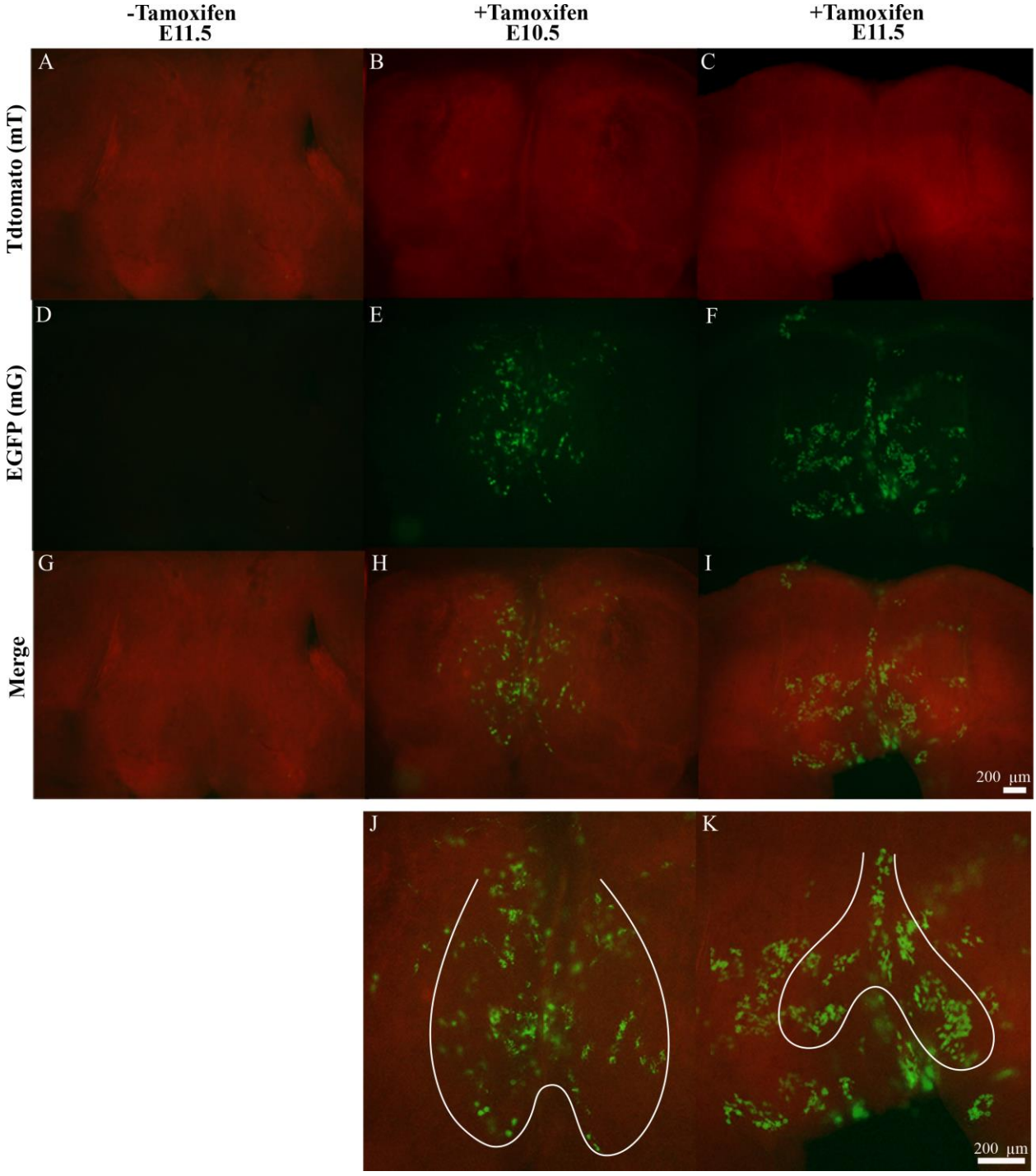
-Tamoxifen
E11.5
+Tamoxifen
E10.5
+Tamoxifen
E11.5
Tdtomato (mT)
EGFP (mG)
Merge
A
B
C
D
E
F
G
H
I
J
K
200 µm
200 µm

Figure 38. Collagen 2 expressing cells are arranged in paired rods in the merging MNPs at E10.5

Morphogenesis of the normal nasal septum at E10.5 **(E, H, J)** and E11.5 **(F, I, K)**. (**A-K**) Col2-Cre^{ERT} mice bred to Tdtomato mice. Ubiquitous red fluorescence from the Tdtomato locus, and the cells that express *Collagen2-Cre* express EGFP and are fluorescing green. (**A, D, G**) In the absence of tamoxifen, there are no EGFP expressing cells. (**B, E, H, J**) Cre-recombination was induced E9.5 with 50 ug/ml tamoxifen and embryos were collected at E10.5. Recombination was induced in many *Collagen2-Cre* positive cells in the MNPs. The *Collagen2-Cre* positive cells are present as two bars along the medial edge of the MNPs. (**C, F, I, K**) Cre-recombination was induced E9.5 with 50 ug/ml tamoxifen and embryos were collected at E11.5. *Collagen2-Cre* positive cells in the bilateral bars condensed together towards the midline of the MNPs at E11.5. Scale bars are 100 μm.

3.3.6 *Unicorn* MNP medial edge epithelial cells have increased epithelial cell markers and loss of apical cell polarity during medial convergence.

Currently within the literature, the merging mechanisms of the anterior facial prominences is unknown, though many have speculated that they may undergo the same epithelial seam regression mechanisms as the palatal shelves (Cox 2004; Gaare and Langman 1977; Jiang et al. 2006; Sun et al. 2000). Though, there is not one proven mechanism of action, but three proposed cellular mechanisms to explain the regression of the palatal epithelial seam. The proposed mechanisms for palatal epithelial regression include an epithelial to mesenchymal transformation (Fitchett and Hay 1989; Griffith and Hay 1992; Jin and Ding 2006; Martınez-Alvarez et al. 2000; Nawshad et al. 2004; Shuler et al. 1991; Shuler et al. 1992), apoptosis (Cuervo and Covarrubias 2004; Martınez-Alvarez et al. 2000; Mori et al. 1994; Taniguchi et al. 1995), and lateral migration of the epithelial cells, and active cell extrusion (Carette and Ferguson 1992; Kim et al. 2015). Given the compelling evidence from these past studies, I have hypothesized that these principles from the palate will likely participate in the convergence of the apical basal polarized epithelium of the MNPs. To test this hypothesis, I have tested the expression and localization of epithelial and mesenchymal markers in the MNP medial edge epithelium before (E10.5) and after (E11.5) medial lip convergence.

β-catenin is involved in the regulation of cell to cell adhesion within epithelial cells by linking to cadherin complexes. At E10.5, the *Unicorn* MNP medial edge epithelium has increased levels of β-catenin that surrounds the proximo-distal surfaces of the epithelial cells in comparison to control levels of β-catenin (Figure 39 B). At E11.5, β-catenin expression surrounds the epithelial cells in *Unicorn* and control embryos, but β-catenin is specifically localized around the cells in the *Unicorn* embryos (Figure 39, C, D). Additionally, *Unicorn* MNP medial edge epithelial cells have

increased levels of Na, K-ATPase, an essential component of epithelial tight junctions at E10.5 (Figure 39 F), as well as, at E11.5 (Figure 39 H). At E10.5, *Unicorn* embryos have increased levels of E-cadherin, an intracellular epithelial adhesion molecule (Figure 40 B). E-cadherin expression is increased proximo-distally in the MNP medial edge epithelial cells in comparison to littermate controls at E10.5 (Figure 40 A, B). At E11.5, E-cadherin expression expands to surround the entire periphery of the MNP epithelial cells in the *Unicorn* embryos (Figure 40 D). The expression level of E-cadherin is largely increased from the low E-cadherin levels present in the littermate controls at E11.5 (Figure 40 C). Additionally, aPKCι, an apical polarity marker, is decreased at the apical surface of the *Unicorn* MNP medial edge epithelium at both E10.5 (Figure 40 F) and E11.5 (Figure 40 H).

Intriguingly, *Unicorn* MNP medial edge epithelial cells are able to upregulate comparable levels of the mesenchymal marker, vimentin at E10.5 (Figure 41 A, B). Though by E11.5, vimentin levels are greatly reduced from those observed in the control animals (Figure 41 C, D).

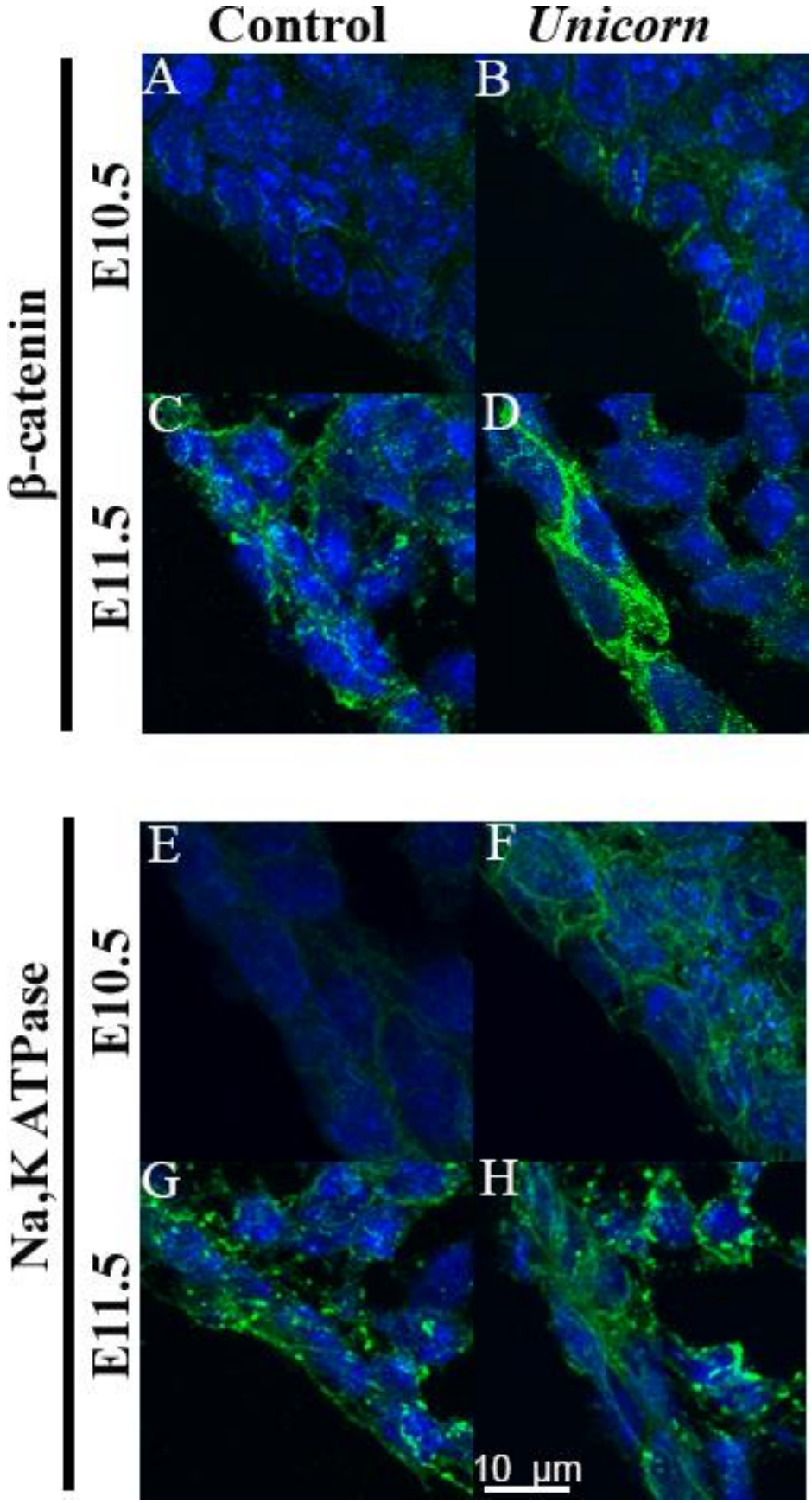
Control
Unicorn
β-catenin
E10.5
E11.5
A
B
C
D
Na,K ATPase
E10.5
E11.5
E
F
G
H
10 µm

Figure 39. *Unicorn* MNP medial edge epithelium have increased cell junctions.

Confocal stacks showing immunofluorescent staining to β-catenin and Na,K ATP-ase in the *Unicorn* MNP medial edge epithelial cells at E10.5 (**A-B, E-F**) and E11.5 (**C- D, G-H).** (**A-D**) β-catenin is increased in *Unicorn* MNP medial edge epithelium at E10.5 (**A-B**) and E11.5 (**C-D**). Scale bar is 10 μm.

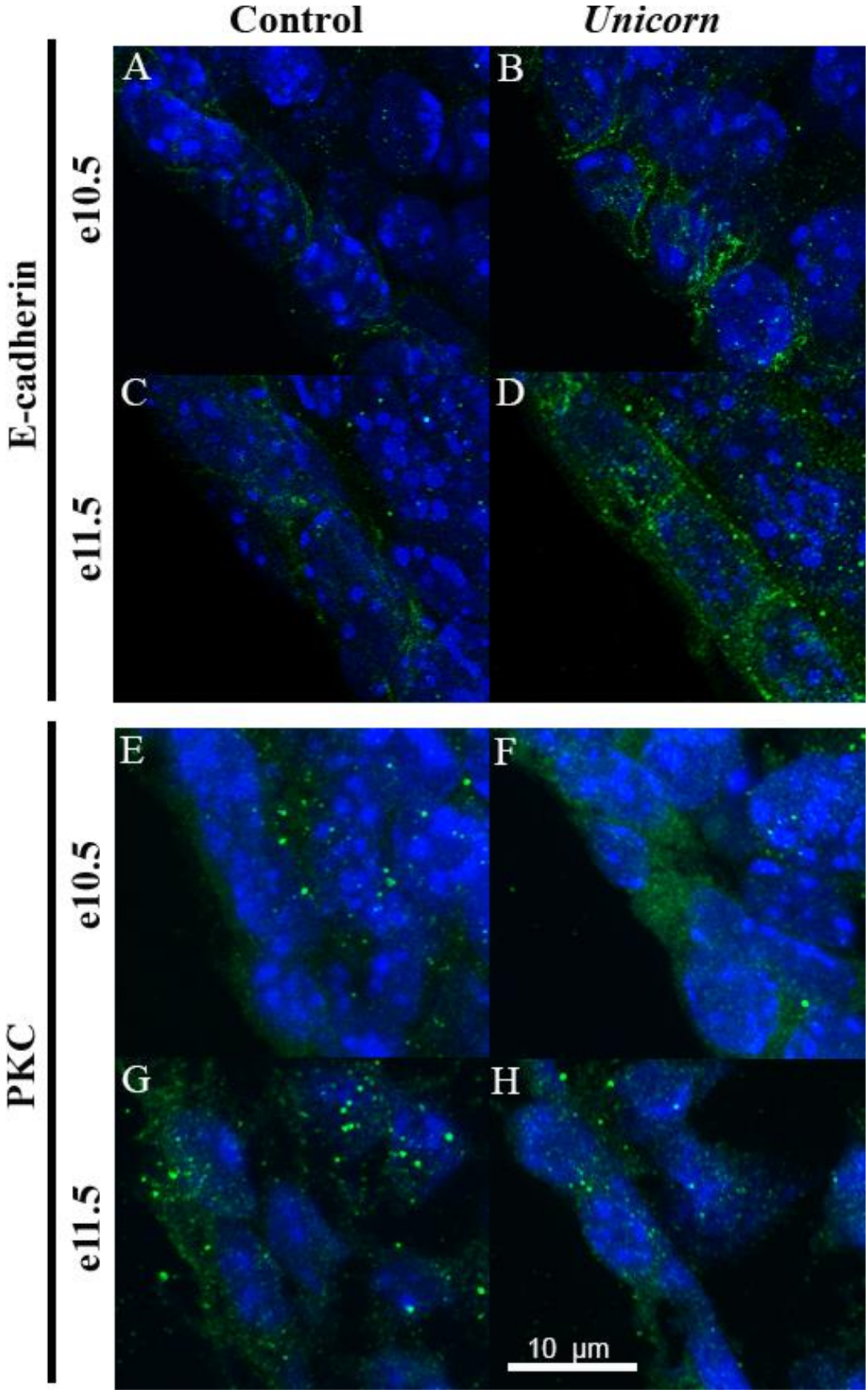
Control
Unicorn
E-cadherin
e10.5
e11.5
PKC
e10.5
e11.5
A
B
C
D
E
F
G
H
10 µm

Figure 40. *Unicorn* embryos have increased junctions and decreased cell polarity in MNP medial edge epithelial cells.

Confocal stacks showing immunofluorescent staining to E-cadherin and PKC in the *Unicorn* MNP medial edge epithelial cells at E10.5 (**A-B, E-F**) and E11.5 (**C- D, G-H).** Increased E-cadherin staining is observed in the *Unicorn* medial edge epithelium at E10.5 (**A-B**) and E11.5 (**C-D**). PKC is decreased at the apical surface of the medial edge epithelium at E10.5 (**E-F**) and E11.5 (**G-H**) in *Unicorn* embryos. Scale bar is 10 µm.

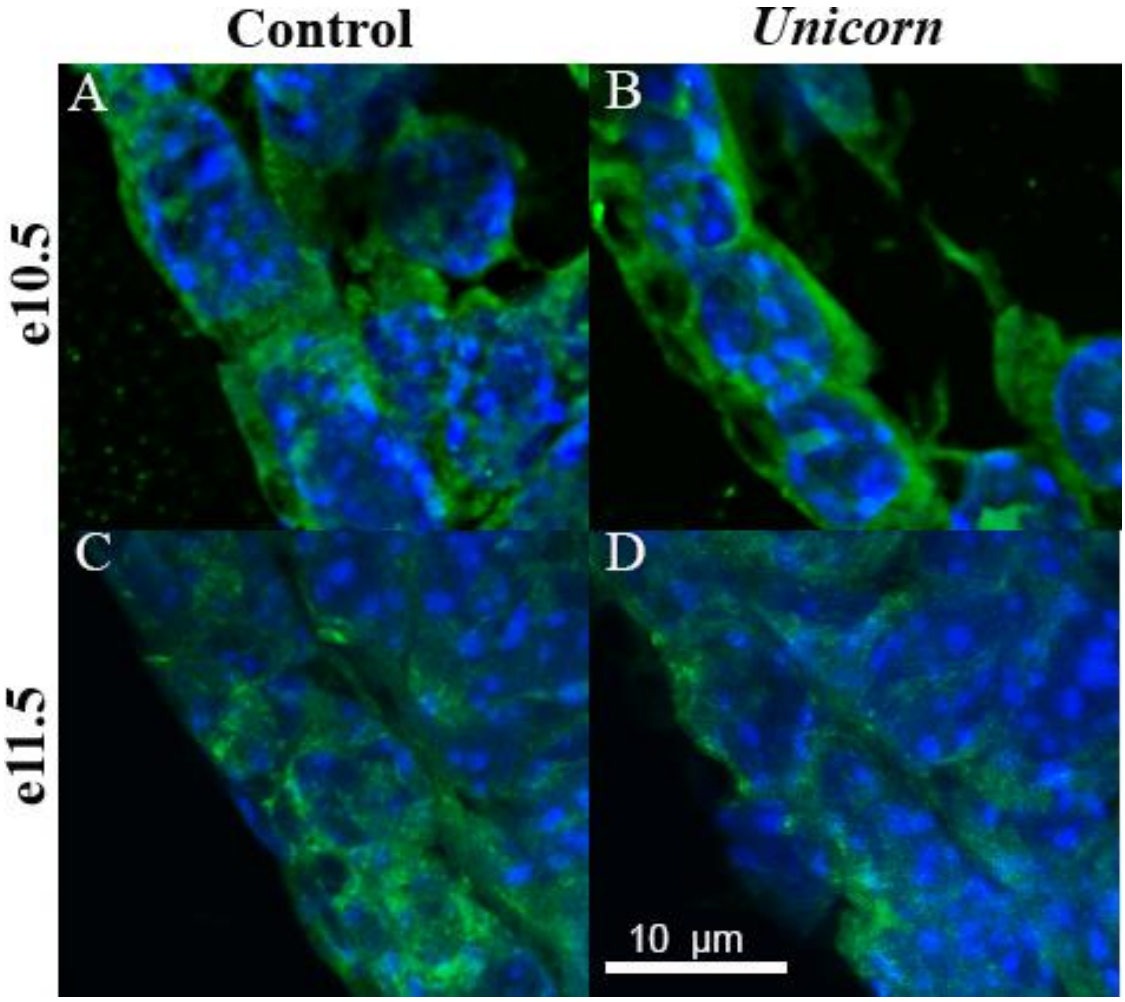
Control
Unicorn
A
B
C
D
e10.5
e11.5
10 µm

Figure 41. *Unicorn* medial edge epithelial cells have decreased mesenchymal markers at E11.5.

Confocal stacks showing immunofluorescent staining to vimentin in the *Unicorn* MNP medial edge epithelial cells at E10.5 (**A, B**) and E11.5 (**C, D**). (**A, B**) *Unicorn* MNP medial edge epithelial cells have similar levels of vimentin compared to littermates at E10.5. (**C, D**) Vimentin is decreased in *Unicorn* MNP medial edge epithelial cells at E11.5. Scale bar is 10 μm.

3.3.7 *Unicorn* embryos have decreased proliferation in caudal MNPs.

Due to the morphological differences present in *Unicorn* embryos facial prominences, we investigated cellular proliferation in the MNPs at E10.5 and E11.5. We tested cellular proliferation in two ways, PHH3 and BrdU (Bromodeoxyuridine). It has been shown that when histone H3 is not undergoing cellular proliferation histone H3 is not phosphorylated (Hendzel et al. 1997). During the G2 and M phase of mitosis, histone H3 is phosphorylated, thus indicating that the cell is undergoing cellular proliferation (Hendzel et al. 1997; Juan et al. 1998). BrdU, a thymidine analog, demarcates cellular proliferation by incorporating into DNA during the S phase of replication. Cells undergoing proliferation were counted in the cranial and caudal mesenchyme at both E10.5 and E11.5 (Figures 42-44 A). At E10.5, proliferating cells were counted in one area of the adjacent epithelium (Figure 42 A, Figure 43 A). Two areas in the medial edge epithelium adjacent to the mesenchymal boxes were counted at E11.5 (Figure 42 A, Figure 44 A).

At E10.5, *Unicorn* embryos have significantly less proliferation within the caudal mesenchyme when evaluated via BrdU (Figure 43 B, C). There were significant differences within the caudal epithelium at E11.5 when evaluated via PHH3 (Figure 42 C). Though, PHH3 differences were not significant at E10.5, but there was a decrease in proliferation within the mesenchyme in *Unicorn* embryos (Figure 42 B, C). AT E11.5, there are no significant differences between the percentage of BrdU positive cells at E11.5, but the *Unicorn* embryos do have less proliferation within the mesenchyme (Figure 44 B, C).

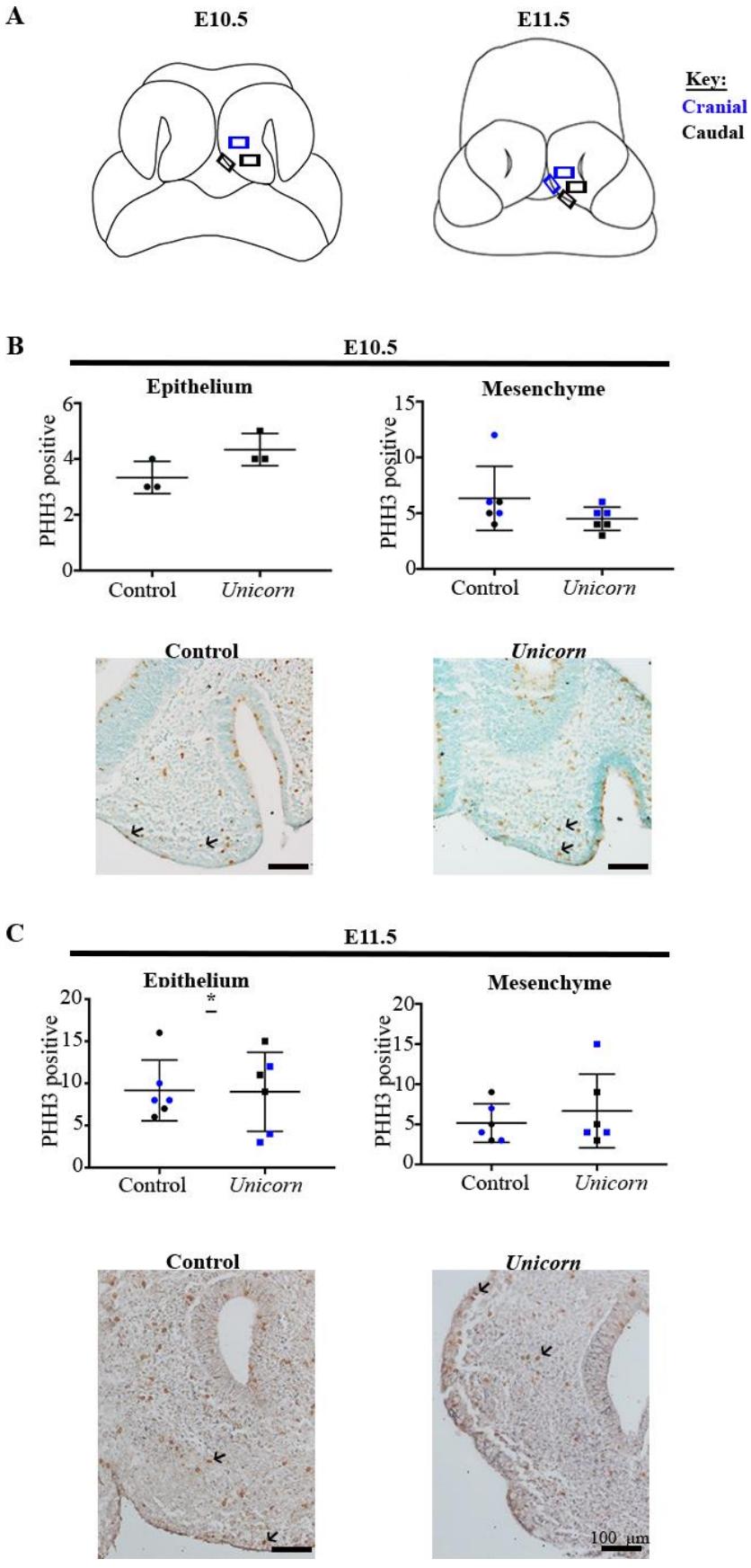
A
E10.5
E11.5
Key:
Cranial
Caudal
B
E10.5
Epithelium
Mesenchyme
PHH3 positive
Control
Unicorn
Control
Unicorn
C
E11.5
Epithelium
Mesenchyme
*
PHH3 positive
Control
Unicorn
Control
Unicorn
100 µm

Figure 42. *Unicorn* embryos have less proliferation in the medial edge epithelium at E11.5.

Proliferation measured in *Unicorn* epithelium and mesenchyme before (E10.5) and after (E11.5) MNP midline fusion. (**A**) Schematics of representing box placement for counting PHH3 positive cells. Two boxes were drawn and counted within the mesenchyme of E10.5 and E11.5 embryos. One box was placed adjacent in the epithelium of E10.5 embryos. Two boxes were placed in the epithelium of E11.5 embryos. (**B**) Categorical scatterplots generated in Prism software for *Unicorn* and control epithelial and mesenchymal PHH3 positive cells at E10.5. Representative images of control and *Unicorn* MNP PHH3 stained sections at E10.5. (**C**) Categorical scatterplots for *Unicorn* and control PHH3 positive cells, and representative images for E11.5 embryos. *Unicorn* embryos epithelium had significantly less PHH3 positive cells at E11.5 (P-value = 0.0274). Scale bars are 100 μm.

A

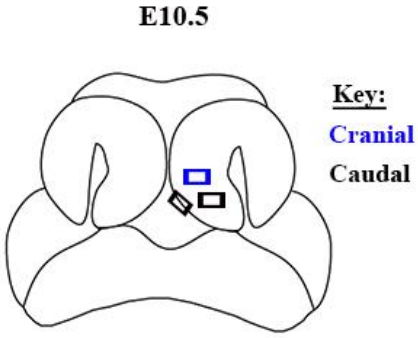
E10.5
Key:
Cranial
Caudal

B

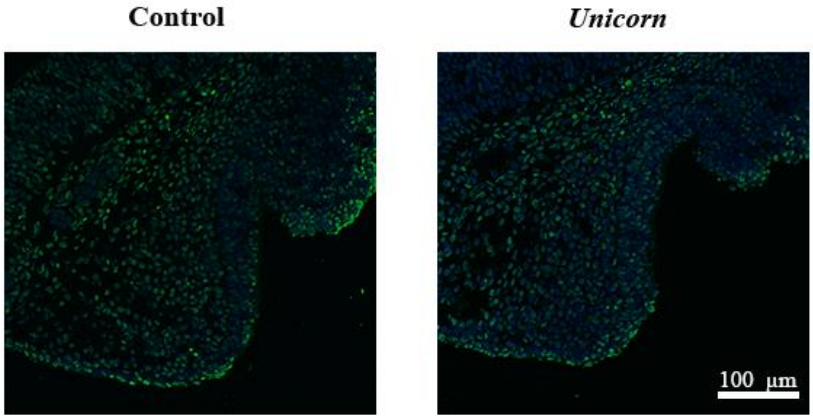
Control
Unicorn
100 µm

C

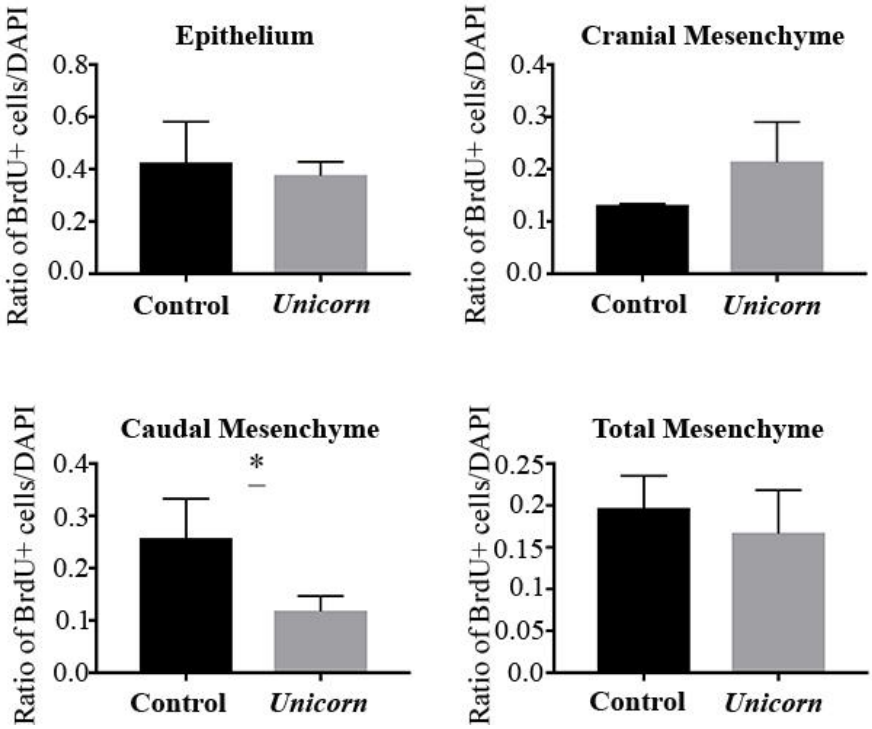
Epithelium
Ratio of BrdU+ cells/DAPI
0.8
0.6
0.4
0.2
0.0
Control
Unicorn
Cranial Mesenchyme
0.4
0.3
0.2
0.1
0.0
Caudal Mesenchyme
*
Total Mesenchyme
0.25
0.15
0.05

Figure 43. *Unicorn* anterior mesenchyme has less DAPI positive cells at E10.5.

(**A**) Schematic representing box placement for counting BrdU positive cells and DAPI nuclei. Two boxes were drawn and counted within the mesenchyme of E10.5 embryos. One box was placed adjacent in the epithelium of E10.5 embryos. (**B**) Confocal stacks showing immunofluorescent staining to BrdU in the MNP at E10.5. (**C**) Ratios of BrdU positive cells/ total DAPI cells. Cells were counted in one area of the epithelium and two areas of the mesenchyme. Individual mesenchymal boxes were added together for the total mesenchyme. *Unicorn* anterior mesenchyme have significantly less BrdU positive cells at E10.5 (p-value= 0.029). Significance evaluated by students t-test.

A

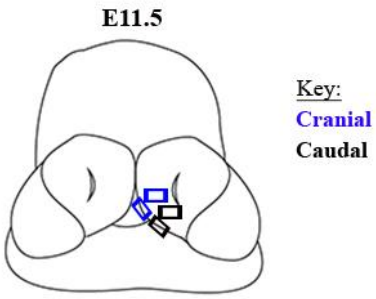
E11.5
Key:
Cranial
Caudal

B

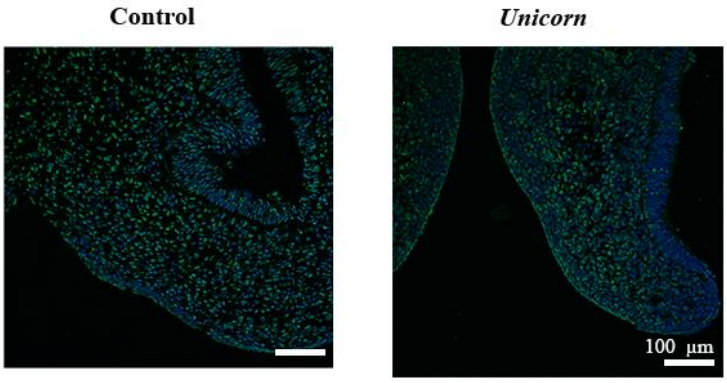
Control
Unicorn
100 µm

C

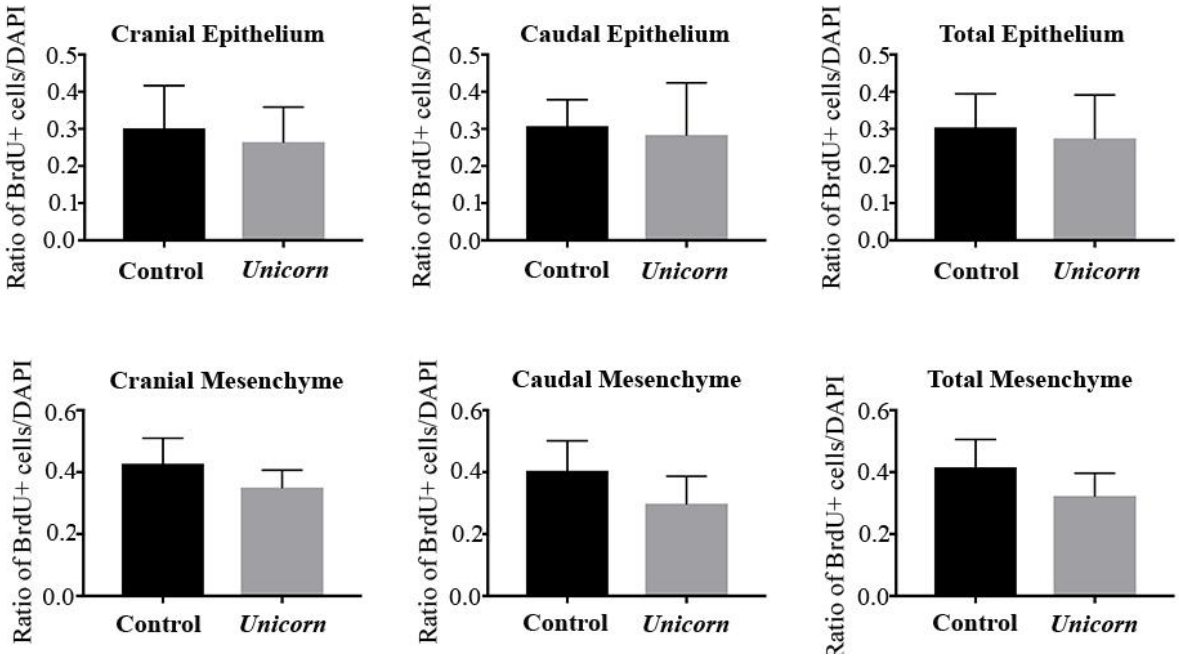
Cranial Epithelium
Caudal Epithelium
Total Epithelium
Cranial Mesenchyme
Caudal Mesenchyme
Total Mesenchyme
Ratio of BrdU+ cells/DAPI
Control
Unicorn

Figure 44. *Unicorn* MNP proliferation is not different at E11.5 when evaluated via BrdU.

(**A** Schematics of representing box placement for counting BrdU positive cells. Two boxes were drawn and counted within the mesenchyme of E11.5 embryos. Two boxes were placed in the epithelium of E11.5 embryos. (**B**) Confocal stacks showing immunofluorescent staining to BrdU in the MNP at E11.5. (**C**) Ratios of BrdU positive cells/ total DAPI cells. Cells were counted in two areas in the epithelium and mesenchyme. Individual epithelial and mesenchymal boxes were added together for the total epithelium and mesenchyme. Significance evaluated by students t-test.

3.3.8 *Unicorn* MNPs do not have increased cell death during MNP fusion.

In the palate, there is evidence that the medial edge epithelial cells disappear via apoptosis (Cuervo and Covarrubias 2004; Martınez-Alvarez et al. 2000; Mori et al. 1994; Taniguchi et al. 1995). Apoptosis is a controlled process of cell death. Apoptotic cellular death is regulated by proteases, called caspases that mediate cleavage during early apoptosis. During later stages of apoptosis, endonucleases are activated and fragment the DNA. TUNEL (terminal deoxynucleotidyl transferase (TdT) nick end labeling) labels the cleaved DNA fragments. Due to the medial edge epithelium data in the palate, we tested whether *Unicorn* embryos have less apoptosis occurring in the MNP medial edge epithelium during MNP midline fusion.

Cells undergoing apoptosis were counted in the cranial and caudal mesenchyme at both E10.5 and E11.5 (Figure 42 A). At E10.5, apoptotic cells were counted in one area of the adjacent epithelium, and two areas in the epithelium at E11.5 (Figure 42 A). We did not find any significant apoptotic differences in the epithelium nor mesenchyme of the *Unicorn* embryos at E10.5 or E11.5 (Figure 42 B, C). Though at E11.5, we did notice significantly more TUNEL positive cells located at the zone of fusion (Figure 42 C).

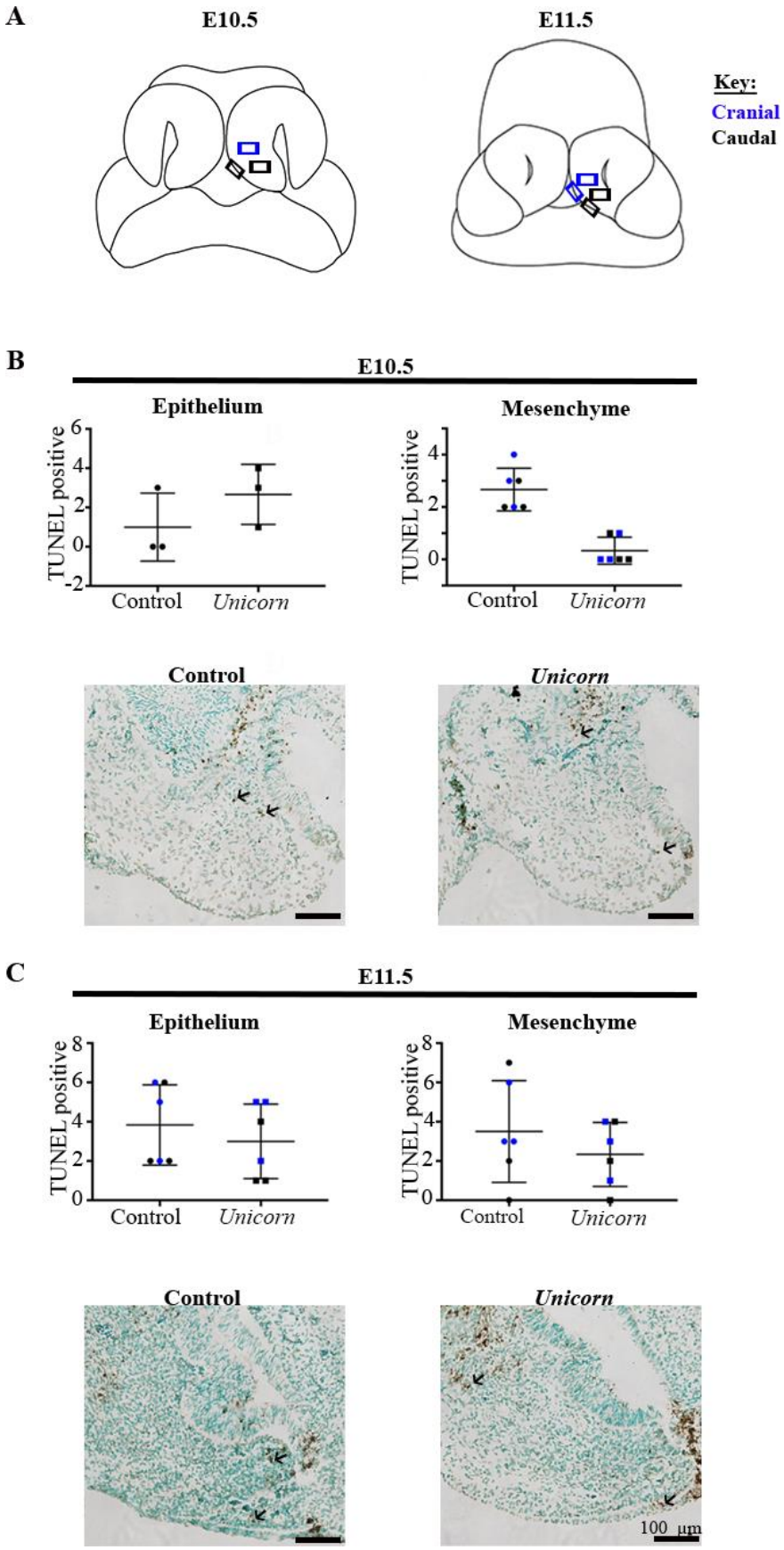
A
E10.5
E11.5
Key:
Cranial
Caudal
B
E10.5
Epithelium
Mesenchyme
TUNEL positive
Control
Unicorn
Control
Unicorn
C
E11.5
Epithelium
Mesenchyme
TUNEL positive
Control
Unicorn
Control
Unicorn
100 µm

Figure 45. *Unicorn* MNPs do not have increased apoptosis before and after medial MNP fusion.

Apoptosis measured in *Unicorn* epithelium and mesenchyme before (E10.5) and after (E11.5) MNP midline fusion. (**A**) Schematics of representing box placement for counting TUNEL positive cells. Two boxes were drawn and counted within the mesenchyme of E10.5 and E11.5 embryos. One box was placed adjacent in the epithelium of E10.5 embryos. Two boxes were placed in the epithelium of E11.5 embryos. (**B**) Categorical scatterplots generated in Prism software for *Unicorn* and control epithelial and mesenchymal TUNEL positive cells at E10.5. Representative images of control and *Unicorn* MNP TUNEL stained sections at E10.5. (**C**) Categorical scatterplots for *Unicorn* and control TUNEL positive cells, and representative images for E11.5 embryos. (**B-C**) No significant differences were measured. Scale bars are 100 μm.

3.4 DISCUSSION

The *Unicorn* line is a novel model that can accurately model severe phenotypes of midfacial clefting (Figure 30). The *Unicorn* mice midfacial cleft results from a bifurcation of the nasal septum and secondarily causes a cleft palate (Figure 30). Though many mouse lines currently available only develop palatal clefts, the *Unicorn* mice develop a midline cleft of the lip, nose, and palate (Figure 30). As in human cases of midfacial clefting, we have shown that the anatomy surrounding the cleft is normal in *Unicorn* embryos (Figure 30, Figure 31, Figure 36). Additionally, the *Unicorn* mice also develop a bifurcated nasal septum, which is a common finding in clinical cases of severe true midfacial clefting (Figure 31). The nasal septum is a key growth site responsible for midfacial chondrocranial growth during embryogenesis (Kvinnsland 1974; Sarnat and Wexler 1966; Scott 1953), though the early morphogenetic mechanisms of nasal septum development have not been studied, until now.

A poor understanding of normal midfacial morphogenesis, as well as, the pathogenesis of midfacial clefting and nasal septum dysmorphologies can be attributed to an overlooked significance of midfacial clefting due to underreporting. The prevalence of diagnosed midfacial clefting cases are low, but the spectrum of severity that midfacial clefting presents as may be accountable for this. Midfacial clefting is estimated to account for 0.43% to 0.73% of all craniofacial clefts, and to occur in approximately 1: 1,000,000 live births (Koh and Do Yeon Kim 2016; Urata and Kawamoto 2003). A small midline notch of the upper lip may go undiagnosed as it may not warrant a corrective surgery if the child is able to thrive and the cleft is not cosmetically concerning. However severe midfacial clefting cases that do require corrective craniofacial surgery to restore function are more likely to be reported and contribute to midfacial clefting prevalence rates. A low reported prevalence rate could attribute to a low necessity to understand normal

midfacial morphogenesis. The *Unicorn* embryos model human midfacial clefting. The *Unicorn* embryos lip, nose, and palate cleft, but are unique in that their causative mutation is unknown. After genome sequencing the *Unicorn* embryos, a novel causative mutation will be identified. Identification of a novel gene that is implicated in midfacial clefting will allow us to understand normal morphogenetic processes of MNP convergence.

We have provided evidence that the nasal septum is a bilaterally paired organ by visualizing with *Collagen2-Cre* positive cells in the MNPs as early as E10.5 (Figure 38). We continued to delineate nasal septum development and found that at E11.5 as the MNPs are beginning to converge, so do the bilaterally paired nasal septa located within the mesenchyme of the MNPs (Figure 37, 38). We found that the nasal septum first merges anteriorly at E11.5 (Figure 37, 38). The nasal septum then continues to fuse medially in the posterior direction as the MNPs continue to converge into a confluent piece of tissue, called the frontonasal process (Figures 31, 36, 37, 38). By E15.5, the nasal septum is fully merged at the midline (Figure 31). In the *Unicorn* embryos, the MNPs never fuse medially, so the nasal septum develops autologously in the nasal capsule (Figures 31, 36, 37).

In the case of severe midfacial clefting, such as that observed in the *Unicorn* embryos, that significant morphological changes within the facial prominences occur sometime between E10.5 and E11.5 (Figure 32, Figure 33). The MNPs of the *Unicorn* mice are turned laterally rather than medially at E10.5, and by E11.5 they develop a large internasal distance between the MNPs (Figure 32, Figure 33). At E10.5, the distance from the lateral edge of the lateral medial prominence to the inferior tip of the MNP (1, 6) was significantly shorter in the *Unicorn* embryos, perhaps contributing towards not pushing the MNPs towards the midline (Figure 32 C).

We initially hypothesized that perhaps the MNPs are turned laterally rather than medially, and do not make midline contact because of polarity defects within the medial edge epithelium. Our data showed that the *Unicorn* embryos do have a loss of apical cell polarity within the MNP medial edge epithelium at E10.5 and E11.5. The loss of apical cell polarity and the large internasal distance also played a part in separating the bilaterally paired FEZ from correctly coordinating cellular signaling pathways during midfacial convergence. My data has not allowed me to distinguish between the loss of apical cell polarity in the medial epithelium of the MNP or a potential loss of mesenchymal polarity as causative of the convergence failure.

I have shown that the FEZ signaling pathways (HH and FGF) are abnormal at E10.5, and E11.5 when we observed significant facial prominence morphology differences. In the *Unicorn* embryos, we have shown that HH signaling is decreased in the MNPs at E10.5 and E11.5 (Figure 34). We additionally show that FGF signaling is increased in the MNPs at E10.5 and E11.5 (Figure 35). We hypothesize that the disturbances within the FEZ signaling pathways has an impact upon the MNP medial edge epithelium as well as the underlying mesenchyme.

We found that during normal medial lip fusion processes that an epithelial to mesenchymal transformation must occur (Figure 39 - 41), similar to what has been shown in the palatal epithelial seam (Fitchett and Hay 1989; Griffith and Hay 1992; Jin and Ding 2006; Martınez-Alvarez et al. 2000; Nawshad et al. 2004; Shuler et al. 1991; Shuler et al. 1992). In the *Unicorn* mice, rather than losing epithelial cell markers like their littermate controls, the *Unicorn* medial edge epithelial cells maintained and even upregulated epithelial markers such as E-cadherin and β-catenin (Figure 39-40). Similar to wildtype embryos, the *Unicorn* medial edge epithelial cells upregulate vimentin at E10.5, but fails to increase its levels compared to control animals at E11.5 (Figure 41).

In conclusion, the midfacial cleft phenotype present in the *Unicorn* mice has revealed clues that has allowed us to understand normal midfacial morphogenesis. Through the *Unicorn* mice, we have been able to describe midfacial convergence and delineate the earliest stages of nasal septum morphogenesis. Additionally, we have presented molecular and cellular signaling that must occur for midfacial morphogenesis to occur.

3.5 SUPPLEMENTAL FIGURES

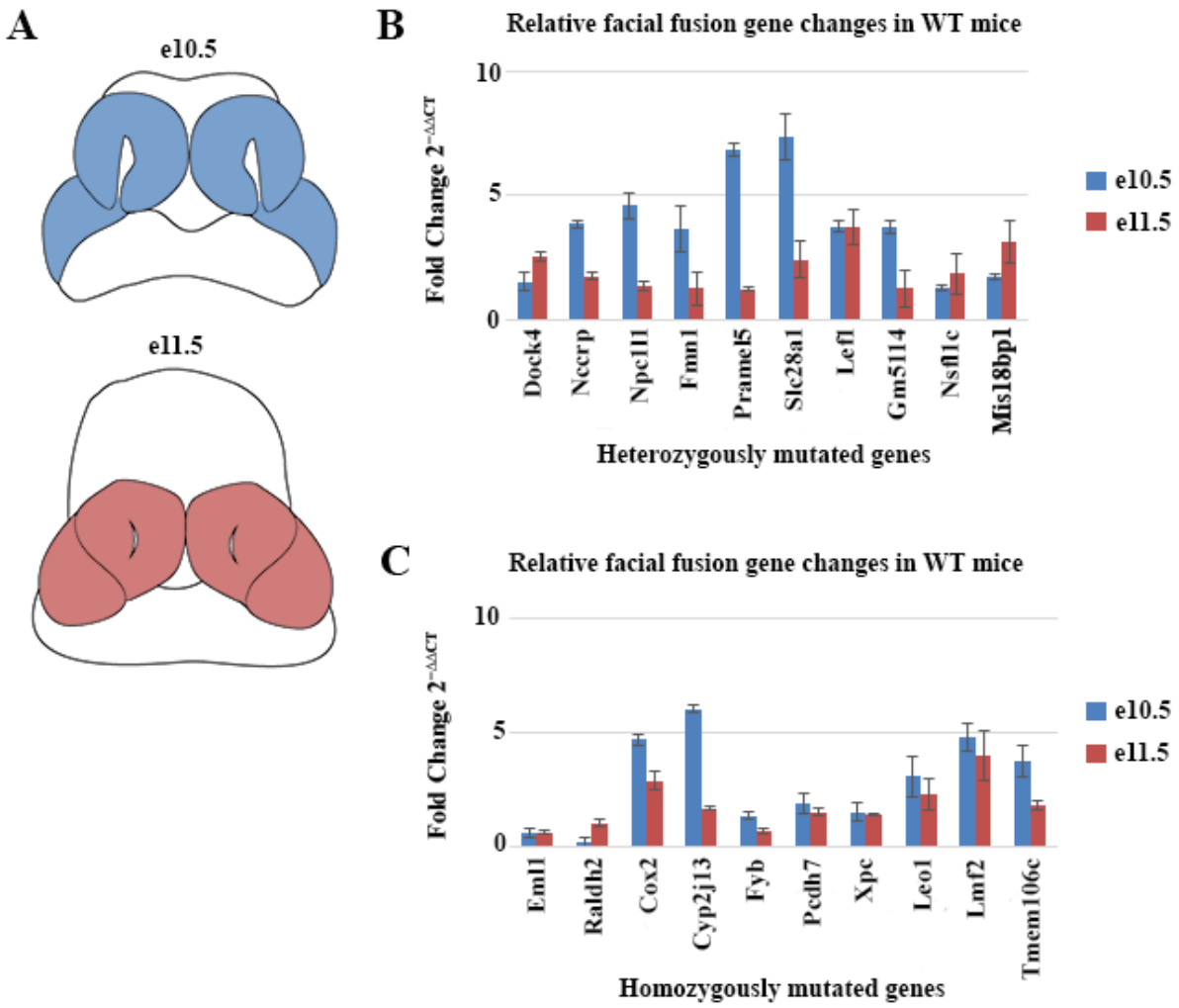

Figure 42. Supplemental 1. Genes mutated in founder *Unicorn* animals are expressed during midfacial convergence in wildtype mice.

Two F3 *Unicorn* phenotypic embryos were exome sequenced and realtime PCR primers were designed to assay if the mutated genes were expressed in the wildtype facial prominences undergoing midfacial convergence. (**A**) Schematic of the facial tissues used from E10.5 and E11.5 wildtype embryos as a source of RNA for Q-PCR. (**B - C**) Homozygous and heterozygous mutated genes in the *Unicorn* exome sequencing was normalized to *Hprt* and the fold change was calculated by normalizing to the expression in the body. We observed that all genes were expressed in the face during the time of medial convergence.

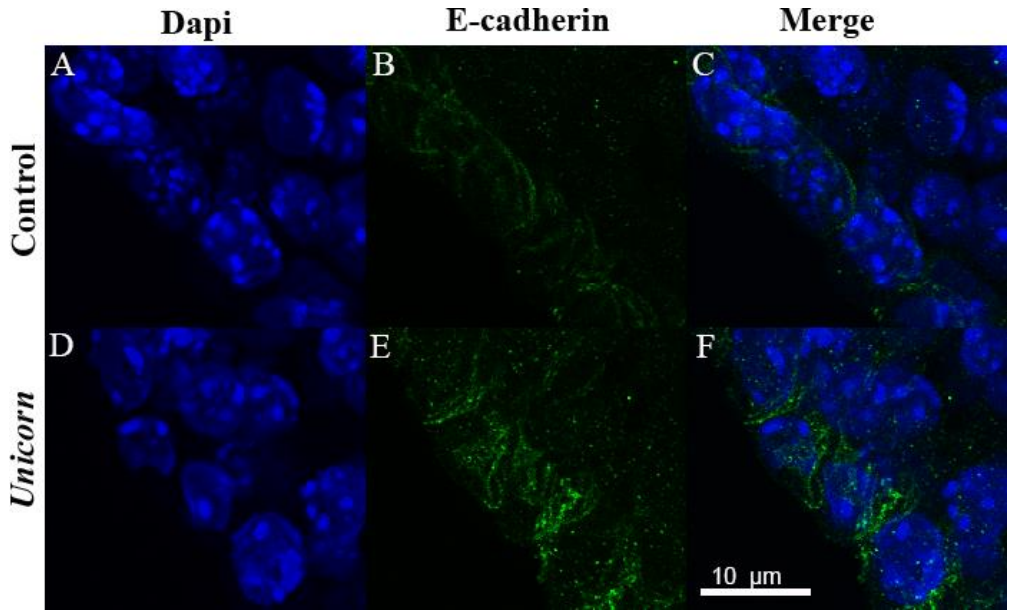

Figure 43. Supplemental 2. *Unicorn* E10.5 E-cadherin single channel.

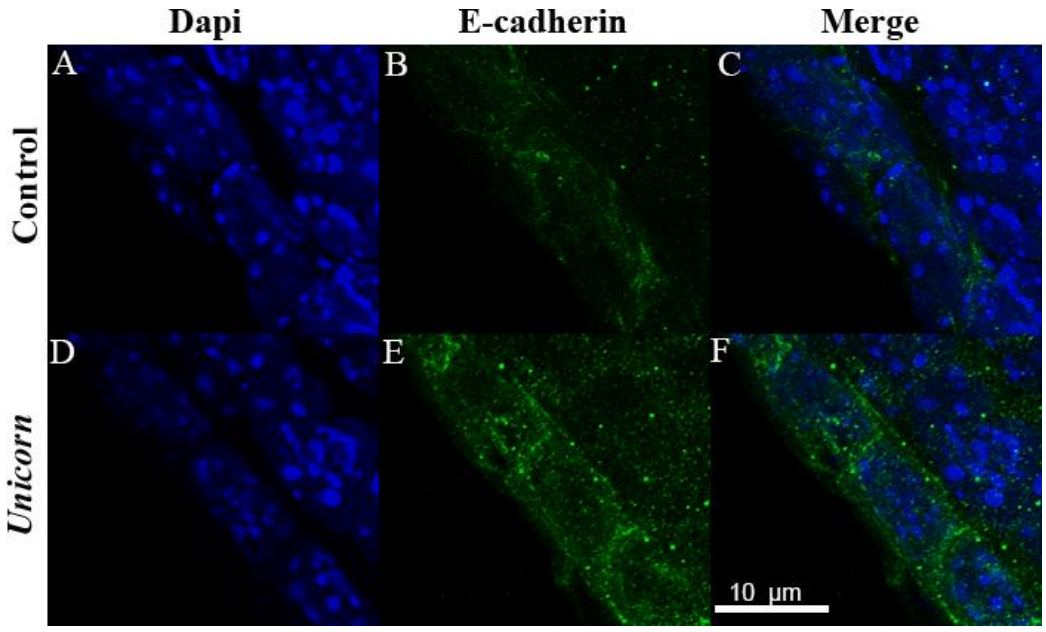

Figure 44. Supplemental 3. *Unicorn* E11.5 E-cadherin single channel.

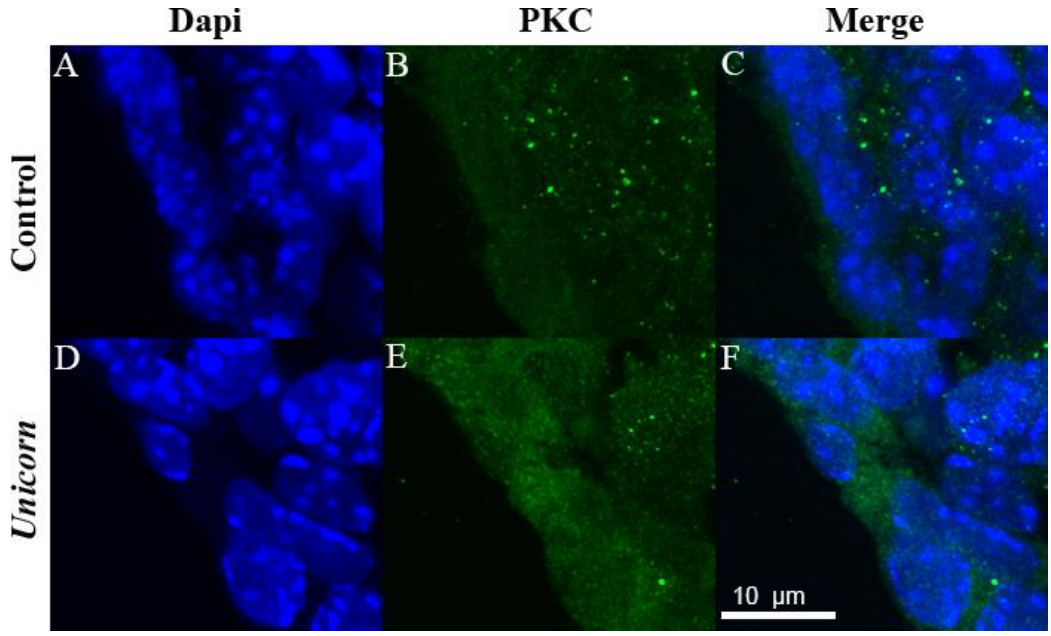

Figure 45. Supplemental 4. *Unicorn* E10.5 PKC single channel.

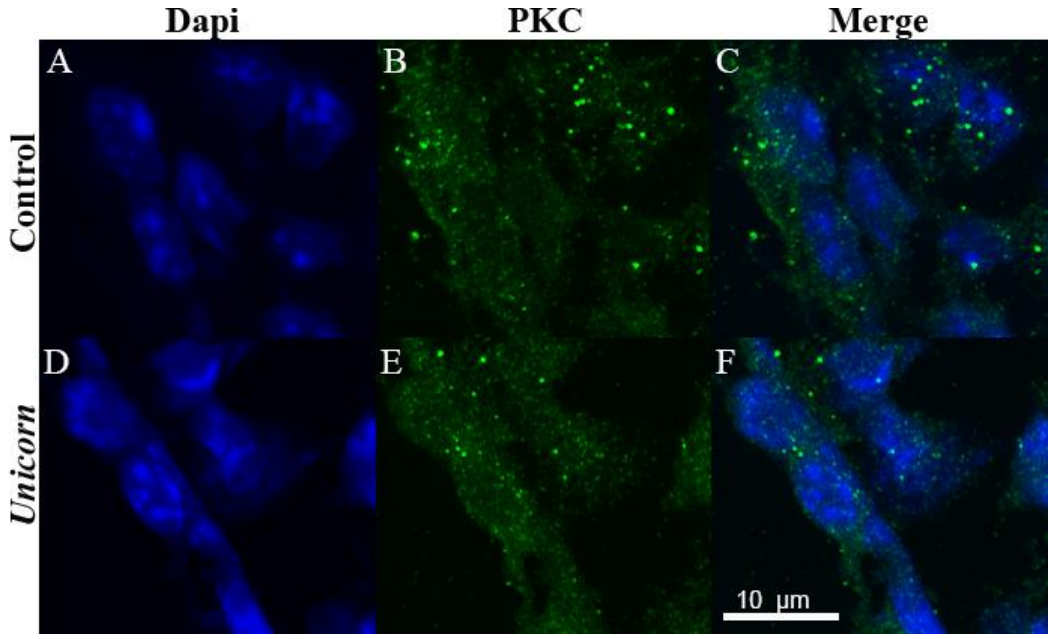

Figure 46. Supplemental 5. *Unicorn* E11.5 PKC single channel.

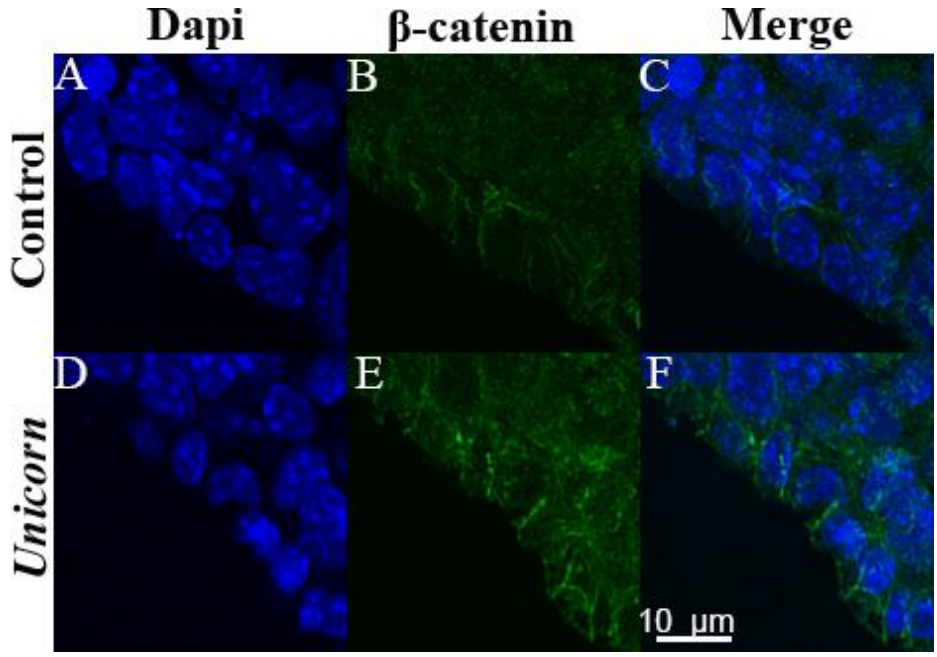

Figure 47. Supplemental 6. *Unicorn* E10.5 β-catenin single channel.

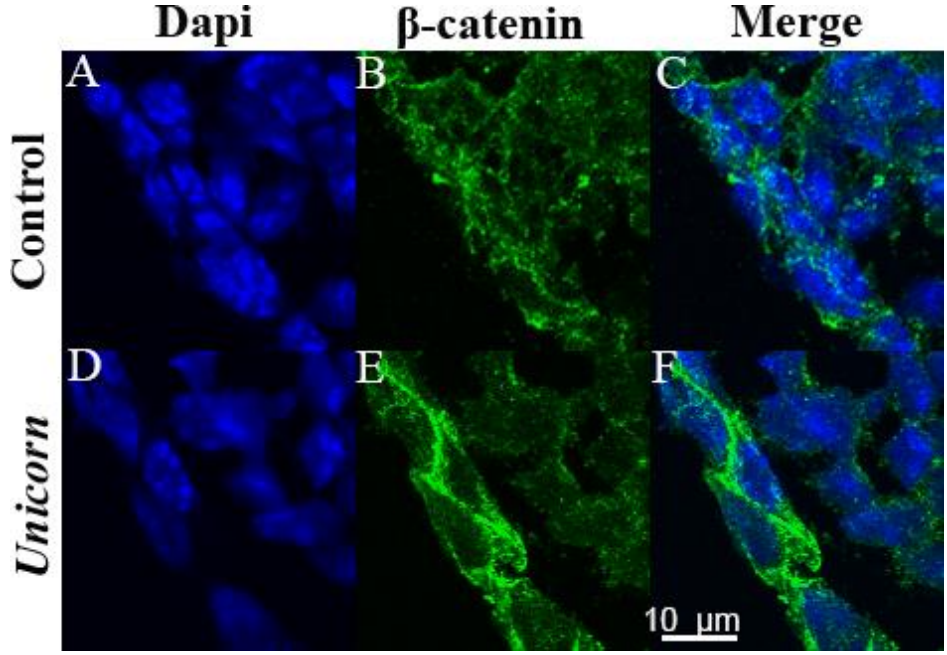

Figure 48. Supplemental 7. *Unicorn* E11.5 β-catenin single channel.

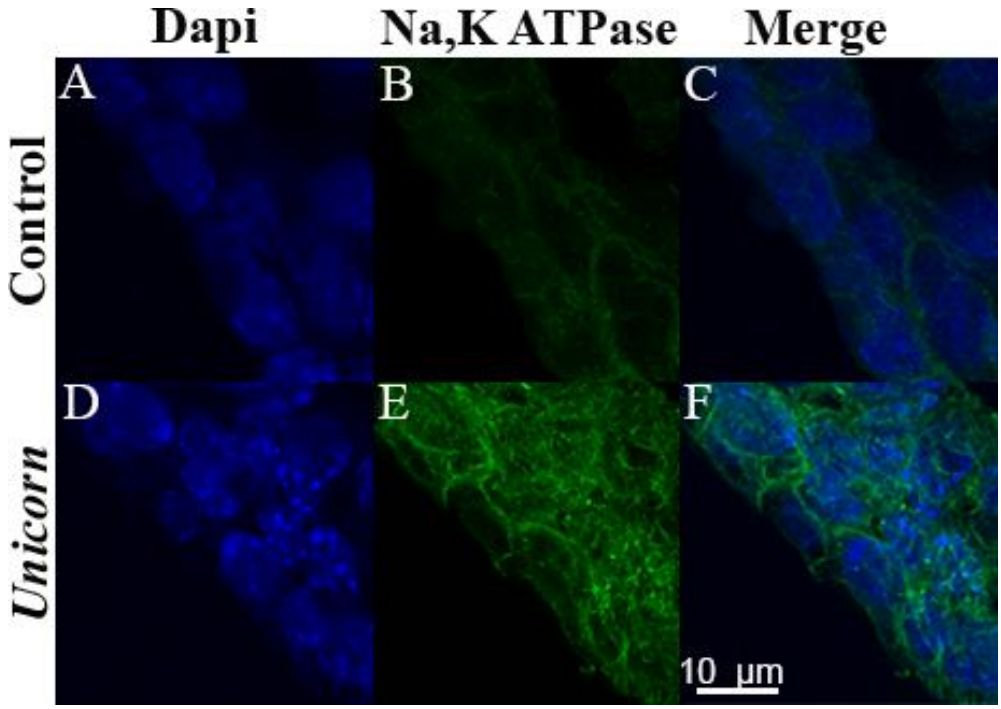

Figure 49. Supplemental 8. *Unicorn* E10.5 Na,K ATPase single channel.

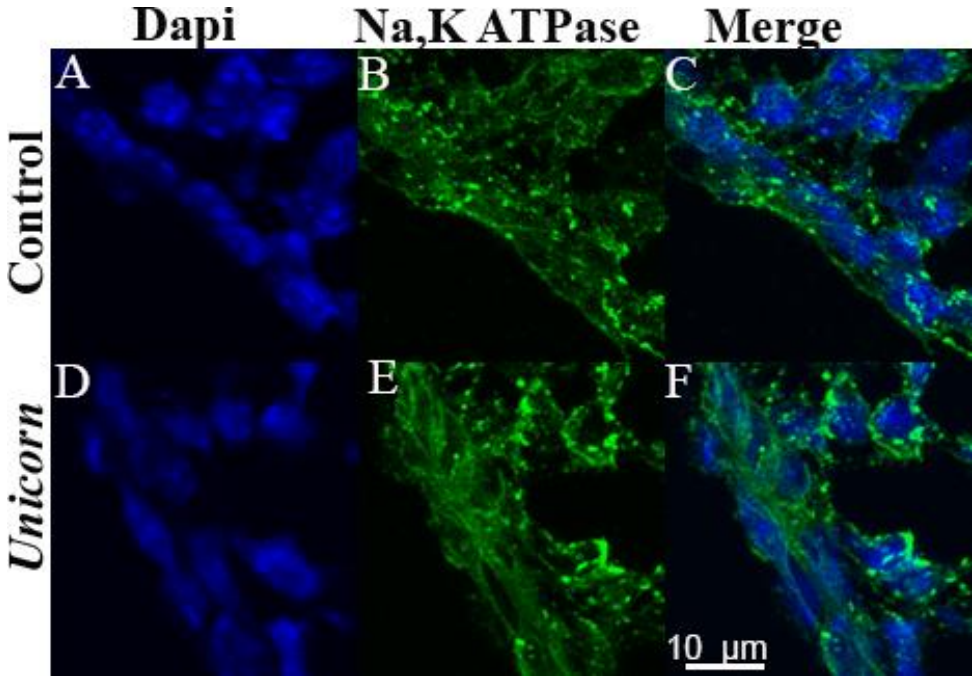

Figure 50. Supplemental 9. *Unicorn* E11.5 Na,K ATPase single channel.

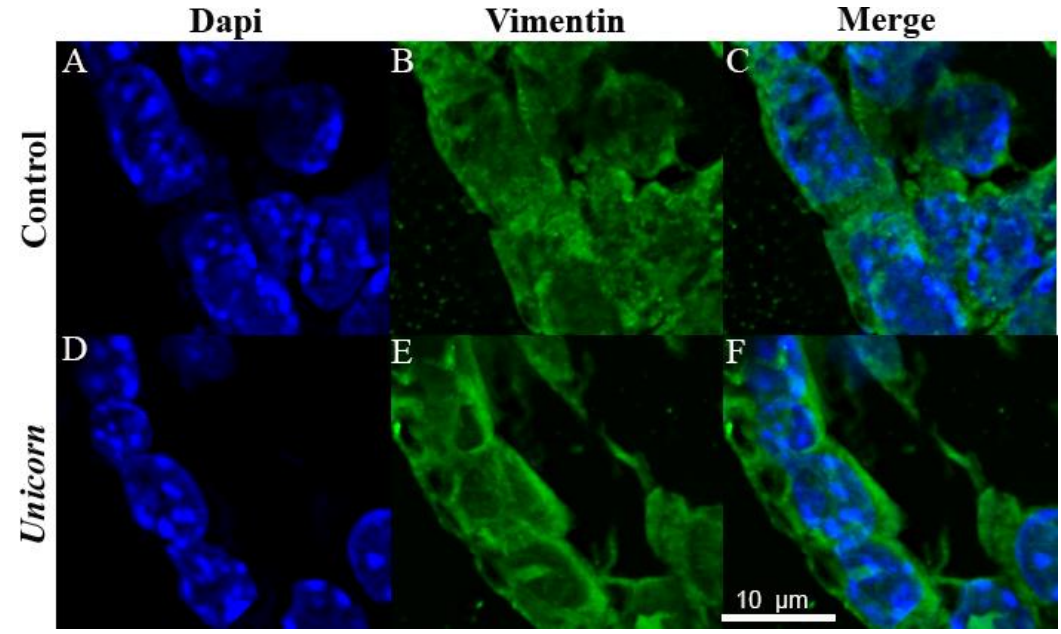

Figure 51. Supplemental 10. *Unicorn* E10.5 vimentin single channel.

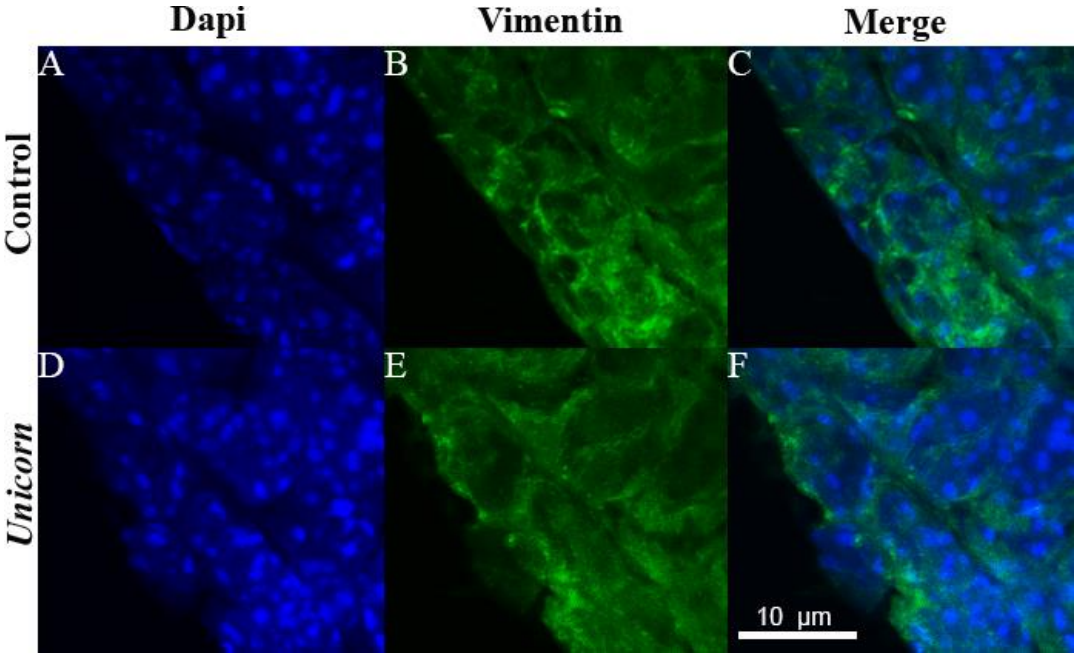

Figure 52. Supplemental 11. *Unicorn* E11.5 vimentin single channel.

4.0 CONCLUSIONS

Orofacial clefting is the most common craniofacial anomaly to affect the population. The prevalence of this life altering morphological defect provides many researchers with the initiative to study the malformation. However, the multifactorial etiology of orofacial clefting suggests that there are many mechanisms that contribute to the development of the different types of orofacial clefting. Through this dissertation, I delineated the spectrum of severity of midfacial clefting through the utilization of two ENU- mutagenized mouse lines. I reasoned that to be able to fully understand the etiology of midfacial clefting, I must first understand the normal morphological processes that occur during midfacial morphogenesis. The midfacial morphogenetic processes that I focused on were the fusion processes of the medial nasal processes and early morphogenesis of the nasal septum. I was able to observe when any morphogenetic, cell signaling, or molecular processes of the embryos from the mild or severe mouse lines began to deviate from the control embryos whilst still allowing us to compare it to normal midfacial development. The data that I have provided within this dissertation is the foundation that clinicians can use to offer better treatment plans and possible prevention strategies to patients.

Traditionally, orofacial clefting has been subdivided into two categories, cleft palate and cleft lip with or without cleft palate. Currently within the literature, nearly all work in orofacial clefting and facial prominence fusion has been largely based upon secondary palatal clefting as there are an abundance of mouse models. The secondary palate develops by means of the bilateral maxillary prominences fusing together medially creating the roof of the mouth. Morphogenesis of the lip is more complex as the lateral and medial segments of the lip are formed separately through the convergence of different facial prominences. The lateral sides of the lip are formed through the

fusion of the maxillary prominence, lateral nasal prominence, and the medial nasal prominence. Whereas, the medial segment of the upper lip is formed through the medial convergence of the medial nasal prominences, and there is a paucity of information about medial nasal prominence movement. It is important to remember that lip morphogenesis occurs much earlier in time than palatal morphogenesis, and that the lip develops from several facial prominences, while the palate develops from one facial prominence. Therefore, it is essential to consider that the morphogenetic processes may be similar, but likely have unique characteristics that arise from each facial prominence involved. Through my dissertation, I focused on nasal septum morphogenesis, as well as, mild and severe clefting of the medial lip, and therefore analyzed the midline convergence processes of the medial nasal prominences in control and medial cleft lip models.

I have demonstrated that the ENU- mutagenized mouse lines, *Unicorn* and *Beetlejuice*, are novel models for anterior midline convergence. During embryonic development, both *Unicorn* and *Beetlejuice* mutants encounter disruptions in midline merging of the medial nasal processes that make them excellent models for the phenotypic spectrum of midfacial clefting. By conducting timed matings in both the *Unicorn* and *Beetlejuice* lines, I was successful in evaluating the anterior midfacial fusion processes that contribute to the medial portion of the lip and nose, as well as, evaluate the earliest stages of nasal septum development in mutant and control embryos. The *Unicorn* mice develop a severe midfacial cleft though the lip, palate, and nose, in addition to a fully bifurcated nasal septum. I have identified that the *Unicorn* phenotype arises between E10.5 to E11.5 of development, suggesting that this day of development is the critical window for midfacial convergence.

We have established that for normal midfacial morphogenesis to occur, specific signaling and molecular processes within the epithelium and mesenchyme must occur. At E10.5, we have

shown that *Ptc1* and *Gli1* is expressed in the medial edge epithelium, and the mesenchyme of the medial nasal process in *Beetlejuice* and *Unicorn* control embryos. The expression domain of *Ptc1* and *Gli1* expression expands in the mesenchyme of the control embryos medial nasal prominence at E11.5. We have also established that in both *Unicorn* and *Beetlejuice* control embryos at E10.5 *Erm1* expression is within the medial edge mesenchyme and posterior tip of the medial nasal prominence. At E11.5 in control embryos, *Erm1* expression shifts lateral to the nasal pit in the mesenchyme.

Additionally, I have provided evidence of the mechanism that the medial edge epithelium uses to disappear during midline medial nasal prominence convergence. Through this dissertation, I have demonstrated that an epithelial to mesenchymal transformation is required for normal midline medial nasal prominence convergence. I have shown that at E10.5 and E11.5, the medial nasal prominence medial edge epithelial cells begin to lose epithelial markers such as, E-cadherin, β-catenin, and Na,K ATP-ase. The control medial edge epithelium also maintains its apical cell polarity at both E10.5 and E11.5. While the medial edge epithelium is losing its epithelial markers, the medial edge epithelium is also acquiring increased levels of the mesenchymal marker, Vimentin. The down-regulation of epithelial markers paired with the upregulation of the mesenchymal marker demonstrates that an epithelial to mesenchymal transformation is occurring. Interestingly though, I did not find any significant differences in apoptosis within the medial edge epithelium or mesenchyme during medial nasal prominence fusion. From this result, I suggest that apoptosis within the medial edge epithelium is not the main mechanism responsible for normal midline convergence of the medial nasal processes.

Through the *Unicorn* and *Beetlejuice* mouse lines, I have demonstrated that precise cell signaling and molecular processes must occur for normal medial lip development to occur. A

coordination of cell signaling, particularly in the frontonasal ectodermal zone (FEZ), is required for fusion of the medial nasal prominences. In both the *Unicorn* and *Beetlejuice* mouse lines, Hedgehog and FGF signaling is altered in the critical developmental window for medial nasal prominence fusion. I found a decrease of HH and FGF signaling in the *Beetlejuice* mice before and during medial lip fusion. I also found a decrease in HH signaling in the *Unicorn* mice, but an increase and shift of domain in FGF signaling during medial lip fusion. I hypothesize that the *Unicorn* mutation affects the induction and location of the FEZ which then secondarily prevents midfacial convergence.

Furthermore, in comparing the *Unicorn* and *Beetlejuice* littermate controls, the mutant embryos medial edge epithelium fails to undergo an epithelial to mesenchymal transformation at E10.5 and E11.5. We have shown that for medial lip development to occur unaffected that the medial edge epithelial cells must lose their epithelial markers and in the process, gain mesenchymal markers. In both the *Unicorn* and *Beetlejuice* mouse lines, the medial edge epithelial cells are able to initially gain mesenchymal markers prior to convergence, but because they never adequately lose their epithelial markers they also never gain enough mesenchymal markers during medial nasal prominence fusion. Additionally, both the *Unicorn* and *Beetlejuice* mice have a loss of apical cell polarity in their MNP medial edge epithelial cells at E10.5 and E11.5. At this point in time, it is unclear from my data the defects in epithelial and mesenchymal status of the medial nasal prominence medial edge epithelium is primary to the midfacial clefting phenotype or secondary to the failure of the epithelial species merging.

I have shown that the *Unicorn* and *Beetlejuice* mutant embryos both fail to undergo an epithelial to mesenchymal transformation and have a loss of apical cell polarity, but the severity of the midline cleft is much more severe in the *Unicorn* embryos. *Unicorn* medial nasal

prominences are turned laterally rather than medially at E10.5, though the width of the medial nasal prominences are normal. By E11.5 the medial nasal prominences are wider and there is a significant internasal distance separating the medial edge of the medial nasal prominences. This internasal distance also laterally displaces the FEZ in the *Unicorn* medial nasal prominences. I observed that at E15.5, one of the *Unicorn* palatal shelves was able to make contact and fuse with the frontonasal process. Together, these data suggest two possibilities 1) the epithelial defects are primary cause of the midfacial cleft phenotype or 2) a secondary outcome of defects earlier patterning defects. To examine these possibilities, I propose to test if the *Unicorn* medial nasal prominences could fuse together if placed in normal proximity of one another via cell culture. Based on my observations, I expect that if the internasal distance is minimized and the medial nasal prominences are placed in close proximity, then the medial nasal prominences will fuse.

Additionally, I have demonstrated that the nasal septum arises from two separate *Collagen2-cre* positive cell populations. I have identified that the *Collagen2-cre* positive cell populations begin developing within the bilaterally paired medial nasal prominences. Through this dissertation, I have shown that the nasal septum anlagen converge at the midline as the medial nasal prominences begin to fuse at the midline. I have shown that like the medial nasal prominences, the nasal septum merges first anteriorly and continues to merge posteriorly as the medial nasal prominences continue to converge. Thus, in severe cases of midfacial clefting, such as in the *Unicorn* mice, the medial nasal prominences fail to converge at the midline and therefore the nasal septum is secondarily inhibited from fusing medially. I have shown that rather than converging into one midline nasal septum, the *Unicorn* dual nasal septi continues to develop autonomously as the embryo develops.

In the future, I aim to better understand the etiology of nasal septum bifurcations that present with severe midfacial clefts of the nose. Ideally, I aim to identify when the nasal septum bifurcation occurs, as well as, to characterize the morphogenesis of the independent nasal septi. To determine when the bifurcations occurs and characterize the independent nasal septum morphogenesis, we will continue these sets of experiments in the *Unicorn* line. I would like to will breed the Col2-CreER^{T} (FVB-Tg(Col2a1-cre/ERT)KA3Smac/J) mouse line into the *Unicorn* mouse line. As I have previously shown that the *Unicorn* nasal septum is bifurcated at E11.5, I would aim to begin collecting embryos at E10.5, and follow the morphogenesis of the nasal septum.

In conclusion, anterior midfacial convergence is an incredibly complex time sensitive process that relies upon precise HH and FGF signaling, as well as, for the medial edge epithelial cells to undergo an epithelial to mesenchymal transformation. Medial nasal prominence midline fusion is vital for medial lip and nasal development, as well as, nasal septum development. To be able to understand orofacial clefting, we must first understand normal craniofacial developmental processes. Working by this principle, we have used the mutant mouse lines to understand abnormal development, but in the process we also uncovered molecular mechanisms that must occur for unaffected craniofacial morphogenesis to occur, and were able to delineate the earliest stages of nasal septum development.

5.0 MATERIALS AND METHODS

5.1 SAMPLE COLLECTION

5.1.1 Embryo collection

Timed matings were performed, and the day of the spermatic plug was designated as day E0.5 of embryonic development. For BrdU labeling, pregnant females were intraperitoneally injected with 10mg/kg BrdU in sterile PBS one hour prior to collection. Pregnant females were euthanized via CO_2 followed by cervical dislocation. Embryos were collected via cesarean section and placed into PBS for transfer and dissection. After dissection, embryos were placed into 4% PFA overnight at 4°C on a rocking plate. Embryos were then placed into 100% ethanol for 2 minutes, 95% ethanol for 2 minutes, followed by two washes of 70% ethanol. Embryos were stored in 70% ethanol until processed and embedded into paraffin wax.

Animal care and use described was approved and complies with the guidelines of the Institutional Animal Care and Use Committee of the University of Pittsburgh.

5.1.2 DNA extraction

Tissues were incubated overnight at 55°C in 10mg/ml Proteinase K and tail lysis buffer (50mM Tris pH 8.0, 5mM EDTA, 50 mM NaCl, 0.5% SDS). Samples were mixed on a shaker and saturated NaCl was added to the samples. The samples were then mixed and centrifuged. The supernatant was poured off to a new centrifuge tube and kept. Isopropanol was added to the

supernatant to precipitate DNA, mixed by inversion, and centrifuged. The supernatant was removed, and the pellet was washed 70% ethanol, vortexed, and centrifuged. After removing the alcohol, DNA was dried in the tubes. Dried DNA was resuspended and stored in 500 µl of 0.1% TE buffer.

5.2 SAMPLE PREPARATION

5.2.1 Processor

Upon collection of embryos in 1% PBS, embryo heads were placed into 4% PFA overnight at 4°C on a rocking plate. The following day, embryo heads were placed into 100% ethanol for 2 minutes, 95% ethanol for 2 minutes, followed by two washes of 70% ethanol. Immediately prior to processing the tissue, 0.1% neutral red in PBS was added to e9.5, e10.5, and e11.5 embryo heads. The addition of the neutral red solution made visualization of the early embryos easier to visualize while embedding under the microscope. Embryo heads were placed into labeled Micromesh biopsy processing/embedding cassettes and placed into a Histoembedder processor for an 8-hour processing cycle. Tissues were dehydrated using graded ethanol changes. Samples were incubated in 70% ethanol at 37°C for 30 minutes, 95% ethanol at 45°C for 30 minutes, 95% ethanol at 45°C for 45 minutes, followed by 3 series of 100% ethanol at 45°C for 30 minutes, 30 minutes, and 45 minutes, respectively. Samples were then incubated in three changes of xylene at 45°C for 30 minutes, 30 minutes, and 45 minutes, respectively. Finally, the samples were incubated in three changes of paraffin wax at 55°C for 45 minutes, 1 hour, and 1 hour time periods. Following the last paraffin wax incubation, samples were immediately embedded.

5.2.2 Embedding

After processing the cranial tissues, samples were embedded using a Leica Histoembedder. Samples were immediately placed into the paraffin wax filled cassette bath set at 65°C. Samples were oriented in the paraffin wax using a Leica S6E stereo microscope. E9.5, e10.5, e11.5, e12.5, and e15.5 heads were placed into the metal cassette with the face pointing towards the microscope. This way, perfectly straight facial orientation sections could be achieved by adjusting the microtome through the back of the head. After correct orientation was achieved, samples were placed onto a -5°C molding tray until the wax hardened.

5.2.3 TESPA coated slides

To ensure that tissue sections adhere tightly and do not detach from the slides during experimentation, slides were coated with triethoxysilylpropylamine (TESPA). Fisherbrand Superfrost Plus Microscope Slides were placed into 2% TESPA for 30 seconds. Slides were then twice placed into 100% acetone for 30 seconds. Slides were rinsed for 30 seconds in miliQ water, wrapped in aluminum foil and dried overnight at 42°C.

5.2.4 Sectioning

After embedding, e9.5, e10.5, e11.5, e12.5, and e15.5 samples were sectioned using a Leica RM2245 microtome. All samples were cut 10 µm thick coronally through the cranium. A water bath was used to adhere sections to the TESPA coated slides. Samples were evaluated using a Leica S6E stereo microscope to check the orientation of the sections. The addition of neutral red

to younger staged embryos allowed for visualization of the sections on the slides. Micro adjustments were made on the microtome until the sections were equilateral coronally. Slides were dried over night at 25°C.

5.3 IMAGING

5.3.1 Pseudo SEM Imaging

E9.5, e10.5, e11.5, and e12.5 embryos were fixed in 4% PFA overnight at 4°C on a shaker. Embryos were washed with 1% PBS and placed into a 0.01% ethidium bromide: 1 % PBS solution for 15 minutes. Embryos were placed back into 1% PBS and imaged via fluorescence using the DsRED filter under fluorescence illumination on the Leica M165FC dissecting microscope using a DFC450 camera microscope. Fluorescence images were compiled in Adobe Photoshop and set to black and white.

5.3.2 Whole mount and skeletal preparation imaging

Samples were imaged in a 1:1 glycerol: ethanol solution. Images were taken on a Leica M165FC dissecting microscope using a DFC450 camera with the Leica LAS software. Images were compiled in Adobe Photoshop.

5.3.3 Histology, immunohistochemistry, and in-situ hybridization imaging

Hematoxylin and eosin staining, sirius red in picric acid and alcian blue staining, immunohistochemistry, and sectioned in-situ hybridization sections were imaged on a Zeiss AXIO microscope with a AxioCam MRc 35 camera. Images were compiled in Adobe Photoshop.

5.3.4 Immunofluorescence and BrdU imaging

Immunofluorescence and BrdU signaling images were taken at The Center for Biological Imaging facilities at the University of Pittsburgh. Z-stacks of the images were taken on an Olympus Fluoview 1000 confocal microscope. Z-stacks were deconvolved and set to maximum projection intensity using NIS software.

5.4 STAINING

5.4.1 TUNEL staining

Apoptosis was detected in paraffin embedded tissue sections using ApopTag Plus Peroxidase *In Situ* Apoptosis Detection Kit (S7101). Sections were deparaffinized using 3 washes of xylene for 5 minutes each, followed by rehydration in 2 changes of 100% ethanol for 5 minutes each, 95% ethanol for 3 minutes, and 70% ethanol for 3 minutes. Sections were washed in PBS for 5 minutes. The tissues were then pretreated with proteinase k (20 µg/mL) for 15 minutes at room temperature, followed by 2 changes of water to wash the sections. Endogenous peroxidases were quenched in

3% hydrogen peroxide for 5 minutes at room temperature. Sections were rinsed twice with PBS for 5 minutes. Next, 75 µL/ 5cm^2 of equilibration buffer was added to the sections. Then, 55 µL/ 5 cm^2 of working strength TdT enzyme was added to the sections and incubated within a humidified chamber at 37°C for 1 hour. The TdT enzyme reaction was stopped with a stop buffer and washed with PBS prior to application of anit-digoxignenin conjugate for 30 minutes at room temperature. Sections were washed four times with PBS for 2 minutes each prior to applying ImmPACT DAB peroxidase substrate staining kit to the slides. DAB color development was monitored under a microscope, and the reaction was stopped using water. Sections were counterstained with methyl green. Slides were dipped 10 times into water, left to air dry, and cover slipped.

5.4.2 Hematoxylin and Eosin staining

Sections were deparaffinized in three changes of xylene for 5 minutes, 3 minutes and 1 minute, respectively. Sections were rehydrated in three changes of 100% ethanol for 1 minute each prior to being rinsed in water for 1 minute. Sections were then moved to Gills hematoxylin (ThermoScientific #7221) for 30 seconds prior to being placed into a clarifier solution (Richard Allan Scientific #7401) for 1 minute. Sections were then placed into running water for 1 minute, followed by a bluing solution (Richard Allan Scientific #7301) for 1 minute. Sections were placed into running water for 1 minute, then were rinsed with 95% ethanol for 20 seconds. Sections were then put into eosin (ThermoScientific #7111) for 1 minute, followed by three changes of 100% ethanol for 20 seconds. Finally, samples were placed into 3 changes of xylene for 3 minutes each. Samples were dried and were subsequently cover slipped.

5.4.3 Sirius red in picric acid and alcian blue staining

Sections were deparaffinized in two changes of xylene for 10 minutes each. Sections were then rehydrated in graded ethanol changes, 100% ethanol for 2 minutes, 90% ethanol for 2 minutes, 70% ethanol for 2 minutes, and 50% ethanol for 2 minutes. After washing in water, sections were placed into 0.5% acetic acid for 10 minutes. Sections were then placed into 1% Alcian blue in 3% acetic acid pH 2.5 for 10 minutes, followed by two washes of 0.5% acetic acid for 3 minutes each. Sections were then placed into 0.5% sirius red in saturated picric acid for 1 hour. Sections were then rinsed twice in 0.5% acetic acid for 1 minute each. Sections were then placed in 100% ethanol three times for 1 minute each, prior to being placed into xylene for 5 minutes. Slides were then allowed to dry and were mounted.

5.5 IMMUNOHISTOCHEMISTRY AND IMMUNOFLOURESCENCE

5.5.1 Immunohistochemistry

Slides were deparaffinized in xylene two times for 10 minutes each. Sections were rehydrated in graded ethanol changes, 100% ethanol for 5 minutes twice, 70% ethanol for 3 minutes, and 50% ethanol for 3 minutes. Sections were then washed with PBS twice for 5 minutes prior to being blocked for peroxidases in 3% hydrogen peroxide in PBS for 5 minutes at room temperature. Slides are then placed into Sodium Citrate buffer pH 6.0 and microwaved for 25 minutes for antigen unmasking. After the slides cool to room temperature, slides are placed into PBS for 2 minutes, followed by 0.1% Triton X-100 in PBS twice for 5 minutes each. The sections are then blocked in

diluted normal goat serum from the Vectastain ABC-HRP Kit for 20 minutes at room temperature in a dehumidifying chamber. Finally, the primary antibody is diluted with the normal goat serum blocking buffer and allowed to incubate overnight at 4°C in a dehumidifying chamber.

The following day, slides were placed into 0.1% Triton X-100 in PBS for 5 minutes at room temperature. Using the Vectastain ABC-HRP Kit, biotinylated goat anti-rabbit IgG secondary antibody was added to the slides for 30 minutes at room temperature in the dehumidifying chamber. The secondary antibody was rinsed off with 0.1% Triton X-100 in PBS for 5 minutes. Vectastain reagents A and B were prepared beforehand and added to the slides for 30 minutes at room temperature in the dehumidifying chamber. Slides were then rinsed with 0.1M Tris pH 7.5, and stained with ImmPACT DAB. The DAB reaction was stopped in water. Sections were counterstained with methyl green. Finally, slides were dipped into water, left to air dry, and cover slipped.

Primary antibody:

P-Histone H3 (S10) produced in rabbit, Cell Signaling #9701S

Secondary antibody:

Biotinylated goat anti-rabbit IgG – Included in Vectastain ABC-HRP Kit

Reagents and Kits used:

Vectastain ABC-HRP Kit– Peroxidase Rabbit IgG, PK-4001

ImmPACT DAB, Peroxidase Substrate Kit – Vector SK-4105

Methyl green, Vector H-3402

5.5.2 Immunofluorescence

Slides were deparaffinized in xylene two times for 10 minutes each. Sections were rehydrated in graded ethanol changes, 100% ethanol for 5 minutes twice, 70% ethanol for 3 minutes, and 50% ethanol for 3 minutes. Sections were then washed with PBS twice for 5 minutes prior to being blocked for peroxidases in 3% hydrogen peroxide in PBS for 5 minutes at room temperature. Slides are then placed into Sodium Citrate buffer pH 6.0 and microwaved for 25 minutes for antigen unmasking. After the slides cool to room temperature, slides are placed into PBS for 2 minutes, followed by 0.1% Triton X-100 in PBS twice for 5 minutes each. The sections are then blocked in normal serum from Vectastain kit for 20 minutes at room temperature in a dehumidifying chamber. Finally, the primary antibody is diluted with the normal serum blocking buffer and allowed to incubate overnight at 4°C in a dehumidifying chamber.

The following day, the primary antibody was rinsed off in three changes of PBS for 3 minutes. The secondary antibody was added for 1 hour at room temperature in a dehumidifying chamber. Following, the secondary antibody was washed off with three changes of PBS for 3 minutes each. Slides were cover slipped and mounted with Prolong-Gold Antifade with DAPI.

Primary antibodies:

Purified mouse Anti- β-catenin 1:100, BD Biosciences #610153

Purified mouse Anti- E-cadherin, BD Biosciences #610181

Purified mouse Anti-Protein Kinase C (PKC), BD Biosciences # 610175

Monoclonal Anti-Vimentin antibody produced in mouse, Sigma #V2258

Rabbit monoclonal Anti-Sodium Potassium ATPase, Abcam #ab76020

Secondary antibodies:

Alexaflour 488 rabbit anti-mouse: 1:200, Invitrogen A11059

Alexaflour 488 donkey anti-rabbit: 1:200, Invitrogen A21206

5.5.3 BrdU

Sections were deparaffinized in 3 changes of xylene for 5 minutes each. Sections were then rehydrated in graded ethanols changes, 100% ethanol two times for 5 minutes, 95% ethanol for 3 minutes, and 70% ethanol for 3 minutes. After washing with PBS three times for 2 minutes, sections were treated with 5 µg/ml Proteinase K in Proteinase K buffer at 37°C for 10 minutes. Sections were washed three times with PBS again for 2 minutes. Next, 300 U/ml Exonuclease III and 15 U/ml Dpn1 were diluted in enzyme buffer. Slides were incubated in the enzyme buffer mix in a humidified chamber for 30 minutes at 37°C. After rinsing the slides in PBS, GE healthcare antibody (RPN202) was added to slides for 30 minutes at 37°C in a humidified chamber. After slides were washed three times for 2 minutes with PBS, Alexa Flour 488 (1:200) in antibody buffer was added to the slides for 30 minutes at room temperature in a humidified chamber. Slides were washed with PBS three times for 5 minutes prior to being mounted and cover slipped with Prolong Gold with dapi (Invitrogen).

The anterior and posterior regions of the medial portion of the medial nasal prominences were analyzed. A box within the anterior portion and posterior portion of the medial nasal prominence was drawn, and the mesenchyme and epithelium was evaluated separately within each area. BrdU positive cells, as well as, all DAPI stained cells were counted in the anterior and posterior regions of the medial nasal prominences. The ratio of BrdU-positive cells within the anterior and posterior regions of the medial nasal prominences were compared to the controls

respective regions using a paired t-test ($p<0.05$). At least 3 Prickle$^{BJ/BJ}$, *Unicorn*, and respective littermate controls were used.

Proteinase K buffer: 0.1M Tris pH 7.5, 0.05M EDTA pH 8.0

Antibody buffer: 1M Tris pH 7.6, 1M $MgCl_2$, 1M β-mercaptoethanol, 1% BSA

5.6 *IN SITU* HYBRIDIZATION

5.6.1 Generation of RNA probes

Dig-labelled RNA probes to the genes of interest were created to detect the location of a mRNA species within the anterior midfacial prominences. One Shot Top10 chemically competent *E. coli* cells were used to transform DNA constructs that contain the gene of interest. DNA was added to the cells, incubated on ice for 30 minutes, heat shocked at 42°C for 30 seconds, placed back on ice for 2 minutes. After, S.O.C medium was added to the vial, and shook horizontally at 37°C for 1 hour at 225 rpm. After cells were incubated overnight on a plate at 37°C, colonies were selected and grown overnight at 37°C in LB media and Amp100.

The following day, a mini prep of the bacterial culture was done to isolate the DNA plasmid using Thermo Scientific GeneJet Plasmid Miniprep Kit. First, cells were resuspended, lysed, and neutralized. The DNA was then bound to a column, prior to the purified DNA being eluted from the column.

After making the mini prep, the DNA construct was linearized. Linearization of the constructs consisted of using a 10x restriction enzyme buffer, DNA, an enzyme that is based on the orientation of the insert in the plasmid, and water. Plasmids were linearized for 2 hours at 37°C. To ensure that the DNA plasmid is digested, a cut and uncut sample were run onto a gel. Linearized samples were then cleaned up using a Qiagen clean-up kit, and the concentration of DNA was calculated on the nano-photometer

Next, the DIG-labelled RNA probe is generated. The probe synthesis reaction consisted of; 1 µg of linearized DNA, Dig-NTP labeling mix, 5x transcription buffer, RNAsin RNAse inhibitor, RNA polymerase, and water. This reaction was incubated for 2 hours at 37°C, and run on a gel. The probe was then precipitated and cleaned. RNAse-free DNAse was added to the probe for 15 minutes at 37°C, followed by 0.5M EDTA to stop the DNAse. Next, 7.5M LiCl and 100% ethanol were added to the sample, mixed, and precipitated for 20 minutes at -80°C. The sample was then centrifuged for 20 minutes. The supernatant was removed, and the pellet was washed with 70% ethanol. The sample was then centrifuged for 5 minutes, and the supernatant was removed, and the pellet was allowed to dry. The pellet was resuspended in 100 µl of DEPC water at 55°C for 10 minutes. After the pellet was dissolved, the concentration of the probe was checked on the nano-photometer. Finally, 1 ml of hybridization buffer was added to the probe to make a stock solution of the probe. Probes were stored at -80°C, and used at 1 µg/ml in in situ experiments.

5.6.2 Whole-mount *in situ* hybridization

Harvested embryos were collected into 1% PBS, and fixed overnight in 4% PFA at 4°C. The following day, embryos were dehydrated in a graded series of methanol, and stored long term in

100% methanol at -20°C until ready to use. Whole mount in-situ hybridization was carried out using a 12-well plate and mesh bottomed well inserts.

DAY 1: Pre-treatment and hybridization

Upon use, embryos were transferred to mesh bottomed well inserts and a small tear was made in the posterior portion of the brain to increase infiltration of solutions. Embryos were rehydrated in a graded methanol series (75%, 50%, and 25% methanol, respectively) for 5 minutes each at room temperature. Embryos were then rinsed twice with 1% PBS for 5 minutes each wash. Embryos were bleached for 1 hour in 6% hydrogen peroxide in PBT, and then washed with PBT three times for 5 minutes each. Embryos were digested using 5 ug/ml Proteinase K depending upon embryonic day. E9.5 embryos were digested for 15 minutes, e10.5 embryos were digested for 30 minutes, and e11.5 embryos were digested for 45 minutes. Digestion reactions were stopped with glycine 2 mg/ml for 5 minutes at room temperature. Embryos were washed in PBT twice for 5 minutes before being re-fixed in 0.2% glutaraldehyde/ 4% PFA in PBT for 20 minutes at room temperature. Embryos were washed in PBT twice for 5 minutes and placed into pre-hybridization buffer for 1 hour at 70°C. After incubation in the pre-hybridization buffer, RNA dig-labelled probe (1 µg/ml) was diluted and incubated with the embryos overnight at 70°C.

Solutions:

PBT: PBS, 0.1% Tween-20

Proteinase K solution (5 ug/ml): Proteinase K (10 mg/ml), PBT

Pre-hybridization buffer: formamide, 5x SSC pH 5.5, 1x Denhardts's, 0.1% Tween-20, 0.1% Chaps, yeast tRNA

Day 2: Post-hybridization washes and antibody hybridization

Embryos were transferred to pre-warmed solution 1 and incubated for 30 minutes at 70°C twice. Embryos were then transferred to a 1:1 solution 1: TNT solution for 10 minutes at 70°C prior to washing the embryos three times in TNT for 5 minutes each at room temperature. Embryos were treated with 100 µg/ml RNAse in TNT solution for 30 minutes at 37°C, and then washed with TNT for 5 minutes at room temperature. Embryos were transferred to solution 2 for 5 minutes at room temperature, followed by two washes of solution 2 for 30 minutes at 65°C. Solution 2 washes were followed by 3 washes of TBST for 5 minutes each at room temperature. Embryos were washed two times in 1x MAB for 10 minutes at room temperature before being pre-blocked with 2% BMB + 1x MAB for 3 hours at room temperature. Finally, Anti-Digoxigenin-AP antibody (1:2000) was added to the pre-block solution and incubated overnight at 4°C.

Solutions:

Solution 1: 50% Formamide, 5x SSC pH 5.5, 1% SDS

Solution 2: 50% Formamide, 2x SSC pH 5.5, 0.2% SDS

TNT: 10 mM Tris HCl pH 7.5, 0.5 M NaCl, 0.1% Tween-20

TBST: 0.14 M NaCl, 2.7 mM KCl, 25 mM Tris HCl pH 7.5, 0.1% Tween-20

Day 3: Post antibody washes and detection

Embryos were washed for 5 minutes with TBST at room temperature. For the next 8 hours, embryos were washed every 2 hours with TBST at room temperature. Embryos were left in TBST overnight at 4°C.

Day 4: Detection

Embryos were washed in TBST for 5 minutes at room temperature, followed by being transferred to AP buffer twice for 5 minutes each at room temperature. Embryos were then placed into BM purple in the dark to develop at room temperature. After staining was identified, embryos were washed in PBT several times, and fixed in 4% PFA overnight at 4°C. Embryos were rinsed in PBT twice, and placed inot 50% PBT/ 50% glycerol for 10 minutes. Embryos were transferred, stored and photographed in 20% PBT/ 80% glycerol.

5.6.3 Sectioned *in situ* hybridization

Harvested embryos were collected into 1% PBS, and fixed overnight in 4% PFA at 4°C. The following day, embryos were dehydrated in a graded series of ethanol, and stored in 70% ethanol. Embryos were processed, and embedded in paraffin wax. Localization of gene expression within specific tissues was evaluated via in-situ hybridization within 10 µm coronally cut sections.

DAY 1: Pre-treatment and hybridization

Sections were deparaffinized with two changes of xylene for 10 minutes each, and washed in 100% ethanol twice for 5 minutes each. Sections were rehydrated through a graded ethanol series consisting of: 95% ethanol, 90% ethanol, 70% ethanol, and 30% ethanol for 2 minutes in each series of ethanol. Slides were washed with PBS for 5 minutes, and post-fixed in 4% PFA for 20 minutes at room temperature. After post-fixation, slides were washed with 2 changes of PBS for 5 minutes each. Sections were digested with 10 µg/ml of Proteinase K in pre-warmed Proteinase K

buffer solution for 10 minutes at 37°C. The digestion was stopped with 2 mg/ml glycine in PBS for 10 minutes at room temperature. The section were washed in PBS for 5 minutes, and fixed in 4% PFA for 5 minutes. Permeability was increased by treating sections with 0.2N HCl for 15 minutes at room temperature. Sections were washed 2 times for 5 minutes each in PBS and acetylated for 10 minutes. Acetylation of the sections consisted of using 0.1M triethanolamine/ 0.25% acetic anhydride pH 8.0. Slides were washed in PBS, then water for 5 minutes each at room temperature. Slides were then placed into a humidifying box and incubated with prehybridization buffer for 2 hours at 65°C. After 2 hours, hybridization buffer was tapped off, and the RNA probe (3 µg probe/ml) was incubated on the sections overnight at 65°C in a humidifying box.

Solutions:

Proteinase K buffer: 0.1M Tris pH 7.5, 0.05M EDTA pH 8.0

Acetylation solution: 0.1M triethanolamine, HCl, acetic anhydride

Prehybridization buffer: formamide, 5x SSC pH 5.5, 1x Denhardts's, 0.1% Tween-20, 0.1% Chaps, yeast tRNA

DAY 2: Post-hybridization washes and antibody incubation

On the following day, slides were put through a series of post hybridization washes and an overnight antibody incubation. Slides were washed twice in pre-warmed solution 1 for 30 minutes each at 65°C. Slides were then washed in TNT three times for 5 minutes each at room temperature. Slides were treated with 40 µg/ml RNAse in TNT at 37°C for an hour. Slides were then washed with TNT: Solution 2 (1:1) for 5 minutes at room temperature prior to washing the slides twice for 30 minutes each with solution 2 at 65°C. Sections were then washed in 1x MAB 3 times for 5

minutes each at room temperature. Sections were pre-blocked for 2 hours at room temperature in a dehumidifying chamber. Finally, the antibody (Anti-Digoxigenin-AP Fab fragments) was added (1:2000) to the blocking buffer, and left overnight in the humidifying chamber at 4°C.

Solutions:

Solution 1: 50% Formamide, 5x SSC pH 5.5, 1% SDS

Solution 2: 50% Formamide, 2x SSC pH 5.5, 0.2% SDS

TNT: 10 mM Tris HCl pH 7.5, 0.5 M NaCl, 0.1% Tween-20

MAB: 100 mM Maleic acid, 150 mM NaCl, 0.1% Tween-20, pH 7.5

Blocking buffer: 1x MAB; 2% BBR (Boehringer Blocking buffer), 10% Sheep serum

Day 3: Post-antibody washes

Slides were washed with MAB three times for 10 minutes each at room temperature. Hourly washes of MAB were done for 4 hours. Three 10 minute washes with NTMT were done at room temperature. Sections were incubated in BM-purple developing solution at room temperature in the dark. After color is detected, reaction was stopped in PBS. Slides were post-fixed in 4% PFA for 15 minutes at room temperature. Slides were then washed in PBS twice for 5 minutes. Sections were counter stained with eosin for 1 minute, then dehydrated with a graded ethanol series and cover slipped.

Solutions:

MAB: 100 mM Maleic acid, 150 mM NaCl, 0.1% Tween-20, pH 7.5

NTMT: 5M NaCl, 1M Tris pH 9.5, 1M $MgCl_2$, 10% Tween-20

5.7 SKELETAL PREPS

In 1% PBS, skin was peeled from embryos, and the contents of the peritoneal and pleural cavities were eviscerated. Embryos were placed into 95% ethanol and fixed overnight at room temperature. Embryos were transferred into 100% acetone and incubated for 6 hours at room temperature to remove fat. Embryos were rinsed in deionized water and placed into alcian blue cartilage stain for 24 hours at room temperature. Embryos were washed every hour for 8 hours in 70% ethanol. Embryos were transferred to 1% potassium hydroxide for 1 hour at room temperature. Bones were counterstained overnight with alizarin red stain. Samples were cleared by placing them into 1% potassium hydroxide/ 20%glycerol. Samples were stored and imaged in a 1:1 glycerol: ethanol solution. Images were taken on a Leica M165FC dissecting microscope using a DFC450 camera with the Leica LAS software. Images were compiled in Adobe Photoshop.

Alcian blue: 90% ethanol, acetic acid, 8GX Alcian Blue (Sigma)

Alizarin red: 0.02% Alizarin Red (Sigma) in 1% KOH

5.8 QUANTITATIVE-PCR

5.8.1 Purifying WT embryonic RNA

Facial prominences (maxillary prominence, lateral nasal prominence, and medial nasal prominence), as well as, bodily tissues were carefully excised from wild type embryos one day prior to facial prominence fusion (e10.5) and one day after the facial prominence fusion (e11.5). Facial and bodily tissues were collected from three e10.5 WT embryos and from three e11.5 WT embryos. Tissues were stored at -80°C until ready to be used.

Upon use, embryonic tissues were removed from the -80°C freezer and placed on ice. Lysis buffer containing 1% 2-mercaptoethanol was added to each microcentrifuge tube containing facial or body tissues. Using a pestle, tissues were minced until the tissue was thoroughly disrupted and lysed. One volume of 70% ethanol was added to the samples and mixed to thoroughly disperse the precipitate. The entire sample was then transferred to a spin cartridge, centrifuged, and disposed of the flow through. Wash buffer was added to the spin cartridge, centrifuged, and the flow through and the collection tube were discarded of. The spin cartridge was placed into a new collection tube and a wash buffer containing ethanol was applied to the spin cartridge, centrifuged, and the flow through was discarded of two separate times. After discarding the flow through from the second wash buffer containing ethanol centrifuge step, the spin cartridge was centrifuged for 1 minute to dry the membrane with the attached RNA. The collection tube was discarded of, and the spin cartridge was placed into a recovery tube. RNAse free water (40 µl) was added to the center of the spin cartridge and incubated for 1 minute at room temperature. The sample was centrifuged for 2 minutes, and the final sample was checked on a nano-photometer to identify the RNA yield and quality.

5.8.2 cDNA synthesis

First strand cDNA was synthesized from RNA made in 6.8.1 for qRT-PCR. The Invitrogen SuperScript VILO cDNA Synthesis Kit was used. cDNA for e11.5 face and body, as well as, e10.5 face and body were generated. A reaction was set up that included 2.5 µg of RNA, 5x VILO Reaction Mix, 10x SuperScript Enzyme Mix, and water. The reaction was gently mixed and incubated at 25°C for 10 minutes. The reaction was then incubated at 42°C for 60 minutes. The reaction was terminated at 85°C for 5 minutes.

5.8.3 qRT-PCR

Custom made Q-PCR forward and reverse primers were designed as listed in Table 1. Initially, each primer was centrifuged, rehydrated with water, vortexed, and centrifuged again prior to use. cDNA was diluted to 1.25 ng/µl. Applied Biosystems Fast SYBR Green Master Mix, forward and reverse primers, cDNA templates, and water were combined and centrifuged in a 96 well reaction plate. For each gene, 3 replicates were done. Additionally, included within each reaction for each gene was a no template control. Reactions were cycled on a StepOnePlus machine.

Table 1. Q-PCR Primers.

Custom made primers from mutated genes identified in the *Unicorn* exome analysis were made to evaluate gene expression during normal lip fusion in WT mouse embryos. Forward and reverse primers for each gene are listed.

Gene	Forward Primer	Reverse Primer
Cyp2j13	AGCTGCTGTCACCTTCCTTTT	TGCGTCAAGTCCATCTGGAAC
Lmf2	AGCTGCTGTCACCTTCCTTTT	AGCGTTGGTGTTTCCCACAG
Tmem106	ATGTCCTCCTGTCGGTCCTG	GATGCCGTTATCGTCCACGAG
Ptgs2	TGAGCAACTATTCCAAACCA	GCACGTAGTCTTCGATCACTAT
Pcdh7	CAGCCATTTCGTAGAGTGAC	CTTGGTGTTTCTGACTCCTCC
Xpc	TCCAGGGGACCCCACAAAT	GCTTTTTGGGTGTTTCTTTGCC
Aldh1a2	CAGAGAGTGGGAGAGTGTTC	CACACAGAACCAAGAGAGAA
Leo1	GTAACAAGGAACTGTTCGGG	AAGCCTCCGACCTATTGTCTG
Eml1	TGAGAACCACCGTCAACAAT	GAGCTGGTCCTATTGATGCTTT
Fyb	TCAACACGGGGAGTAACCC	CGAGCTTTGTCCTGCAACT
Dock4	TGGGGAACCATGTGGAAACA	CGTCGCAGATCGAGGATTTCA
Fmn1	CAAGGGAAGGGTTGCCTATG	TCCCGGAACTATGAGTCTCAG
Gm5114	CCAGCCGCTCATGGGTAATG	CAATCCCACTTGAGAGCACCT
Lef1	TGTTTATCCCATCACGGGTGG	CATGGAAGTGTCGCCTGACAG
Mis18bp1	GTATCACAGTATTGCCGGTCC	CTCTCCCGATTCAGCCTTTCT
Nccrp1	CCCAGTCGCCCAAACCTTAG	TTCCTCCGAGTTCAGGGACC
Npc1l1	TGTCCCCGCCTATACAATGG	CCTTGGTGATAGACAGGCTAC
Nsfl1c	GACTGGCACTGAGGAGGAC	GGGGTTGCTTGTGAAATGGTC
Pramel5	CCCTCACTGTCCCGAACTG	TCCTGTAGGTCTGCAAGGTCA
Slc28a1	TGCCTTTCAGGTTTTGCCCAT	GCAATCTTCAGGATCACCCAC
Gapdh	TGGATTTGGACGCATTGGTC	TTTGCACTGGTACGTGTTGAT
Hprt	TCAGTCAACGGGGGACATAA	GGGGCTGTACTGCTTAACCAG

5.8.4 Analysis

Relative gene expression was quantified in the face of normal fusing facial tissues relative to bodily tissues in WT mice embryos at e10.5 and e11.5. Changes in expression of the target facial tissues relative to the reference bodily tissue were analyzed via the $2^{-\Delta\Delta CT}$ method (Livak and Schmittgen 2001).

BIBLIOGRAPHY

Ashique AM, Fu K, Richman JM. 2002. Endogenous bone morphogenetic proteins regulate outgrowth and epithelial survival during avian lip fusion. Development. 129(19):4647-4660.

Bailey AP, Bhattacharyya S, Bronner-Fraser M, Streit A. 2006. Lens specification is the ground state of all sensory placodes, from which fgf promotes olfactory identity. Developmental cell. 11(4):505-517.

Berk NW, Marazita ML. 2002. Costs of cleft lip and palate: Personal and societal implications. Cleft lip and palate: from origin to treatment.458.

Brinkley L, Basehoar G, Avery J. 1978. Effects of craniofacial structures on mouse palatal closure in vitro. Journal of dental research. 57(2):402-411.

Burdi A, Feingold M, Larsson K, Leck L, Zimmerman E, Fraser F. 1972. Etiology and pathogenesis of congenital cleft lip and cleft palate, an nidr state of the art report. Teratology. 6(3):255-268.

Bush JO, Jiang R. 2012. Palatogenesis: Morphogenetic and molecular mechanisms of secondary palate development. Development. 139(2):231-243.

Carette M, Ferguson M. 1992. The fate of medial edge epithelial cells during palatal fusion in vitro: An analysis by dii labelling and confocal microscopy. Development. 114(2):379-388.

Chai Y, Jiang X, Ito Y, Bringas P, Han J, Rowitch DH, Soriano P, McMahon AP, Sucov HM. 2000. Fate of the mammalian cranial neural crest during tooth and mandibular morphogenesis. Development. 127(8):1671-1679.

Chong HJ, Young NM, Hu D, Jeong J, McMahon AP, Hallgrimsson B, Marcucio RS. 2012. Signaling by shh rescues facial defects following blockade in the brain. Developmental Dynamics. 241(2):247-256.

Clark J, Mossey P, Sharp L, Little J. 2003. Socioeconomic status and orofacial clefts in scotland, 1989 to 1998. The Cleft palate-craniofacial journal. 40(5):481-485.

Cobourne MT. 2004. The complex genetics of cleft lip and palate. European journal of orthodontics. 26(1):7-16.

Cox TC. 2004. Taking it to the max: The genetic and developmental mechanisms coordinating midfacial morphogenesis and dysmorphology. Clinical genetics. 65(3):163-176.

Cuervo R, Covarrubias L. 2004. Death is the major fate of medial edge epithelial cells and the cause of basal lamina degradation during palatogenesis. Development. 131(1):15-24.

DeMyer W. 1967. The median cleft face syndrome differential diagnosis of cranium bifidum occultum, hypertelorism, and median cleft nose, lip, and palate. Neurology. 17(10):961-961.

Diewert V. 1974. A cephalometric study of orofacial structures during secondary palate closure in the rat. Archives of oral biology. 19(4):303-315.

Diewert V. 1980a. The role of craniofacial growth in palatal shelf elevation. Current Research Trends in Prenatal Craniofacial Development.165-186.

Diewert V. 1982. A comparative study of craniofacial growth during secondary palate development in four strains of mice. Journal of craniofacial genetics and developmental biology. 2(4):247-263.
Diewert VM. 1976. Graphic reconstructions of craniofacial structures during secondary palate development in rats. Teratology. 14(3):291-313.
Diewert VM. 1978. A quantitative coronal plane evaluation of craniofacial growth and spatial relations during secondary palate development in the rat. Archives of oral biology. 23(8):607-629.
Diewert VM. 1979. Correlation between mandibular retrognathia and induction of cleft palate with 6-aminonicotinamide in the rat. Teratology. 19(2):213-227.
Diewert VM. 1980b. Differential changes in cartilage cell proliferation and cell density in the rat craniofacial complex during secondary palate development. The Anatomical Record. 198(2):219-228.
Diewert VM. 1983. A morphometric analysis of craniofacial growth and changes in spatial relations during secondary palatal development in human embryos and fetuses. Developmental Dynamics. 167(4):495-522.
Diewert VM, Wang K-Y. 1992. Recent advances in primary palate and midface morphogenesis research. Critical Reviews in Oral Biology & Medicine. 4(1):111-130.
Dixon MJ, Marazita ML, Beaty TH, Murray JC. 2011. Cleft lip and palate: Understanding genetic and environmental influences. Nature Reviews Genetics. 12(3):167.
Eriksson JE, Dechat T, Grin B, Helfand B, Mendez M, Pallari H-M, Goldman RD. 2009. Introducing intermediate filaments: From discovery to disease. The Journal of clinical investigation. 119(7):1763-1771.
Farbman AI. 1969. The epithelium-connective tissue interface during closure of the secondary palate in rodent embryos. Journal of dental research. 48(5):617-624.
Fawcett E. 1911. The development of the human maxilla, vomer, and paraseptal cartilages. By professor fawcett, md, university of bristol. The usually accepted descriptions of the development of the maxilla of man state that it arises by a number of separate centres—the number varying. The Journal of Anatomy and Physiology. 45:378.
Ferguson MW. 1988. Palate development. Development. 103(Supplement):41-60.
Firnberg N, Neubüser A. 2002. Fgf signaling regulates expression of tbx2, erm, pea3, and pax3 in the early nasal region. Developmental biology. 247(2):237-250.
Fitchett JE, Hay ED. 1989. Medial edge epithelium transforms to mesenchyme after embryonic palatal shelves fuse. Developmental biology. 131(2):455-474.
Forbush III B, Kaplan JH, Hoffman JF. 1978. Characterization of a new photoaffinity derivative of ouabain: Labeling of the large polypeptide and of a proteolipid component of the (sodium-potassium ion)-dependent atpase. Biochemistry. 17(17):3667-3676.
Fulton JT. 1957. Closure of the human palate in embryo. American Journal of Obstetrics & Gynecology. 74(1):179-182.
Gaare JD, Langman J. 1977. Fusion of nasal swellings in the mouse embryo: Regression of the nasal fin. Developmental Dynamics. 150(3):477-499.
Gavert N, Ben-Ze'ev A. 2007. B-catenin signaling in biological control and cancer. Journal of cellular biochemistry. 102(4):820-828.
Gavrieli Y, Sherman Y, Ben-Sasson SA. 1992. Identification of programmed cell death in situ via specific labeling of nuclear DNA fragmentation. The Journal of cell biology. 119(3):493-501.

Gibbs BC, Damerla RR, Vladar EK, Chatterjee B, Wan Y, Liu X, Cui C, Gabriel GC, Zahid M, Yagi H. 2016. Prickle1 mutation causes planar cell polarity and directional cell migration defects associated with cardiac outflow tract anomalies and other structural birth defects. Biology open. 5(3):323-335.

Gilles C, Polette M, Zahm J-M, Tournier J-M, Volders L, Foidart J-M, Birembaut P. 1999. Vimentin contributes to human mammary epithelial cell migration. J Cell Sci. 112(24):4615-4625.

Gorlin R, Cohen M, Levin L. 1990. Syndromes of the head and neck.(3rdedn). Oxford University Press, UK. Pg.

Gray H. 1918. Anatomy of the human body. In: Lewis WH, editor. Philadephia: Philadephia: Lea & Febiger.

Griffin JN, Compagnucci C, Hu D, Fish J, Klein O, Marcucio R, Depew MJ. 2013. Fgf8 dosage determines midfacial integration and polarity within the nasal and optic capsules. Developmental biology. 374(1):185-197.

Griffith C, Hay ED. 1992. Epithelial-mesenchymal transformation during palatal fusion: Carboxyfluorescein traces cells at light and electron microscopic levels. Development. 116(4):1087-1099.

Gritli-Linde A. 2012. The mouse as a developmental model for cleft lip and palate research. Cleft lip and palate. Karger Publishers. p. 32-51.

Gritli-Linde A. 2008. The etiopathogenesis of cleft lip and cleft palate: Usefulness and caveats of mouse models. Current topics in developmental biology. 84:37-138.

Gubb D, Green C, Huen D, Coulson D, Johnson G, Tree D, Collier S, Roote J. 1999. The balance between isoforms of the prickle lim domain protein is critical for planar polarity in drosophila imaginal discs. Genes & development. 13(17):2315-2327.

Guion-Almeida ML, Richieri-Costa A, Saavedra D, Cohen Jr MM. 1996. Frontonasal dysplasia: Analysis of 21 cases and literature review. International journal of oral and maxillofacial surgery. 25(2):91-97.

Hay ED. 1995. An overview of epithelio-mesenchymal transformation. Cells Tissues Organs. 154(1):8-20.

Hayward A. 1969. Ultrastructural changes in the epithelium during fusion of the palatal processes in rats. Archives of oral biology. 14(6):661-IN620.

Hendzel MJ, Wei Y, Mancini MA, Van Hooser A, Ranalli T, Brinkley B, Bazett-Jones DP, Allis CD. 1997. Mitosis-specific phosphorylation of histone h3 initiates primarily within pericentromeric heterochromatin during g2 and spreads in an ordered fashion coincident with mitotic chromosome condensation. Chromosoma. 106(6):348-360.

Henrique D, Schweisguth F. 2003. Cell polarity: The ups and downs of the par6/apkc complex. Current opinion in genetics & development. 13(4):341-350.

Hinrichsen D. 1985. The early development of morphology and patterns of the face in the human embryo. Advances in anatomy, embryology, and cell biology.

Hirano S, Nose A, Hatta K, Kawakami A, Takeichi M. 1987. Calcium-dependent cell-cell adhesion molecules (cadherins): Subclass specificities and possible involvement of actin bundles. The Journal of Cell Biology. 105(6):2501-2510.

Hu D, Helms JA. 1999. The role of sonic hedgehog in normal and abnormal craniofacial morphogenesis. Development. 126(21):4873-4884.

Hu D, Marcucio RS. 2009. Unique organization of the frontonasal ectodermal zone in birds and mammals. Developmental biology. 325(1):200-210.

Hu D, Marcucio RS, Helms J. 2003. A zone of frontonasal ectoderm regulates patterning adn growth in the face. Development. 130:1749-1758.
Iizuka T. 1973. Stage of the closure of the human palate. Okajimas folia anatomica Japonica. 50(4):249-257.
Jeong J, Mao J, Tenzen T, Kottmann AH, McMahon AP. 2004. Hedgehog signaling in the neural crest cells regulates the patterning and growth of facial primordia. Genes & development. 18(8):937-951.
Jiang R, Bush JO, Lidral AC. 2006. Development of the upper lip: Morphogenetic and molecular mechanisms. Developmental Dynamics. 235(5):1152-1166.
Jiang X, Iseki S, Maxson RE, Sucov HM, Morriss-Kay GM. 2002. Tissue origins and interactions in the mammalian skull vault. Developmental biology. 241(1):106-116.
Jin J-Z, Ding J. 2006. Analysis of cell migration, transdifferentiation and apoptosis during mouse secondary palate fusion. Development. 133(17):3341-3347.
Juan G, Traganos F, James WM, Ray JM, Roberge M, Sauve DM, Anderson H, Darzynkiewicz Z. 1998. Histone h3 phosphorylation and expression of cyclins a and b1 measured in individual cells during their progression through g2 and mitosis. Cytometry: The Journal of the International Society for Analytical Cytology. 32(2):71-77.
Justice MJ, Noveroske JK, Weber JS, Zheng B, Bradley A. 1999. Mouse enu mutagenesis. Human molecular genetics. 8(10):1955-1963.
Kalluri R, Neilson EG. 2003. Epithelial-mesenchymal transition and its implications for fibrosis. The Journal of clinical investigation. 112(12):1776-1784.
Kato Y, Hirano T, Yoshida K, Yashima K, Akimoto S, Tsuji K, Ohira T, Tsuboi M, Ikeda N, Ebihara Y. 2005. Frequent loss of e-cadherin and/or catenins in intrabronchial lesions during carcinogenesis of the bronchial epithelium. Lung Cancer. 48(3):323-330.
Katoh M, Katoh M. 2003. Identification and characterization of human prickle1 and prickle2 genes as well as mouse prickle1 and prickle2 genes homologous to drosophila tissue polarity gene prickle. International journal of molecular medicine. 11(2):249-256.
Kawauchi S, Shou J, Santos R, Hébert JM, McConnell SK, Mason I, Calof AL. 2005. Fgf8 expression defines a morphogenetic center required for olfactory neurogenesis and nasal cavity development in the mouse. Development. 132(23):5211-5223.
Kemphues KJ, Priess JR, Morton DG, Cheng N. 1988. Identification of genes required for cytoplasmic localization in early c. Elegans embryos. Cell. 52(3):311-320.
Kim S, Lewis AE, Singh V, Ma X, Adelstein R, Bush JO. 2015. Convergence and extrusion are required for normal fusion of the mammalian secondary palate. PLoS biology. 13(4):e1002122.
Kinzler KW, Bigner SH, Bigner DD, Trent JM, Law ML, O'Brien SJ, Wong AJ, Vogelstein B. 1987. Identification of an amplified, highly expressed gene in a human glioma. Science. 236(4797):70-73.
Koh KS, Do Yeon Kim TSO. 2016. Clinical features and management of a median cleft lip. Archives of plastic surgery. 43(3):242.
Kolker AR, Sailon AM, Meara JG, Holmes AD. 2015. Midline cleft lip and bifid nose deformity: Description, classification, and treatment. Journal of Craniofacial Surgery. 26(8):2304-2308.
Kvinnsland S. 1974. Partial resection of the cartilaginous nasal septum in rats; its influence on growth. The Angle Orthodontist. 44(2):135-140.

Lee J, Platt KA, Censullo P, i Altaba AR. 1997. Gli1 is a target of sonic hedgehog that induces ventral neural tube development. Development. 124(13):2537-2552.
Lee JM, Dedhar S, Kalluri R, Thompson EW. 2006. The epithelial–mesenchymal transition: New insights in signaling, development, and disease. J Cell biol. 172(7):973-981.
. Genetics of cleft lip and cleft palate. American Journal of Medical Genetics Part C: Seminars in Medical Genetics; 2013: Wiley Online Library.
Li Y, Klena NT, Gabriel GC, Liu X, Kim AJ, Lemke K, Chen Y, Chatterjee B, Devine W, Damerla RR. 2015. Global genetic analysis in mice unveils central role for cilia in congenital heart disease. Nature. 521(7553):520.
Liu C, Lin C, Gao C, May-Simera H, Swaroop A, Li T. 2014. Null and hypomorph prickle1 alleles in mice phenocopy human robinow syndrome and disrupt signaling downstream of wnt5a. Biology open. 3(9):861-870.
Livak KJ, Schmittgen TD. 2001. Analysis of relative gene expression data using real-time quantitative pcr and the 2− δδct method. methods. 25(4):402-408.
Luke D. 1976. Development of the secondary palate in man. Cells Tissues Organs. 94(4):596-608.
Macara IG. 2004. Par proteins: Partners in polarization. Current biology. 14(4):R160-R162.
Macatee TL, Hammond BP, Arenkiel BR, Francis L, Frank DU, Moon AM. 2003. Ablation of specific expression domains reveals discrete functions of ectoderm-and endoderm-derived fgf8 during cardiovascular and pharyngeal development. Development. 130(25):6361-6374.
Macklin CC. 1914. The skull of a human fetus of 40 mm. Developmental Dynamics. 16(3):317-385.
Macklin CC. 1921. Preliminary note on the skull of a human fetus of 43 mm. Greatest length. The Anatomical Record. 22(4):251-265.
Marcucio RS, Cordero DR, Hu D, Helms JA. 2005. Molecular interactions coordinating the development of the forebrain and face. Developmental biology. 284(1):48-61.
Marigo V, Davey RA, Zuo Y, Cunningham JM, Tabin CJ. 1996a. Biochemical evidence that patched is the hedgehog receptor. Nature. 384(6605):176.
Marigo V, Johnson RL, Vortkamp A, Tabin CJ. 1996b. Sonic hedgehog differentially regulates expression ofgliandgli3during limb development. Developmental biology. 180(1):273-283.
Martınez-Alvarez C, Tudela C, Perez-Miguelsanz J, O'kane S, Puerta J, Ferguson M. 2000. Medial edge epithelial cell fate during palatal fusion. Developmental biology. 220(2):343-357.
McMahon AP, Ingham PW, Tabin CJ. 2003. 1 developmental roles and clinical significance of hedgehog signaling.
McNeill H, Ozawa M, Kemler R, Nelson WJ. 1990. Novel function of the cell adhesion molecule uvomorulin as an inducer of cell surface polarity. Cell. 62(2):309-316.
Mendez MG, Kojima S-I, Goldman RD. 2010. Vimentin induces changes in cell shape, motility, and adhesion during the epithelial to mesenchymal transition. The FASEB Journal. 24(6):1838-1851.
Minor NT, Sha Q, Nichols CG, Mercer RW. 1998. The gamma subunit of the na, k-atpase induces cation channel activity. Proceedings of the National Academy of Sciences. 95(11):6521-6525.
Mori C, Nakamura N, Okamoto Y, Osawa M, Shiota K. 1994. Cytochemical identification of programmed cell death in the fusing fetal mouse palate by specific labelling of DNA fragmentation. Anatomy and embryology. 190(1):21-28.

Moss ML, Bromberg BE, Song IG, Eisenman G. 1968. The passive role of nasal septal cartilage in mid-facial growth. Plastic and Reconstructive Surgery. 41(6):536-542.

Mousa SA. 2008. Cell adhesion molecules: Potential therapeutic & diagnostic implications. Molecular biotechnology. 38(1):33-40.

Müller F, O'Rahilly R. 1980. The human chondrocranium at the end of the embryonic period, proper, with particular reference to the nervous system. Developmental Dynamics. 159(1):33-58.

Nawshad A, LaGamba D, Hay E. 2004. Transforming growth factor β (tgfβ) signalling in palatal growth, apoptosis and epithelial mesenchymal transformation (emt). Archives of oral biology. 49(9):675-689.

Negoescu A, Lorimier P, Labat-Moleur F, Drouet C, Robert C, Guillermet C, Brambilla C, Brambilla E. 1996. In situ apoptotic cell labeling by the tunel method: Improvement and evaluation on cell preparations. Journal of Histochemistry & Cytochemistry. 44(9):959-968.

Ohno S. 2001. Intercellular junctions and cellular polarity: The par–apkc complex, a conserved core cassette playing fundamental roles in cell polarity. Current opinion in cell biology. 13(5):641-648.

Osumi-Yamashita N, Ninomiya Y, Eto K, Doi H. 1994. The contribution of both forebrain and midbrain crest cells to the mesenchyme in the frontonasal mass of mouse embryos. Developmental biology. 164(2):409-419.

Ozawa M, Baribault H, Kemler R. 1989. The cytoplasmic domain of the cell adhesion molecule uvomorulin associates with three independent proteins structurally related in different species. The EMBO journal. 8(6):1711-1717.

Pascual-Castroviejo I, Pascual-Pascual S, Pérez-Higueras A. 1985. Fronto-nasal dysplasia and lipoma of the corpus callosum. European journal of pediatrics. 144(1):66-71.

Rajasekaran SA, Palmer LG, Moon SY, Soler AP, Apodaca GL, Harper JF, Zheng Y, Rajasekaran AK. 2001. Na, k-atpase activity is required for formation of tight junctions, desmosomes, and induction of polarity in epithelial cells. Molecular biology of the cell. 12(12):3717-3732.

Rohatgi R, Milenkovic L, Scott MP. 2007. Patched1 regulates hedgehog signaling at the primary cilium. Science. 317(5836):372-376.

Russell W, Kelly E, Hunsicker P, Bangham J, Maddux S, Phipps E. 1979. Specific-locus test shows ethylnitrosourea to be the most potent mutagen in the mouse. Proceedings of the National Academy of Sciences. 76(11):5818-5819.

Sarnat BG, Wexler MR. 1966. Growth of the face and jaws after resection of the septal cartilage in the rabbit. Developmental Dynamics. 118(3):755-767.

Scher RL, Koch WM, Richtsmeier WJ. 1993. Induction of the intercellular adhesion molecule (icam-1) on squamous cell carcinoma by interferon gamma. Archives of Otolaryngology–Head & Neck Surgery. 119(4):432-438.

Schneider R, Helms J. 2003. The cellular and molecular origins of beak morphology. Science. 299(5606):565-568.

Scott J. 1953. The cartilage of the nasal septum. British Dental Journal 95:37-40.

Shen Y, Leatherbury L, Rosenthal J, Yu Q, Pappas M, Wessels A, Lucas J, Siegfried B, Chatterjee B, Svenson K. 2006. Cardiovascular phenotyping of fetal mice by noninvasive high-frequency ultrasound facilitates recovery of enu-induced mutations causing congenital cardiac and extracardiac defects. Physiological genomics. 24(1):23-36.

Shuler C, Guo Y, Majumder A, Luo R. 1991. Molecular and morphologic changes during the epithelial-mesenchymal transformation of palatal shelf medial edge epithelium in vitro. The International journal of developmental biology. 35(4):463.

Shuler CF, Halpern DE, Guo Y, Sank AC. 1992. Medial edge epithelium fate traced by cell lineage analysis during epithelial-mesenchymal transformation in vivo. Developmental biology. 154(2):318-330.

Song Y, Hui J, Fu K, Richman J. 2004. Control of retinoic acid synthesis and fgf expression in the nasal pit is required to pattern the craniofacial skeleton. Developmental biology. 276(2):313-329.

Sperber G. 2002. Formation of the primary palate.; Wyszynski D, editor. Cleft lip & palate: From origin to treatment.

Sperber GH, Guttmann GD, Sperber SM. 2001. Craniofacial development (book for windows & macintosh). PMPH-USA.

Stenstrom SJ, Thilander BL. 1970. Effects of nasal septal cartilage resections on young guinea pigs. Plastic and reconstructive surgery. 45(2):160-170.

Stone DM, Hynes M, Armanini M, Swanson TA, Gu Q, Johnson RL, Scott MP, Pennica D, Goddard A, Phillips H. 1996. The tumour-suppressor gene patched encodes a candidate receptor for sonic hedgehog. Nature. 384(6605):129.

Sun D, Baur S, Hay ED. 2000. Epithelial–mesenchymal transformation is the mechanism for fusion of the craniofacial primordia involved in morphogenesis of the chicken lip. Developmental biology. 228(2):337-349.

Szabo-Rogers H, Yakob W, Liu KJ. 2016. Frontal bone insufficiency in gsk3β mutant mice. PloS one. 11(2):e0149604.

Szabo-Rogers HL, Geetha-Loganathan P, Nimmagadda S, Fu KK, Richman JM. 2008. Fgf signals from the nasal pit are necessary for normal facial morphogenesis. Developmental biology. 318(2):289-302.

Szabo-Rogers HL, Geetha-Loganathan P, Whiting CJ, Nimmagadda S, Fu K, Richman JM. 2009. Novel skeletogenic patterning roles for the olfactory pit. Development. 136(2):219-229.

Takeichi M. 1977. Functional correlation between cell adhesive properties and some cell surface proteins. The Journal of cell biology. 75(2):464-474.

Takeichi M. 1990. Cadherins: A molecular family important in selective cell-cell adhesion. Annual review of biochemistry. 59(1):237-252.

Takeichi M. 1991. Cadherin cell adhesion receptors as a morphogenetic regulator. Science. 251(5000):1451-1455.

Taniguchi K, Sato N, Uchiyama Y. 1995. Apoptosis and heterophagy of medial edge epithelial cells of the secondary palatine shelves during fusion. Archives of histology and cytology. 58(2):191-203.

Trainor PA, Tam P. 1995. Cranial paraxial mesoderm and neural crest cells of the mouse embryo: Co-distribution in the craniofacial mesenchyme but distinct segregation in branchial arches. Development. 121(8):2569-2582.

Tree DR, Shulman JM, Rousset R, Scott MP, Gubb D, Axelrod JD. 2002. Prickle mediates feedback amplification to generate asymmetric planar cell polarity signaling. Cell. 109(3):371-381.

Trumpp A, Depew MJ, Rubenstein JL, Bishop JM, Martin GR. 1999. Cre-mediated gene inactivation demonstrates that fgf8 is required for cell survival and patterning of the first branchial arch. Genes & development. 13(23):3136-3148.

Urata MM, Kawamoto HK. 2003. Median clefts of the upper lip: A review and surgical management of a minor manifestation. Journal of Craniofacial Surgery. 14(5):749-755.
Walker B, Fraser F. 1956. Closure of the secondary palate in three strains of mice. Development. 4(2):176-189.
Wang K-Y, Juriloff DM, Diewert VM. 1995. Deficient and delayed primary palatal fusion and mesenchymal bridge formation in cleft lip-liable strains of mice. Journal of craniofacial genetics and developmental biology. 15(3):99-116.
Waterman RE, Meller SM. 1974. Alterations in the epithelial surface of human palatal shelves prior to and during fusion: A scanning electron microscopic study. The Anatomical Record. 180(1):111-135.
Watkins SE, Meyer RE, Strauss RP, Aylsworth AS. 2014. Classification, epidemiology, and genetics of orofacial clefts. Clinics in plastic surgery. 41(2):149-163.
Weinberg SM, Neiswanger K, Richtsmeier JT, Maher BS, Mooney MP, Siegel MI, Marazita ML. 2008. Three-dimensional morphometric analysis of craniofacial shape in the unaffected relatives of individuals with nonsyndromic orofacial clefts: A possible marker for genetic susceptibility. American Journal of Medical Genetics Part A. 146(4):409-420.
Wood PJ, Kraus B. 1962. Prenatal development of the human palate: Some histological observations. Archives of oral biology. 7(2):137-IN137.
Wu P, Jiang T-X, Suksaweang S, Widelitz RB, Chuong C-M. 2004. Molecular shaping of the beak. Science. 305(5689):1465-1466.
Yang T, Jia Z, Bryant-Pike W, Chandrasekhar A, Murray JC, Fritzsch B, Bassuk AG. 2014. Analysis of prickle1 in human cleft palate and mouse development demonstrates rare and common variants involved in human malformations. Molecular genetics & genomic medicine. 2(2):138-151.
Yoshida T, Vivatbutsiri P, Morriss-Kay G, Saga Y, Iseki S. 2008. Cell lineage in mammalian craniofacial mesenchyme. Mechanisms of development. 125(9):797-808.
Young NM, Chong HJ, Hu D, Hallgrímsson B, Marcucio RS. 2010. Quantitative analyses link modulation of sonic hedgehog signaling to continuous variation in facial growth and shape. Development. 137(20):3405-3409.
Zallen JA. 2007. Planar polarity and tissue morphogenesis. Cell. 129(6):1051-1063.